TAMPEREEN TEKNILLINEN YLIOPISTO
TAMPERE UNIVERSITY OF TECHNOLOGY

ANTTI HILDEN

POWER QUALITY AND POWER MONITORING IN A MODERN OFFICE BUILDING UTILIZING DIVERSE METERING

Master of Science Thesis

Examiner: D.Sc. (Tech.) Pertti Pakonen

The examiner and topic of the thesis were approved on 30 May 2018

ABSTRACT

ANTTI HILDEN: Power quality and power monitoring in a modern office building utilizing diverse metering
Tampere University of Technology
Master of Science Thesis, 88 pages
December 2018
Master's Degree Programme in Electrical Engineering
Major: Power Systems and Market
Examiner: D.Sc. (Tech.) Pertti Pakonen

Keywords: building, distortion, Fryze, ICT, machine learning, measurements, monitoring, power, power quality, solar power

The monitoring and measuring of power quality and power is becoming increasingly important in distribution networks as a consequence of developing electricity markets, distributed generation and the proliferation of power electronics devices. The correct measurements and adequate monitoring result in an effective and secure supply of electrical energy. The studies of the thesis utilize the diverse measurements of the piloted modern office building expanding examination to low voltage distribution networks. During the study, the complete monitoring of the electrical energy system of the building was implemented and the measurements were analyzed focusing on their significant aspects.

The thesis consists of three parts considering the theory and practices of measuring, the implementation of the data acquisition system in the pilot building and the analyses of the measurements. First the concerns over power quality and power are discussed in conventional and modern cases and the principles of measuring and the quantities used are described. Also, the consequences of inaccurate power measurements and poor power quality are listed. Then the thesis continues with the introduction of the pilot environment and the ICT system comprising IoT- and Linux platforms. Finally, the measurements are presented by the means of a general overview and more sophisticated analyses of time averaging of power and distortion in current, voltage and power.

The analyses focus on total distortion and Fryze's power theory and provide an overview of the electrical behaviour of the building. In addition, various time averages are calculated for active, fundamental frequency reactive and Fryze's reactive power and, also, distortion in current and voltage and their combined effect on Fryze's reactive power are discussed. The time resolution of 1 second was utilized with the different types of loads and the solar power plant. The impact of the solar power plant and electric car charging was found to mainly relate to active power. Ventilation and tenants' appliances were observed to draw the highest distortion current, and thus affect the voltage distortion of the building confirmed by correlation coefficients and random forest method of machine learning. Time averaging of 1 minute was noted to conform with the averages of 1 second. The results indicate that Fryze's reactive power quantifies distortion relevantly and distortion current requires quantification in an absolute manner.

TIIVISTELMÄ

ANTTI HILDEN: Sähkön laadun ja tehon monitorointi nykyaikaisessa toimistorakennuksessa hyödyntäen kattavaa mittarointia
Tampereen teknillinen yliopisto
Diplomityö, 88 sivua
Joulukuu 2018
Sähkötekniikan diplomi-insinöörin tutkinto-ohjelma
Pääaine: Sähköverkot ja -markkinat
Tarkastaja: TkT Pertti Pakonen

Avainsanat: aurinkovoimala, Fryze, ICT, mittaukset, monitorointi, rakennus, sähkön laatu, särö, teho, yliaallot

Sähkön laadun ja tehon mittaamisen ja seurannan merkitys kasvaa jakeluverkoissa sähkömarkkinoiden kehityksen, hajautetun tuotannon ja yleisesti tehoelektroniikan lisääntyneen määrän seurauksena. Asianmukaiset mittaukset ja riittävä seuranta auttavat tehokkaaseen ja turvattuun sähköenergian toimitukseen. Diplomityö hyödyntää pilottirakennuksen monipuolisia mittauksia ja laajentaa tutkimukset käsittämään myös pienjännitejakeluverkot. Työn aikana toteutettiin pilottirakennuksen sähköenergiajärjestelmän kokonaan kattava mittarointi, jonka mittauksien erityisiä ominaisuuksia korostettiin analyyseissä.

Diplomityö koostuu kolmesta osasta, joissa käsitellään mittaamisen teoriaa ja käytäntöjä, pilottirakennuksen mittausjärjestelmän toteutusta ja mittauksien analyyseja. Aluksi käydään läpi sähkön laatuun ja tehoon liittyviä huolia perinteisestä ja nykyaikaisesta näkökulmasta ja perehdytään mittaamisen perusteisiin ja käytettyihin mittasuureisiin. Lisäksi selvitetään huonon sähkön laadun ja epätarkkojen tehomittausten seurauksia. Sen jälkeen esitellään pilottirakennus ja siihen kehitetty ICT-järjestelmä, joka sisältää Linux- ja IoT-alustat. Työn analyysiosiossa tarkastellaan mittaustuloksia yleisesti ja syvennytään aikakeskiarvoihin ja särön osuuteen virrassa, jännitteessä ja tehossa.

Työn analyyseissä keskitytään kokonaissäröön ja Fryzen tehoteoriaan, joita hyödynnetään rakennuksen sähköenergiajärjestelmän yleisen käyttäytymisen tarkastelussa. Lisäksi pätöteholle, perusaallon loisteholle ja Fryzen loisteholle lasketaan moninaisia aikakeskiarvoja eri mittauspisteissä ja pohditaan virran ja jännitteen säröä ja niiden yhdistymistä Fryzen loistehossa. Erityyppiset kuormat ja aurinkovoimala, joita mitattiin 1 sekunnin tarkkuudella, olivat työn kannalta huomattavia etuja. Aurinkovoimalan ja sähköauton latauksen todettiin olevan merkityksellisiä ainoastaan pätötehon osalta. Ilmanvaihto ja vuokralaisten laitteet aiheuttivat suurimman virtasärön ja näkyivät myös jännitesärössä. Tämä vahvistettiin laskemalla korrelaatiokertoimia ja kouluttamalla random forest -koneoppimismalli. Työssä tehtyjen tarkastelujen perusteella 1 minuutin aikakeskiarvot kuvaavat riittävän tarkasti 1 sekunnin aikakeskiarvoja. Tulokset myös osoittivat, että Fryzen loisteho on käyttökelpoinen työkalu särötehon seurannassa, ja että virtasärön mittaamisessa kannattaa suosia absoluuttisia suureita suhteellisten sijasta.

PREFACE

This Master of Science Thesis was completed as part of the Prosumer Centric Energy Ecosystems - Social Energy (ProCem) project at the Laboratory of Electrical Energy Engineering at Tampere University of Technology. Professor Pertti Järventausta made it possible to participate in the project. D.Sc. (Tech.) Pertti Pakonen, examiner, and professor Pekka Verho, supervisor, guided in the selection of the subject.

Also, I thank D.Sc. (Tech.) Pertti Pakonen for his expert opinions and the staff of MX Electrix Oy for the flexible cooperation. The special thanks go to D.Sc. (Tech.) Jyri Kivimäki, D.Sc. (Tech.) Aapo Aapro, D.Sc. (Tech.) Antti Mutanen and M.Sc. Kalle Ruuth for pushing me forward and creating a joyful work environment. Furthermore, I owe to M.Sc. Nyyti Kinnunen and B.Sc. Ville Heikkilä for aiding me in the examinations of the studies of the thesis.

Finally and with all my heart, I want to express my gratefulness to Vuokko and my family for the love and support.

In Tampere, Finland, on 19 November 2018

Antti Hilden

CONTENTS

LIST OF FIGURES

LIST OF TABLES

LIST OF ABBREVIATIONS AND SYMBOLS

AC	Alternating current
AMR	Automatic meter reading
API	Application programming interface
BC	Blockchain
BREEAM	Building Research Establishment's Environmental Assessment Method
CEER	Council of European Energy Regulators
CIGRE	Conseil International des Grands Réseaux Électriques
DC	Direct current
DFT	Discrete Fourier transform
DR	Demand response
DSM	Demand side management
DSO	Distribution system operator
ecdf	Empirical cumulative distribution function
EU	European Union
FFT	Fast Fourier transform
FMI	Finnish Meteorological Institute
HIRLAM	High Resolution Limited Area Model
ICT	Information and communication technology
IEC	International Electrotechnical Commission
IEEE	Institute of Electrical and Electronics Engineers
IoT	Internet of Things
IT	Information technology
JWG	Joint working group
LED	Light-emitting diode
LV	Low voltage
LV3	Laatuvahti 3 meter
L1	Phase L1
L2	Phase L2
L3	Phase L3
ML	Machine learning
MV	Medium voltage
N	Neutral conductor
NIALM	Nonintrusive appliance load monitoring
PC	Personal computer
PCC	Point of common coupling
PFC	Power factor correction
PM3255	Power meter PM3255
PM820	Power meter PM820MG
ProCem	Prosumer Centric Energy Ecosystem
PV	Photovoltaic
RTDS	Real Time Digital Power System Simulator
RVC	Rapid voltage change
SMPS	Switched-mode power supply
TSO	Transmission system operator
TUT	Tampere University of Technology
V2G	Vehicle-to-grid technology

a_n	Fourier series coefficient
a_0	Mean value of periodic signal in Fourier series
A_n	Magnitude of harmonic frequency
b_n	Fourier series coefficient
D_B	Budeanu's distortion power
D_I	Distortion power caused by distortion current
D_V	Distortion power caused by distortion voltage
DPF	Displacement power factor
I_n	Magnitude of harmonic frequency current
I_1	Magnitude of fundamental frequency current
I_R	Maximum demand current
I_{TD}	Total distortion current
mse	Mean squared error
n	Number of harmonic order
N	Maximum number of harmonic components
P	Active power
P_1	Fundamental frequency active power
PF	Power factor
ppm	Particles per million
Q_B	Budeanu's reactive power
Q_f	Fryze's reactive power
Q_1	Fundamental frequency reactive power
rms	Root mean square
R^2	Correlation of prediction and data
S_1	Fundamental frequency apparent power
S	Apparent power
S_H	Distortion power caused by distortion voltage and current
S_N	Nonactive apparent power
t	Time instant in periodic signal of Fourier series
T	Length of time period in Fourier series
TD	Total distortion
TD_I	Total distortion of current
TD_U	Total distortion of voltage
TDD	Total demand distortion
THD	Total harmonic distortion
THD_U	Total harmonic distortion of voltage
THD_I	Total harmonic distortion of current
U	Phase voltage
U_{TD}	Absolute total distortion voltage
U_n	Magnitude of harmonic frequency voltage
U_1	Magnitude of fundamental frequency voltage
$x\,(t)$	Intant value of periodic signal in Fourier series
θ_1	Phase difference of fundamental frequency voltage and current
ϕ_n	Phase of harmonic frequency

1. INTRODUCTION

Distribution networks and grid-connected appliances have gone through evident changes during the past decade urged by distributed generation and the proliferation of power electronics. Concurrently, the imbalance settlement period (ISP) of European day-ahead electricity market is shifting from 1 hour towards 15 minutes, and power tariffs of distribution networks are evolving continuously. These transitions, in addition to the ”smart grid” concept, raise the concern over power quality and need for measuring the power flows in the distribution network more accurately in time and frequency domain [6, 62, 63]. Therefore, it is essential to study sufficient time resolution and quantities for power measurements considering modern loads and power generation. If chosen accordingly, power measurements describe the behaviour of a device relevantly in the distorted voltage conditions of distribution networks.

Understanding the issues in time averaging and quantification of power requires knowledge of the variety of power theories and investigating of conventional and modern loads and power generation in the distribution networks. The power of the distribution network is generally divided into active and reactive power in brevity of common conversations without more detailed definitions. The calculation methods of active and reactive power and their combinations alternate depending on the source and organization, which easily causes additional confusion in the quantification of power [17, 30]. The solution of using rather a simplistic approach to power has been adequate up to the present days but the future of distribution networks may require revising the measurement of power.

In addition to power, power quality is studied in this thesis in a distribution network hosting modern loads and power generation. Power quality represents a surprisingly wide and complex area of electrical engineering with obscure consequences to the consumers. Currently, voltage and current distortion, among others, are contemporary topics due to the proliferation of nonlinear devices connected to the distribution networks. The modern loads, e.g. power converters, and introduction of solar and wind power have been proven to affect the power quality of the distribution networks [24]. To examine the distorted voltage and current conditions of the distribution networks, knowledge should be gathered considering the basic theory of harmonics and measuring of distortion factors. Various practices are available to measure the distortion and a couple of them are utilized in the measurements of the thesis [14].

Usually it is encouraged to make the connection between theory and practice with real measurements. A modern multi-user office building named Kampusareena at Tampere University of Technology (TUT) served as the framework of the measurements in the thesis. Additionally, Kampusareena provided a pilot platform for various other studies

within the Prosumer Centric Energy Ecosystem (ProCem) project. Modern loads and power generation are found in Kampusareena including power converters of ventilation, solar photovoltaic power plant and electric vehicle charging station. As a part of the thesis, a monitoring system of the building was designed and implemented. The system continuously collects data from several sources, stores it in databases and delivers data for applications. In addition to this thesis, the monitoring system was utilized in product development, research, demonstrations and visualizations of an IoT platform (Internet of Things). The data sources consist of meters in the electrical energy system, building automation data, inverters of solar power plant, weather station, weather forecast, hourly electricity market price and information about the national grid status. Building automation systems are inspected in Luoma's thesis and integration of electrical energy system and building automation is called for. Also, power measurements are requested in less than 1 hour intervals, in addition to energy readings, to utilize demand response (DR) [41]. Saari presents a similar data collection system as implemented in Kampusareena and promotes an advanced kWh meter [52]. The pilot of Kampusareena combines comprehensively the data of the electrical energy system and building automation and measures power in various quantities with 1 second time resolution using the next generation advanced kWh meter.

The most valuable data for the thesis was acquired from the separately measured electrical loads, solar power plant and main distribution boards. The analysis utilized simultaneous measurements of the loads in accurate time resolution of 1 second. The meters recorded a comprehensive selection of power and power quality quantities over a time period of several months. These features of the measurements allowed observing the typical behaviour of the electrical energy system of the building considering power and power quality. In the more sophisticated analyses, time averaging of power was studied, in addition to considerations of power in the distorted conditions of the electrical network of the building. Furthermore, a large set of data was fed to machine learning methods to discover the source of the voltage distortion.

The thesis begins by exploring the present power quality concerns in distribution networks and how the electrical loads and power generation have changed until this day. The latter part of Chapter 2 summarizes the theory behind quantities of power and distortion and measurement practices are explained in general. In addition, the consequences of poor power quality and inaccurate power measurements are listed. The pilot of Kampusareena is described in Chapter 3 including general information about the building and an overview of the electrical energy system and its loads and solar power plant. In the same chapter, the ICT system of the pilot and data collection are covered as necessary for the thesis. Chapter 4 reports separately the electrical behaviour of the main electricity distribution, loads and solar power plant from the viewpoints of power and distortion of voltage and current. Eventually in Chapter 5, the data of the monitoring system is used in analysis considering time averaging of power and overall quantification of power justified with distortion current measurements and studies of the source of voltage distortion.

2. POWER QUALITY AND POWER IN DISTRIBUTION NETWORKS

Due to the on-going evolution of distribution networks, which introduces new ways of producing and consuming power, the practices of measuring power quality and power should also be reconsidered. The change from conventional towards modern loads and generation, e.g. electric vehicle (EV) charging stations and solar power plants, adds growing interest on power quality and power in the distribution networks. Consequences of deteriorated power quality and inaccurate power measurements can eventually cause expenses for distribution system operators (DSO) and their customers.

This thesis and chapter concentrates on power quality and power and combines them using alternate power theories and voltage and current distortion in low voltage (LV) distribution networks. The considerations are supported with a review of power quality and power concerns and the difference between conventional and modern loads and power generation. Power quality section focuses on voltage and current distortion and measuring them. Power is discussed by comparing the commonly used power theories with other proposed power theories in the literature. Lastly, the importance of proper power quality and power measurements is argued for with the consequences of adverse conditions.

2.1 Power quality and power concerns

Power quality in the distribution networks has been addressed to remain topical in the future [63]. The legislators in Europe have also realized the critical dependency of customers on electricity leading to more strict regulation of security of energy supply and guidelines of power quality monitoring [24]. At worst, the poor power quality of a distribution network results in an unexpected blackout. Meanwhile power quality is under concern, the measurement principles of power in the distribution networks should also receive attention. As the tariffs of active and reactive power are developed, the measuring practices of power should be exact and congruent. Inaccuracies in the measurements or unsuitable measurement method in terms of time average or power theory may affect the electricity bill in the increasingly nonsinusoidal conditions.

The standardization and academics have addressed the issues in power quality and measuring of power in the future of distribution networks [4, 17, 30, 63]. Bollen discusses on power quality concerns at application level of the future smart grids, and describes potential issues as introduction of microgrids, advanced voltage control, feeder reconfigurations and demand side management (DSM). These concerning issues are made possible by, among others, the proliferation of distributed generation, e.g. solar power, and the changes at

demand-side, e.g. controllability of electric vehicle (EV) charging and other loads. It is expected that the magnitude and direction of power flows are greatly affected, and overall, the upcoming smart functionalities in the distribution networks may redefine the principles of electricity distribution. [4] Another publication of CIGRÉ joint working group (JWG) C4.24 adds power electronics in general as a source of distortion and rises the question of how devices and distribution networks interfere with each other as the power systems evolve [63].

The concerns on power and measuring it are related to power quality through voltage and current distortion induced by proliferation of nonlinear loads. The thesis also addresses fluctuation of power as a consequence of distributed generation and implementation of demand side management (DSM). The definitions of electrical power have been investigated thoroughly over the last decades but it still remains undecided how the power is correctly quantified under nonsinusoidal conditions. [30] In addition, a few studies have speculated the proper time averaging of power, the calculation of demand, in distribution network environments [15, 48, 53, 62]. Anyway, the advanced computing capabilities of today's electronics enable to design versatile and accurate meters with desired specifications. The IEEE (Institute of Electrical and Electronics Engineers) standard IEEE Std 1459 gives a comprehensive introduction to the current state of power definitions.

The thesis considers power quality from the viewpoint of distortion and its sources and connects power to power quality by means of power theories. If the costs of disturbances in the distribution networks is desired to be divided between the customers and DSO, the quantification of power has to be revised for billing purposes. Also, the source of distortion should be reliably determined. Time averaging of power in this thesis is studied based on high time resolution measurements of several load types. The results indicate sufficient time interval of power measurements for different load types and solar power plant in a modern multi-user office building. Additionally, the measurements of the thesis pointed out, and other authors have also underlined, that the enormous amount of power quality and power data from numerous meters requires efficient, unified and automatic analysis with well-defined quantities. [36, 44, 46]

2.2 Conventional and modern loads and power generation

As the concept of smart grid is becoming reality driven by environmental factors and security of supply, especially the distribution networks are affected. Distributed renewable generation is connected to the distribution networks accompanied by electrical energy storages. The customers of the distribution networks are making their loads available for control to third parties to participate in various electricity markets. Furthermore, an overall change is occurring in the type of power generation and loads, which is discussed concentrating on LV distribution network viewpoints more or less excluding large industrial loads due to the scope of the thesis. [31]

Conventionally distribution networks have been described to solely comprise loads of the customers. The electricity has been generated in large centralized power stations and transferred over the transmission and distribution networks eventually to the customer. The production of power has been regulated to match with the consumption of the customers' loads. The conventional loads include incandescent lamps, directly coupled electric motors and mechanically switched resistive loads e.g. stoves. The usage of conventional loads has been predictable, and thus load profiles have been created for consumers. Traditionally the power generation has mainly consisted of nuclear, coal, CHP (Combined Heat and Power) and hydroelectric power plants with nominal powers of tens or hundreds of megawatts. The largest power plants have been operated at relatively constant active power and the smaller ones have balanced the production and demand. Technically the generators have involved inertia proportional to the mass and angular velocity of the rotor of the generator. In brief, the power has been generated in centralized plants at considerable distance from the consumers, which have used directly coupled linear loads.

During the past decades modern power generation and loads have been introduced at the distribution networks. The power generation has been greatly impacted by several forms of distributed generation, while the loads are turning into electronically coupled appliances. The energy resources of the distributed generation include solar photovoltaic (PV) power plants, fuel cells and wind turbines, of which solar power represents the highest penetration in the LV distribution networks. The modern loads are mostly nonlinear power electronics appliances, e.g. adjustable speed drives, electronic ballast and LED (light-emitting diode) lamps and PCs (personal computer) [30]. In addition, nowadays numerous other commonly used appliances contain nonlinearly behaving switched-mode power supply (SMPS). Additionally, energy storages, mainly batteries, and electric cars are more often connected to the distribution networks. Battery energy storages and electric cars can be utilized as controllable loads but also as power supplies. Both the modern power generation and loads bring variability to the distribution networks because of the intermittent nature of weather conditions, and dependence of the loads on certain control strategies. For example, Firth reports unpredictable variability of domestic loads [22].

Articles of Ipakchi and Guerrero review the evolution of distribution networks from several viewpoints giving special attention to distributed generation and demand response [23, 31]. In Finland, the use of the conventional CHP and coal plants is constantly reduced because of environmental reasons, thus nuclear power is increasing its share in the power generation [58]. Simultaneously, small units of the distributed generation are installed around the distribution networks. This is creating a potential issue in balancing the production and demand: nuclear power plants are operated at constant active power and the distributed generation has limited control of power production. The issue is being addressed with the control of the loads and activating even the smaller customers of the distribution networks in it. Altogether, the developments in the power generation and loads are inevitable when the climate change is fought to be restrained.

2.3 Power quality

The quality of the electricity, commonly called power quality, is a wide area of research in the electrical networks. A part of power quality is voltage quality and also the quality of current and the security of supply are considered in power quality. Power itself is seldom mentioned as a quantity when power quality is determined. Power quality in the LV distribution networks generally involves properties of voltage including frequency, magnitude, rapid variations, waveform distortion and various other disturbances. [3, 54] Also, limits for distortion current and interruptions are defined [27, 56]. The interest in power quality results from DSOs intention to deliver proper quality of electricity within standards to the customers and their increasingly sensitive devices [60]. Furthermore, the customers have become critically dependent on the supply of electricity nowadays, and thus the security of supply is essential [42].

Voltage quality is normally the main concern of DSOs because the loads creating the flow of current are operated by the customers. In addition, DSOs are in general responsible for power quality because no cost is listed for the customer in case of poorly operating electrical devices. Usually voltage at the access point to the distribution network is determined to comply with standard SFS-EN 50160 in Finland [60]. Nevertheless, standards and publications are starting to show concern about power quality and its costs, and how the costs should be quantified and divided between DSOs and customers [30, 42].

As stated that power quality is a diverse and complex matter, this thesis studies merely voltage and current distortion of LV distribution networks. The thesis also combines distortion with power, and quantifies the distortion using Fryze's reactive power. The following sections explain the basics of distortion in the distribution networks and consider the factors of total distortion that are used in the analysis of the thesis. Lastly, measurement practices of distortion are shortly reviewed on a general level.

2.3.1 Distortion

Distortion of voltage and current is the deviation of their waveforms from an ideal fundamental frequency sine-wave that is 50 Hz in Finland. In more detail, distortion consists of frequency components differing from the fundamental frequency. In Finland, voltage distortion has been increasing in the distribution networks during the decades due to the increase of nonlinear loads and power generation [40]. The standardization has reacted to the deteriorated conditions with revising of the definitions and limits of voltage and current distortion, and in addition numerous studies have been reported in the literature.

The distortion of voltage and current can be quantified in several manners enabled by the significantly improved processing capabilities of microprocessors and advanced mathematical models. In the very basic theory, Fourier series is used to divide any periodical waveform into DC (direct current) component, fundamental frequency sinusoidal component and integer multiple components of the fundamental frequency. For these components,

magnitude and phase angle can be solved, and thus the components of the distortion, called harmonics, are found. With Fourier series a periodical waveform function is presented as follows [1]:

$$x(t) = a_0 + \sum_{n=1}^{\infty} \left(a_n \cos\left(\frac{2\pi nt}{T}\right) + b_n \sin\left(\frac{2\pi nt}{T}\right)\right). \tag{2.1}$$

The order of harmonic is denoted with n, one equaling to the fundamental frequency. The time instant is t and T the length of the period. Finally, after deriving coefficients a_n and b_n at a time instant the magnitude, A_n, and the phase angle, ϕ_n, are calculated using Equations 2.2 and 2.3. The term a_0 represents the average, DC component, of the periodical function.

$$A_n = \sqrt{a_n^2 + b_n^2} \tag{2.2}$$

$$\phi_n = \tan^{-1}\left(\frac{b_n}{a_n}\right) \tag{2.3}$$

Further knowledge on Fourier series and how the time domain converts to frequency-domain with Fourier transform are explained more profoundly in the literature [1, 8]. In practice voltage or current is sampled at a certain rate and the discrete data requires discrete Fourier transform (DFT). Using the transformation the acquired samples of a periodical waveform are converted into frequency domain and the magnitudes and phase angles of the harmonics of the distortion can be calculated. Modern applications, e.g. smart power meters, frequently utilize a procedure of fast Fourier transform (FFT), which decreases the needed resources and time for computation by simplifying the method of DFT.

Generally, only odd number harmonics are notably measured in three-phase AC (alteranting current) power systems. Even number harmonics result from asymmetry of waveform meaning that the half waves of the waveform differ. Even harmonics may be related to, for instance, saturation of a transformer or a faulty rectifier bridge. [1] The harmonics above the first order are frequently compared with the fundamental frequency component or a defined constant value [27, 60]. It is also typical that the harmonic concentration of the waveform fluctuates continuously due to relation to the magnitude of active power as stated in the analysis of section 5.3.

In addition to individual harmonics that are integer multiples of the fundamental frequency component, harmonics are separated to several other groups in standard IEC 61000-4-7 [14]. These groups comprise harmonic and interharmonic groups and their subgroups. In brief, the harmonic group involves the harmonic frequency and the adjacent frequencies until the half of the distance to the next and previous harmonic frequency in frequency domain. Interharmonic group includes frequencies between two adjacent harmonic frequencies. The subgroups of harmonics and interharmonics limit the considered harmonics to a chosen smaller bandwidth of frequencies. The frequencies below the second harmonic excluding the fundamental frequency component can be named as interharmonics also, or possibly

subsynchronous harmonics [27,30]. The equal considerations can be performed for voltage and current waveform, although different limits are given in standards.

Total values of distortion in standardization and power quality studies calculate a sum of the magnitudes of harmonics or frequencies of certain bandwidth [12, 27, 60]. The total distortion and harmonics overall are usually limited until a specific frequency, normally 2 kHz or 2.5 kHz [27, 60]. Above these frequencies standards provide less guidance until 150 kHz [13]. Research on frequencies 2.5 kHz–150 kHz has proposed the term of supraharmonics to standardize these frequencies frequently polluted by switching designs of power electronics [51]. This thesis considers only the total values of distortion, which are further described in the next section. Standards applicable for the studies in the thesis involve SFS-EN 50160, IEC 61000-4-7 and IEEE Std 1459 [12, 14, 60]. Standard IEC 61000-4-7 establishes a concrete foundation regarding the measurement techniques of harmonics. Additionally, numerous other standards, e.g. VDE-AR-N 4105, specifically address the distributed generation.

In addition to certain frequency components and total distortion, current distortion can be assessed in terms of summation at point of common coupling (PCC). Harmonic or interharmonic currents of various orders of different loads are aggregated at PCC, e.g. a distribution board, and can either cancel each other completely, be superimposed maximally or something in between. In principle, the magnitude of each harmonic current component at PCC varies between zero and root mean square (rms) of the harmonic currents of the loads. Hence, the summation of distortion currents has a significant impact on the resulting distortion current at PCC. The summation depends on the phase angles of certain harmonic current of the aggregated loads. If the phase angles of the harmonic current are equal, the harmonic currents represent maximum superposition and no cancellation of harmonic currents occurs. In contrast, the maximum cancellation occurs when the phase angles have difference of 180 degrees, in case of two sources of harmonic current. Every harmonic current component has a specific phase angle, which can be calculated, for instance, as in Eq. 2.3. [54] In practical cases the phase angles of certain order harmonic current of different loads seldom match, which results in cancellation of some degree in distortion current of PCC. For example, the publication of Meyer reports that harmonic currents of modern lamps considerably cancel each other, if large number of lamps is installed in the same feeder [45]. A study considering summation of distortion currents is also performed in the analysis section 5.2.1, in which the summation of total distortion currents of the loads at main distribution board is measured and calculated based on the measurements of the loads.

2.3.2 Cause of distortion

Usually in power engineering nonlinearity is highlighted when distorted, nonsinusoidal current of AC system is discussed. The nonlinearity of a device distorts the flowing current leading into a situation, where the relationship between current and voltage deviates from

linear behaviour. In other words, if an ideal sinusoidal voltage is applied to the device, it produces a nonsinusoidal current. Although, it should be reminded that even a purely resistive linear load consumes distorted current, if the voltage is distorted. The sources of distorted current, the nonlinear devices, commonly include saturating transformers, arcing devices and power electronics converters in general consisting of switching and rectifying components. The power converters, for instance, drive an electric motor, a fan of ventilation system or convert DC solar power suitable for the AC electrical network. [1, 8] Common distorted current waveforms and their causes are described in the review of Kalair [33].

The voltage of an electrical network is mainly distorted due to flowing distortion currents. However, the source of voltage distortion is more complex to solve than measuring the distortion current of a device. The voltage distortion may inherit from synchronous machine that is generating the voltage of the electrical network, or the voltage is distorted by nonlinearities of the electrical network itself, e.g. due to transformer. At consumer side, nonlinear loads draw distorted current that is reflected into the voltage through the impedance of the network. The voltage distortion caused by the synchronous machines and electrical networks is normally considered small compared to the nonlinear loads of the customers. The distorted current of the consumer device can be generated because of its design principles or due to the background voltage distortion of the electrical network, which rises the question about the compatibility of the device and the electrical network [1, 8]. Ultimately, the problem of finding the source of voltage distortion is difficult [19, 44].

The stiffness of the electrical network defines, how the voltage is affected by the distortion current. Stiffness is quantified with short-circuit impedance, current and power. The short-circuit current and power measure the values that would flow in case of short-circuiting phase to neutral wire or phase to phase at the measurement point. The short-circuit impedance depicts the impedance of the network either as the sum of phase and neutral conductor or two phase conductors. To decrease the risk of overly high voltage distortion one should prefer higher short-circuit current and power and low short-circuit impedance. Also three-phase short-circuit measurements are performed, though the impedance of the conductors can be determined separately. The maximum limits of distortion current in standards can be dependent on the short-circuit current as in IEEE Std 519 [27].

2.3.3 Total of distortion

The analyses of the thesis focus on utilizing various definitions of total distortion quantities for voltage and current distortion. Total distortion describes the overall magnitude of the distortion without separating individual harmonics. In this section the calculation of the total values is explained and the features of each quantity are considered. The quantities of the total distortion include total harmonic distortion (THD), total distortion (TD) and total demand distortion (TDD). Also, an absolute value for the total distortion is derived in contrast to total values usually being related to fundamental frequency component. The quantities of THD and TDD are common knowledge for electrical engineers but the

quantity of TD makes a different approach to the distortion measurements by considering a more comprehensive range of frequency components.

The technical specifications and standards create a frame for the measurement of total distortion. The distortion limits are set for phase-to-neutral measurements and measurement bandwidth is either 0–2 kHz or 0–2.5 kHz at 50 Hz [13, 14, 27, 60]. This thesis uses measurements of phase 1 (L1) and measurement bandwidth of 2 kHz, which complies with standards IEC 61000-4-30 and SFS-EN 50160 [13,60]. Phase 2 (L2) and 3 (L3) and neutral conductor (N) are outlined out of the scope of the thesis to explicitly compare distortion of different loads and solar power plant.

The factor of THD represents the most common method to observe the distortion of voltage or current at the measurement point. THD is used for voltage and current and normally presented as the ratio of root mean square (rms) of rms magnitudes of harmonic components to the rms magnitude of the fundamental frequency component, as shown in Equation 2.4. The rms of the harmonic frequencies comprises the rms values of the harmonic components between the second and 40th or 50th order depending on the measurement practice [27,60]. This thesis involves harmonics until 40th order (2 kHz). The magnitudes of the harmonic components contain only the value of the specific harmonic frequency. In other words, no interharmonic frequencies are considered. The formula for calculating THD of voltage is as follows [1]:

$$THD_U = \frac{\sqrt{\sum_{n=2}^{N} U_n^2}}{U_1} \times 100\,[\%] \tag{2.4}$$

The harmonic order of rms value is denoted with n and U_1 is the rms value of fundamental frequency component. N denotes the last harmonic component included in the calculation. Finally, the ratio is converted to percentage value. The larger the magnitudes of the harmonic components in the numerator are, the higher is the distortion and percentage related to the ideal fundamental frequency component. The same equation applies for THD_I, THD of current, when U_n and U_1 are replaced by I_n and I_1. [1] Standardization provides limits for voltage and current THD in different contexts [27, 60].

In the analyses later in this thesis, it has been noted that in low load conditions the value of THD_I occasionally rises unreasonably high, even though the distortion current represents only low absolute value, thus having no effect on voltage distortion. Hence, THD_I can be misleading because it uses by definition the fluctuating value of fundamental frequency current. If the absolute value of I_1 is small, even a moderate amount of distortion current results in high value of THD_I. On the other hand, the devices are designed to operate around the nominal power, at which the fundamental frequency related total distortion of THD_I is more feasible measure. In case of voltage in the distribution networks, THD_U is more practical since the voltage is assumed to remain around the nominal value.

The ratio of TDD relates the harmonic distortion components to a reference current rather than the fundamental frequency component that depends on the operating point of the appliance. This constant is defined based on the maximum or rated magnitude of current of the load or power generation. Otherwise, the computation of TDD is identical to THD.

$$TDD = \frac{\sqrt{\sum_{n=2}^{N} I_n^2}}{I_R} \times 100\,[\%] \tag{2.5}$$

The selection of constant I_R is guided in standard IEEE Std 519 [27]. The constant reference current removes the fluctuating fundamental frequency current of THD but requires a correct choosing of I_R. For voltage, TDD is less relevant due to practically constant level of the fundamental frequency phase voltage in THD.

Total distortion (TD) of voltage and current includes every frequency component of a waveform limited by the bandwidth of the measurement device. Thus, no restriction of only individual harmonic frequencies is present and interharmonics generated by devices can be measured, even below the fundamental frequency. In detail, TD involves all the frequencies excluding the fundamental frequency and DC component according to the manufacturer of the meters used in this thesis. Measurements of TD include frequencies until 2 kHz and mainly constitute the utilized voltage and current distortion measurements in this thesis. The calculation of total distortion of voltage (TD_U) is described in general in Equation 2.6. Koponen considers more profoundly the deriving of TD from the measurements [38]. The measurements of TD are averaged for 1 second in accordance with IEC 61000-4-30 in the studies of the pilot building [13].

$$TD_U = \frac{U_{TD}}{U_1} \times 100\,[\%] \tag{2.6}$$

In Equation 2.6, the value of TD_U is presented as a percentage value simplified to the division of rms distortion (U_{TD}) and rms magnitude of fundamental frequency component (U_1). The same equation applies for the total distortion of current (TD_I) when the voltage values are replaced by the values of current of I_{TD} and I_1.

Lastly, an absolute value of distortion current is used in the analyses of the thesis to present the exact behaviour and value of distortion. Especially the values of absolute total distortion current, I_{TD}, are presented. Equation 2.7 illustrates the method that was derived to convert percentages of TD_I to the absolute values of I_{TD} in amperes. This was possible because of I_1 measurement of the meters.

$$I_{TD} = \frac{I_{TD}}{I_1} I_1 \times 0.01 = TD_I I_1 \times 0.01\,[A] \tag{2.7}$$

The absolute value of I_{TD} is straightforwardly solved when I_1 is eliminated from the ratio of TD_I. Also, the percentage form is removed with the simple multiplication.

2.3.4 Measuring

Power quality measurements in practice require considerations of different aspects including what is the subject of the measurements, how can you measure the desired quantities and what is the process of data management and analysis. These issues were faced during the design, measurements, and eventually, in the data analysis of the piloted building of the thesis. In this section, the prevailing and possible future measurement practices are discussed in general. Special attention is dedicated to the measuring of the distortion because of the scope of the thesis. Lately in the literature, joint working group (JWG) C4.112 of CIGRÉ in particular has addressed the current state and the future of power quality monitoring [36, 46].

According to survey pointed at DSOs and transmission system operators (TSOs), measuring of harmonics as a part of power quality monitoring is among the most popular ones after voltage level, sags and swells. In distribution networks, the measurements are largely motivated and performed due to customer complaints. Furthermore, the survey found that the measurements are frequently performed only after an exception in power quality, and fewer continuous measurements are installed. In addition, the compliance regulations strongly influence the utilized power quality quantities, though still confusion has been noticed in the selection and understanding of power quality quantities. As an example, a meter or power quality analyzer produces certain quantities or a report of power quality that are accepted without further questioning the measurement setup or the attributes of the meter. JWG C4.112 also concludes that a great variation is found between distribution networks considering the investments in power quality measurements. [36, 46]

The future of power quality measurements is promising because of the technological advances of measurement instruments, communication, data storages and processing resources. Additionally, power quality is a topical subject when modern loads and power generation are concerned. The advances in technology result in cheaper, smaller and more capable measurement devices. The new devices can measure at higher sampling rate, calculate numerous quantities and be more accurate. However, the user still has to acknowledge the shortcomings and limitations of the measurement devices and other instruments e.g. current probes, and also be able to understand the measurement environment and the results. Researchers promote unification of data models and reporting to facilitate data sharing and reduce misunderstandings. Although the current technology can continuously collect enormous amounts of data, only relevant data is preferred to decrease diversification of power quality monitoring. Automatic analysis can also assist with the continuous data flow and utilize the full potential of the data. [46]

The thesis touches the trends of power quality measurements by continuously monitoring the pilot building with several compact and diverse power quality meters. Machine learning algorithms are tested to analyze a larger amount of data, and in addition to traditional figures, the measurement data is visualized with dashboards of an IoT-platform (Internet of Things). In a sense, the thesis also discovers the benefits of a wider utilization and

integration of power quality quantities in AMR-meters (automatic meter reading), which has been proposed before [38, 52]. A more comprehensive power quality assessment with AMR-meters could lead to more effective usage of the distribution network. Fortunately, standards IEC 61000-4-30 and IEEE Std 1159 have been updated recently to clarify the power quality measurements [13, 28]. Standard SFS-EN 50160 gives limits for the voltage of distribution network, and standards IEEE Std 519 and IEC 61000-4-7 concentrate on distortion [14, 27, 60]. In addition, Council of European Energy Regulators (CEER) has written harmonized guidelines for voltage quality monitoring [24].

2.4 Power

Power in electrical network consists of active and reactive power that compose apparent power. This thesis considers power in LV distribution networks by means of frequency domain and investigates power theories differing from the most commonly used ones. Several power theories for AC systems have been developed since 1910 to split apparent power to appropriate components [17]. The interest to explore these power theories arises from the increasing values of voltage and current distortion in the distribution networks. Traditionally active and reactive power include power of the fundamental frequency neglecting distortion power at higher frequencies. Also, the distortion power could be involved, and thus quantified, in the operation of the modern distribution networks. In addition, power in form of power tariffs is becoming a meaningful part of the electricity bill even for smaller private customers in the future, which motivates to inspect the measurement of power also in time domain with time averages.

This section begins by describing the common theory of active and reactive power and apparent power in the LV distribution networks. Furthermore, apparent power is divided into various compositions depending on the power theory finally focusing on Fryze's power theory. The relation of voltage and current distortion to power is explained using the theories and also power factors are examined. At the end, measuring of power is considered from the viewpoints of historical, current and future practices.

2.4.1 Power theories

The usefulness of a power theory is an important criterion. It is essential that an average engineer understands the meaning of the measured power, which relates strongly to the physical meaning of the power. Furthermore, it should be possible to implement the measurement method in the design of power meter feasibly. These reasons may have led to the decision of using the current power theory of active and reactive power. Here, the conventional power theory is compared with other theories finally choosing Fryze's power theory. The calculations behind the measurements of this thesis are introduced preparing for the analysis chapters.

The power theories presented here consider powers measured between phase and neutral conductor leaving the complexities of three-phase theories out of the thesis. The measurement bandwidth is limited to 0–2 kHz due to the measurement device used. The naming of power quantities varies between different sources but confusions are tried to be avoided by mentioning different names of the same quantities. The cited literature provides significantly more profound explanations of power starting from the measurements of instant values. For example, Emanuel and standard IEEE Std 1459 address thoroughly the measuring of power in the literature [2, 16, 30]. The fundamentals of AC power theories have been developed throughout the 20th century and the evolution of the distribution networks makes the theories timely to discuss again [17].

For single phase, apparent power is the product of phase voltage and current. The phase voltage is measured between phase and neutral wire. Apparent power illustrates the maximum power, at which net energy can be delivered, if the voltage and current are sinusoidal and no phase shift is present between them causing reactive power.

$$S = UI \tag{2.8}$$

Voltage U and current I are rms values over a certain time period of sampling. Further, apparent power is usually presented as orthogonal components of active power and reactive power. However, the following definition applies only for sinusoidal conditions.

$$S = \sqrt{P_1^2 + Q_1^2} \tag{2.9}$$

Active power, P_1, is the fundamental frequency active power, which is the arithmetical average of instantaneous active power samples. Active power can also be called real power according to IEEE Std 1459. Reactive power, Q_1, is derived based on the amplitude of the oscillating power of the fundamental frequency component. [30] Equation 2.9 is commonly known, however, the fundamental frequency component is usually neglected in the notations. In practice, distortion is always found in the waveforms of voltage and current, thus the definition of S changes to apparent power of fundamental frequency, S_1, and S is defined as follows according to IEEE Std 1459 [30]:

$$S_1 = \sqrt{P_1^2 + Q_1^2} \tag{2.10}$$

$$S = \sqrt{S_1^2 + S_N^2} = \sqrt{(P_1^2 + Q_1^2) + (D_I^2 + D_V^2 + S_H^2)} \tag{2.11}$$

In nonsinusoidal conditions apparent power S consists of the fundamental frequency components P_1 and Q_1 and the distortion components that include distortion power caused by harmonic current, voltage and current and voltage together. The distortion components are denoted respectively: D_I, D_V and S_H. This definition resolves apparent power to several components resulting in complexity for practical cases. Another composition of apparent power, derived by Budeanu, was recently abandoned in IEEE Std 1459 due to criticism [7].

The composition splits S to P, Q_B and D, which represent respectively: active power equaling to the sum of the fundamental and harmonic frequency components, Budeanu's reactive power including fundamental and harmonic frequency reactive power and distortion power that contains the remaining effect of the distortion in voltage and current [7].

$$S = \sqrt{P^2 + Q_B^2 + D_B^2} \tag{2.12}$$

To reduce the number of components and simplify the complexity in apparent power this thesis utilizes Fryze's power theory, Equation 2.13, which defines S consisting of active power of fundamental and harmonic frequencies (P) and reactive power of fundamental and harmonic frequencies (Q_f). Fundamentally, the theory divides current into orthogonal active and reactive components. The reactive part is named as Fryze's reactive power. According to Emanuel, no directional flow can be defined for Q_f, thus the value of it is unsigned. [16]

$$S = \sqrt{P^2 + Q_f^2} \tag{2.13}$$

Fryze's reactive power is congruent with nonactive power and fictitious power mentioned in standard IEEE Std 1459 [30]. In the measurements of the thesis, P and Q_f also involve the power of interharmonics enabled by the design of the meter. The harmonics and interharmonics normally represent an extremely minor part in P, which is stated in the analysis of the thesis and by De La Rosa [8]. Fryze's reactive power is studied utilizing the measurements in real environment of the pilot building including conventional and modern loads and solar power plant. One of the possible downsides of Fryze's theory is that nonactive powers are included overall in the term Q_f, thus no distinction can be made between fundamental frequency reactive power and distortion power. Nevertheless, Q_f may be used to monitor the values of Q_1 and distortion together both of them being unwanted at the customer's devices in the LV distribution networks. Also Q_1 is available in the measurements and included in the studies later in this thesis, hence it is possible to compare Q_f and Q_1, and for instance, address the difference and the need for fundamental frequency reactive power compensation.

The analysis in the thesis also uses a power factor to describe the electrical behaviour of the pilot building. Next, the concept of power factor is presented as the ratio of active and apparent power from the viewpoints of fundamental frequency and distortion. Also other definitions of power factors are found in the literature, e.g. named as true power factor and total power factor, which equal to PF and the product of PF and DPF respectively [8]. However, the definitions shown here are the most common and easily understandable [1, 8, 30]. The factors of power in IEEE Std 1459 are called as displacement power factor (DPF) and power factor (PF), which are calculated with the following formulas in the standards and also in the measurements of the thesis.

$$DPF = \cos(\theta_1) = \frac{P_1}{S_1}\ [p.u.] \tag{2.14}$$

$$PF = \frac{P}{S}\ [p.u.] \tag{2.15}$$

The phase difference between the fundamental frequency voltage and current is denoted with θ_1. It is stated that, in addition to phase difference, DPF can be calculated as the ratio of fundamental frequency active and apparent power, which can also be expressed as fundamental power factor [30]. In PF, the overall distortion in the system is considered because P and S are utilized. Values of DPF and PF can help to evaluate the concentration of fundamental frequency reactive and overall nonactive power of a electrical system, and furthermore, show the effectiveness of compensation and filtering [30]. The values of the factors are displayed between 0 and 1 in the thesis, thus capacitive or inductive nature of DPF needs to be observed from the measurement of Q_1. The reactive nature of PF is unknown, as is for Q_f, because the total of reactive distortion components is hardly defined.

As a conclusion, the physical meanings of different power quantities depend significantly on the fact that are the quantities related to the fundamental frequency of the electrical system and are the quantities reactive. Fundamental frequency active power (P_1) carries the net energy to the customers. In addition to P_1, fundamental frequency reactive power (Q_1) interacts with the electromagnetic field of the fundamental frequency, though Q_1 transfers no net energy because of the oscillation between reactive components in the network. Active distortion power integrates as a net energy for the load but distortion is very local in the vicinity of the voltage source of the electrical network and the load. Additionally, active distortion power has no contribution to torque of electric motor. Reactive distortion power solely causes losses in the vicinity of their source without transferring net energy. At the moment, the billing of electrical energy and power in distribution networks is based on active and fundamental frequency reactive power. [10, 16, 30, 57]

2.4.2 Measuring

Power theories have been developed over the past 100 years and the basics of electrical energy are nowadays well understood. Still various candidates of power theories exist to measure and evaluate energy billing, the quality of the electric energy and the source of distortion in the system. Especially it is considered how the electricity meters behave in the increasingly distorted conditions of the distribution networks, and which power theory handles the measurement of distortion the most feasibly [6, 20, 21]. In this section, the conventional, and even historical, measuring practices are described and compared with the current and future needs of the distribution networks.

Conventionally, the electricity is measured with kWh and kVArh meters. Before the digital age, a rotating induction-disk technology was utilized in kWh meters. Active energy and power were available from the revolutions of the disk. The error in power measurement was strongly related to the ability to measure the time of a certain amount of revolutions. Reactive power was measured using kVArh meters that frequently were the combination of kWh meter and phase-shifting transformer of 90 electrical degrees. kVArh meters

were only able to measure either lagging or leading kVArh, which was chosen during the installation of the meter. The maximum and average power over a time period, also known as demand, was previously measured with demand meters. These meters utilized the thermal characteristics of the meter to move pointer in scale, or a module was added on kWh meter to record impulses. Overall, it can be said that traditional electricity meters have indeed been electromechanical devices regarding their properties. [29]

The type of modern electricity meters is defined as solid-state or static because the meters include no moving parts and embrace electronics advances. One meter can measure active and reactive energy, various power quantities, voltage and current, to mention a few, of the measurement point. The electronics of the meter can compute any defined quantities using the programmed mathematical methods. Fundamentally, solid-state meters sample values of voltage and current, frequently through transducers, and observe the phase difference between voltage and current of the fundamental frequency. [29] The features of the electronic meters widen the possibilities of power measurements in the distribution networks allowing, for example, to utilize variety of power theories.

The introduction of the solid-state meters has been addressed in the literature considering the accuracy of the meters in nonsinusoidal conditions and compared to the traditional electromechanical meters. The variety of the solid-state meters designed with different principles creates uncertainty in measurements. Previously, Cataliotti [6] and Filipski [20, 21] have investigated the errors of electromechanical and static kVArh meters in distorted environments. The results showed that electromechanical and static meters measure reactive power accurately at sinusoidal conditions but increase of distortion led to large errors in the readings of the electromechanical meters when compared to a reference power analyzer measurement [21]. In addition, variation was found in the measurement results of different static meters in distorted conditions [6]. Fortunately, standards have been improved, and for example, IEC 62053-21 defines accuracy test in the presence of harmonics for static active energy meters [10]. However, active power measurements are under less concern because active distortion power represents only minor part of active power [8].

Paper [6] emphasizes that meter manufacturers should specify in detail the principles of their meter, and even better, if the meters are implemented using similar principles. The nonsinusoidal conditions remain unclear for meter designers because no exact power theory has been selected, thus it is recommended to measure fundamental frequency reactive power separately from distortion power [6, 18]. Paper [21] promotes definitions of only relevant and physically meaningful quantities of power. Ultimately, the static meters are capable of metering accurately and correctly, if designed well. It is fortunate that standards including 62052-11, 62053-21 and 62053-23 are being developed currently [9, 10, 11].

2.5 Consequences of adverse power quality and inaccurate power measurements

At worst, poor power quality results in a blackout or a broken device of the customer, and thus interrupts the normal operation and causes financial losses for the distribution network customer and DSO. Additional costs may also be billed due to inaccurate measurement of energy or power. Furthermore, distorted voltage and current and inadequate metering yield false values in the monitoring of an electrical energy system. The consequences of adverse power quality are well known, however occasionally incidents are hardly related to power quality due to its indirect nature. The false measurements of power and energy are difficult to reveal without comparison to a reference meter at the same point. Consequently, power quality and measurement issues can frequently be left unnoticed without a noticeable exception in the behaviour of a consumer device or electrical network. Especially the issues caused by voltage and current distortion are discussed here.

Most commonly mentioned consequences of voltage and current distortion in the distribution networks involve issues regarding the electrical network components and customer devices. In the network components, power losses are increased in transformers, capacitor banks and conductors because distortion increases the rms value of current and elevates dielectric losses. Eventually, the operating life of the transformer and capacitor bank is reduced. In case of the conductors, particularly neutral wire can experience overloading, and further overheating, if distortion current of three-phase system is accumulated in the neutral wire. This results from the odd order and divisible by three harmonics of the three-phases that sum at the same phase to the neutral wire. Distortion also creates the threat of resonant conditions in the electrical network. The resonances between inductive and capacitive components, e.g. conductor inductance and capacitor bank, can lead to series or parallel resonance that causes dangerous magnitude of current or voltage. The resonances occur at harmonic frequencies above the fundamental frequency, thus the resonant currents and voltages are harmonic. [1, 8]

At the customer side, voltage distortion can produce abnormal behaviour of electronics, for instance, flickering of electronic ballast fluorescent and LED (light-emitting diode) lamps and issues in the systems that utilize zero-crossing detection. It has been also observed that solar power plant can introduce flickering by generating interharmonics below the fundamental frequency [49]. In case of electric motors, distortion may induce unwanted torques that e.g. increase vibration resulting in wearing of bearings. In general, distorted conditions increase power losses and cause various abnormalities in the operation of the consumer devices. [1, 8]

As it was stated, the inaccuracy of power and energy measurements can lead to unintentional costs for the customer. The issues of the power meters in distorted conditions have been discussed profoundly in articles of Filipski and Cataliotti but no generalized answer has been found according to standard IEEE Std 1459 [6, 21, 30]. In an unfortunate case, the electrical energy meter can record overly high energy value for the customer and finally the

incorrect energy reading is transferred to the billing system. In other cases, the performance of the distribution network can be falsely evaluated or the control of the electrical energy system reacts undesirably due to inaccurate readings. [29]

Solutions are available to avoid the listed consequences of poor power quality and inaccurate power measurements. Harmonic assessment should be performed in the distribution networks to monitor the voltage and current distortion conditions of the network, and if required, harmonics can be filtered with passive and active applications. Power quality issues can also be prevented by confirming the compatibility between the device and the electrical network. A well implemented device operates normally in the conditions that remain within the voltage distortion limits of standard [60]. In addition, the device should comply with distortion current emission regulations [12]. In case of power measurements, unified power theory and design principles are promoted [6, 21].

3. PILOT BUILDING

Kampusareena, an eight-storey modern multi-user office building at Tampere University of Technology (TUT), served as a pilot environment in this thesis and ultimately in the project titled Prosumer Centric Energy Ecosystem (ProCem) [55]. The project and its participants enabled the designing and implementation of an extensive measurement and data collection system at Kampusareena, and further, the building was utilized as a research platform for measurements and smart building demonstrations. This chapter describes the pilot environment and the implemented ICT system and its data sources.

This thesis focuses on power and power quality measurements provided by the implemented system monitoring the electrical energy system of Kampusareena. In the project, nine advanced kWh meters were installed in the building, and in addition data was collected from various other sources available in the building. Data sources accessible through Application Programming Interfaces (API) over Internet were also integrated in the monitoring system as external data sources. Overall, the pilot brought together commonly poorly utilized data and used it in several applications. The data sources in general delivered information about the electrical energy system, solar photovoltaic (PV) power plant, building automation, weather, hourly electricity price and the national grid status. The applications, besides the studies in this thesis, involved IoT-platform visualizations, blockchain (BC) demonstration of energy usage accounting and electric car charging and discharging demonstration with mobile battery storage. Moreover, the data was made open for the collaborators in the project and for the future projects and research.

Prosumer Centric Energy Ecosystem - Social Energy -project (ProCem), the founder of the pilot, completed also other studies aiming to investigate the role of prosumer and how various kind of distributed energy resources could be integrated to the electrical energy system [55]. The aspects of the project included political, regulatory and business case studies with technical considerations. Microgrid project of Marjamäki area had also cooperation with ProCem in terms of energy management. The investigations in the project were performed in interdisciplinary manner uniting the strengths of four laboratories of TUT: Electrical Energy Engineering, Pervasive Computing, Automation Science and Engineering and Industrial and Information Management. Additionally, the companies involved in the project collaborated in the process. The project was funded by Tekes, Finnish funding agency for technology and innovation that is currently named Business Finland, and by energy and IT industry companies that participated in the project.

3.1 Building

The pilot building, Kampusareena, that is described as a modern multi-user office building, is located at the middle of the campus at TUT in Tampere, Finland. Photograph of the building complex is presented in Figure 3.1. Kampusareena is mainly occupied by the personnel of the companies having premises at Kampusareena, in addition to researchers, students and university staff. The floor area of Kampusareena covers 16 000 m^2 on eight storeys. The building is owned by University Properties of Finland Ltd. and was completed in fall 2015. The facilities are divided between the university, companies and commercial premises in respective percentages: 60 %, 30 % and 10 %. Two restaurants, library, offices of companies and conference facilities, among others, are located at Kampusareena. In addition to 300 people working at offices, thousands of people visit the premises weekly. [34]

Kampusareena has achieved overall Class B energy rating and 'Very Good' rating from Building Research Establishment's Environmental Assessment Method (BREEAM), which represents environmental rating for the building and addresses issues including energy, water and internal environment. The building is kept warm with district heating but cooling is implemented with free cooling system comprising two cooling units with several compressors. Hence, the heating is in a minor role contrary to the cooling from the viewpoint of the electrical energy system.

Figure 3.1. *Photograph of Kampusareena on 10th of July 2018.*

The building consists of base and high-rise part on top of each other as seen in Fig. 3.1. The panels of solar PV power plant are installed on the darker coloured walls. The library and restaurants are located at the base part and the high-rise premises are reserved for companies.

3.2 Electrical energy system

The topology of the main electricity distribution in the building is distinctly partitioned giving a possibility to monitor separately different types of loads, solar power plant and their sum. The loads of the building are topically interesting, e.g. modern elevators, and solar power plant represents distributed generation providing energy for the building. Thus, the studies in the thesis considering power flows and power quality are taking an advantage of the pilot environment. The pilot specific electrical energy system also sets limitations for the studies due to the type, size and interconnection of the loads and solar power plant. In general, the electrical energy system comprises the behaviour of an office building, and thus differentiates from private apartments and industrial facilities. Nevertheless, in the pilot the behaviour of the loads and solar power plant is also measured separately, which allows studies of individual appliances. The measurements of the electrical energy system of the pilot building are the foundation of the data analysis in the thesis.

The thesis considers the electrical energy system of Kampusareena electrically in three levels: the 20 kV access point, the main distribution boards and the loads and the power generation. The electrical energy system operates in a traditional manner using radial structure. Even though Kampusareena has distributed generation, it is unqualified for the definition of microgrid. JWG C6.22 of CIGRE has summarized the various definitions of microgrid in their publication [43]. For brevity, the building is unable to form an island network because of inadequate power generation and energy storage. However, the electrical energy system of the building contains controllable loads, large cooling units and own power generation, and consequently embraces similar features, for instance, as the microgrid area of Marjamäki in LEMENE-project [39].

3.2.1 Electrical network

The building has its own access point to medium voltage (MV) distribution network at TUT. The MV network is operated radially but backup connection is available from the ring network around TUT. In the distribution substation of the building 20 kV medium voltage is transformed to 400 V level for the electrical network of the building. The distribution substation contains two 1000 kVA transformers that supply two main distribution boards, which further distribute electricity for the loads. The main electricity distribution of the building is drawn in Figure 3.2 as handled in the thesis. Both the MV network and the LV network of the building utilize three-phase topology.

In this thesis, the two main distribution boards are called service electricity and tenants' electricity. Service and tenant side of the main distribution have distinct tasks as service side provides electricity to maintain the functionality and conditions of the building and tenant side feeds the appliances of the tenants. Also lighting is included in tenants' electricity. The loads of service electricity are well-known and clearly separated in contrast to tenants' electricity, which has countless smaller loads mixed in groups.

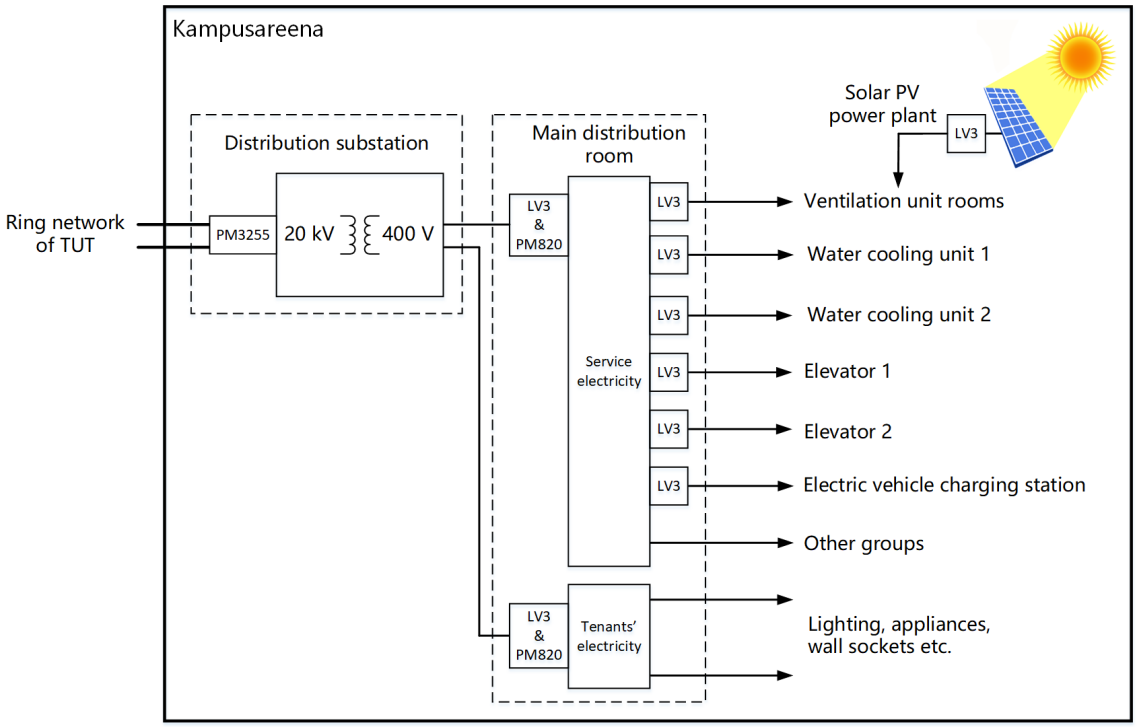

Figure 3.2. *Main electricity distribution system of Kampusareena.*

In Fig. 3.2, measurement devices called Laatuvahti 3 and Schneider PM820 and PM3255 are denoted at the measurement locations. The figure shows the locations of the measurement devices and identifies the loads utilized in the studies of the thesis. Additionally, Fig. 3.2 points out that solar power plant is supplying ventilation units in parallel with the main distribution board.

The voltage stiffness of the electrical network in Kampusareena was evaluated with Fluke 1653B installation tester at the main distribution boards and at the top floor where the inverters of solar power plant are found. The resolution of the tester was exceeded at every measurement point the tester simply displaying short-circuit current of > 10 kA, which indicates a very strong electrical network. The stiffness is the consequence of the two large transformers separately supplying the two main distribution boards via conductor rails. The cable rising to the top floor was also observed to have a substantial diameter. The stiffness of the electrical network reduces voltage fluctuations and voltage distortion caused by the loads and solar power plant. The analyses of the thesis concentrate on current measurements rather than voltage because of the stiffness of the system.

3.2.2 Loads

Power consumed by the building is divided among the loads connected to the electrical network. The amount of appliances is large and only few of them are considered separately in the pilot and in the thesis. As a financial and technical compromise service electricity was chosen to be monitored as marked with the measurement points in Fig. 3.2. Also the sum quantities of the loads were measured at the main distribution boards and at the access

point to the distribution network. The daily electrical behaviour of each measurement point is depicted in Chapter 4. The following list gathers the individually measured loads:

- Ventilation units
- Water cooling unit 1
- Water cooling unit 2
- Elevator 1
- Elevator 2
- Electric vehicle charging station
- Tenants.

The listed loads can be examined separately but many loads, e.g. lighting and appliances of the restaurants, are aggregated at the main distribution board of tenants' electricity. Therefore, one can only estimate the effects of the tenants' loads on the electrical energy system. On the other hand, the main distribution board of service electricity is almost completely monitored because of the installed meters in the pilot. The loads of service electricity are a blend of conventional directly coupled electric motors of the cooling and power converter driven ventilation units, elevators and electric vehicle charging.

Ventilation units, in brief ventilation, regulates the indoor air quality of the building. Nine exhaust and 13 supply air systems of ventilation are scattered around the building, and presumably the majority of the loads are frequency converters driving the fans of the ventilation systems. The measurement at the main distribution board contains all the ventilation units. Ventilation as a whole is one of the largest loads in the building peaking at 80 kW. Building automation controls ventilation, hence the measurements present an active power pattern repeating daily according to required ventilation. Interestingly, one of the ventilation unit rooms is supplied by solar power plant, in addition to the main distribution board, and occasionally the power production of solar power plant exceeds the power consumption of all the ventilation unit rooms.

Water cooling units chill the coolant that is used to cool the building. The coolant mostly flows in the panels at the ceilings of the rooms but also convectors are used. The cooling units utilize free cooling taking advantage of the cool outside air, if possible. Cooling unit 1 contains four compressors, which are run separately introducing steps in power flows. Cooling unit 2 uses six compressors in the same manner. The control of the cooling is based on following certain set points for the coolant temperatures. The rated electrical power is 170 kW for cooling unit 1 and 226 kW for cooling unit 2, and they are manufactured by Chiller Oy. The electric supplies of the cooling units are measured individually at the main distribution board of service electricity.

Elevators include two passenger elevators that are in public use and rise from the bottom floor to eight floor at the high-rise part. Also a third freight elevator is found in the building

lifting goods for the restaurants and other building users within the base part. Only the passenger elevators, elevators 1 and 2, are included in the measurements of the pilot. The weight limit of the passenger elevators is 900 kg and the maximum number of persons is 12. The elevators are manufactured by Kone and are installed without machine room and driven by three-phase power converters. The measured elevators are summoned with a single panel of buttons, thus the elevators synchronize the lifting among themselves.

Electric vehicle charging station consists of five charging parking spots at the front yard of Kampusareena. The fuses are rated at 32 A for each charging spot and the charging requires from the car owner a cable that is compatible with Schuko socket. One of the spots additionally supports three-phase charging with a plug complying to IEC 62196-2. The parking is paid with a mobile application. The electric cars are charged almost daily according to the browsing of the measurement data, and generally one car loads the electrical energy system with active power of 4–8 kW per phase. Nowadays, vehicle-to-grid (V2G) is still rarely supported by electric cars and charging stations, which is the case also at Kampusareena. However, the pilot inspired a V2G demo that was in progress during the writing of the thesis.

Tenants' electricity is the most difficult load to analyze in the building because of the complex composition of the loads. At the early stage of the pilot decision was made to measure only the mains of tenants' electricity, i.e. the mains of the second distribution board. Various types of loads are coupled in the groups of tenants' electricity resulting in impracticable measurements, if the behaviour of the loads is desired to be observed separately. The loads of tenants' electricity include lighting, wall sockets and overall the appliances of the tenants in the building. Electrically the most significant loads could be ovens, dish washing machines and cold storage rooms of the restaurants. The lighting may also represent a remarkable load as a whole. Fluorescent lamps are used for the lighting, although the development of lighting suggests that fluorescent lamps will be converted to LED lamps in the near future.

Other groups of service electricity that are outside of monitoring but denoted in Fig. 3.2 include the freight elevator and a few smaller distribution boards, which have minor impact on active power of the electrical energy system. In addition, no reactive power compensation circuits are installed at the main distribution boards of service electricity and tenants' electricity.

3.2.3 Power generation

Distributed generation is installed in a form of solar photovoltaic (PV) power plant in the building. The solar panels of the power plant can be seen on the darker walls of the building in Fig. 3.3. The panels are directed towards west, south-east and south-west due to the angles of the walls. The west wall is located at the left-hand side of Fig 3.3. In addition to power generation, the solar panels act as sunshades for the premises of the building.

Figure 3.3. *Photograph of Kampusareena showing solar panels on the darker walls facing west, south-east and south-west.*

Solar power plant uses four solar inverters to feed power to one of the ventilation unit rooms located at the top of the building. The nominal powers of the inverters are: 8 kW, 15 kW and 2 × 17 kW equaling to total nominal power of 57 kW. Peak power of the solar panels is 81 kW generated by 561 solar panels. The inverters are connected to the panels at different walls roughly as follows: 8 kW for west, 2 × 17 kW for south-east and 15 kW for south-west. The inverters are manufactured by SMA Solar Technology AG. Solar power plant is incapable of forming an island network, and thus solar power plant is disconnected from the LV network in case of blackout.

3.3 ICT system

The pilot of Kampusareena, and the thesis work, involved design and implementation of the ICT system. It was required to collect data from several data sources and store it in unified and accessible manner. Due to designed monitoring and control features communication between the parts of the ICT system was essential. Eventually, the data and ICT system was made available for users to develop applications and perform data analysis. The architecture of the ICT system is presented in Figure 3.4 illustrating the data and information flows. The advantages of the ICT system can be noted as gathering comprehensively the available data of the building into a single place and dividing the system into real-time and user-time, that is long-term and application based, domains.

The architecture in Fig. 3.4 generally comprises two virtual platforms of Linux and IoT (Internet of Things) implementations. The Linux platform operates in real-time within the limitations of the implementation gathering data from sources, storing the data in local database and making instantaneous control decisions. The data is collected from various sources including the electrical energy system of the building, building automation

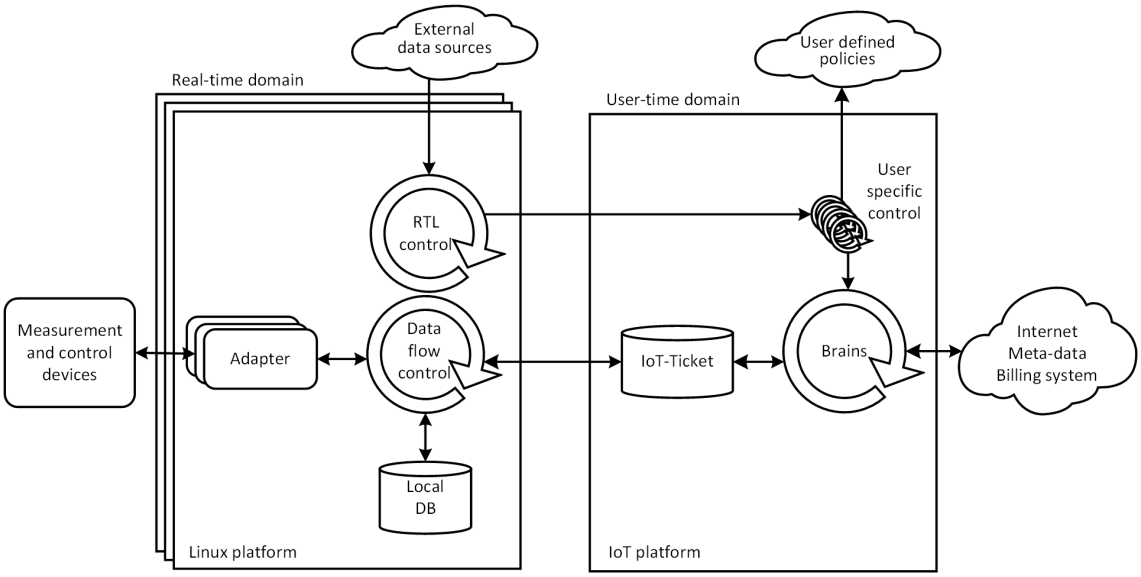

***Figure 3.4**. Architecture of ICT system designed in ProCem project.*

and weather data. IoT platform focuses on visualization of the data and applications that consider more complex and long-term management of the building. The feedback loop from the IoT platform to the Linux platform was not implemented by the time of writing of this thesis but should be developed in the upcoming projects.

This thesis utilizes the collected data of the electrical energy system in the analysis, hence this chapter focuses on the electrical measurements of the ICT system. Explanation of the architecture in Fig. 3.4 is provided in the following sections considering the data sources, data collection and the usage of the data. However, technical details of the ICT system are excluded because they are not in the scope of the thesis. More profound description of the ICT system can be read from the thesis of Heikkilä [25] that is in progress, and from the website of ProCem [55].

3.3.1 Data sources

Data sources of the building are listed in Table 3.1, in which the sources and communication methods are described in general. The data sources include on-site measurements from the building and information gathered over the public Internet. This section specifies each of the data sources and emphasizes the sources utilized in the thesis.

Building automation monitors and controls the variables of indoor conditions including temperature, CO_2 concentration and presence of people. Overall, the building automation manages the ventilation, heating and cooling of the building, and for instance, provides data about the frequency control set points of the inverters of the fans and the measurements of the air flows of individual spaces. The ICT system collects the values of 2883 variables from the building automation and receives a new value once the previous value has changed

Table 3.1. *Data sources of the ICT system in the pilot of Kampusareena.*

Data source	Data provider	Connection	Communication protocol
Building automation	Desigo (Siemens)	BACnet	UDP
Power quality	Laatuvahti (Electrix)	Ethernet	TCP
Power consumption	Measurement hub (ISS Palvelut)	Ethernet	Modbus TCP/IP
Solar power plant	Solar inverters (SMA)	Ethernet	Modbus TCP/IP
Weather station	TUT weather station (Vaisala etc.)	Internet	SQL database
Energy storage	Battery pack built by TUT	CAN/Ethernet	Modbus TCP/IP
Weather forecast	HIRLAM (FMI)	Internet	REST
Electricity spot price	Nord Pool	Internet	REST
National grid status	Fingrid	Internet	REST

enough. Consequently, the number of values for a variable per day varies between 1 and 100 000. The data of the building automation was left out of this thesis but utilized in other applications, e.g. IoT platform visualizations, that are presented briefly in section 3.3.3.

Power quality of the electrical energy system of the building was monitored with a measurement device called Laatuvahti 3 (LV3). The device is manufactured by MX Electrix Oy and was under development during the pilot. The device is designed for monitoring of power quality in the distribution networks embracing large amount of power and power quality quantities, in addition to energy measurements, alerts, fault recording and nonintrusive appliance load monitoring (NIALM). Power quality quantities include e.g. voltage and current harmonics and rapid voltage changes (RVC). Voltage, current and power are quantified by means of fundamental frequency, individual harmonics, and distortion over whole measurement bandwidth of 2 kHz including harmonics and interharmonics. Frequency measurement is specified in collaboration with Finnish transmission system operator Fingrid Oyj. The device follows the guidelines of the distribution network and power quality standards SFS-EN 50160 and IEC 61000-4-30 [13, 60]. The validity of the measurements was confirmed with Real Time Digital Power System Simulator (RTDS) and Dranetz PX5 power quality analyzer at TUT. Figure 3.5 shows Laatuvahti 3 installed in one of the measurements locations.

In the pilot, Laatuvahti 3 measures voltage from terminal blocks and senses current with current transformers from three phases at nine locations in the building, that are marked in Fig. 3.2. Normally measurements are recorded as 1 minute averages but for the pilot time resolution was increased to 1 second averages, and even 100 millisecond time period was tested. Measurement data is saved at the memory of the device and is also sent as a stream using Ethernet to the ICT system of the pilot enabling constant monitoring of the electrical energy system.

Figure 3.5. *Laatuvahti 3 installed at the main distribution room of Kampusareena.*

Electrical power consumption of the building was already widely measured before the pilot. Company called ISS Palvelut Oy monitors the electrical energy of the building using power meters manufactured by Schneider. These meters are recording the consumed energy of each tenant in the building, and further reporting the consumption to measurement hubs and electrical energy billing system. The installed power meters mainly consisted of the models iEM3235, PM3255 and PM820MG. Three of the most sophisticated meters were added in the data collection of the ICT system as denoted in Fig. 3.2. The pilot had no necessity to collect the data of the simpler iEM3235 meters because of the vast number and constricted capabilities of them in terms of measured quantities and data transfer. Most importantly the measurement hub of ISS provided primary measurement from the MV network side of the transformer since no other meter could be installed at the distribution substation. Also, the two utilized meters at the main distribution boards introduced references for Laatuvahti 3 meters. The measurements of Schneider meters included the basic power, current and voltage quantities with harmonic, energy and frequency readings. The measurements are updated once a second and every 30 seconds depending on the quantity but the manuals of the meters contain no explicit information about over which time interval the measurements are averaged. Anyway, the ICT system collects the measurements at 1 minute interval due to delay in the measurement hub. Especially the measurements of the meter at the MV network connection point were utilized in this thesis.

Solar power plant was monitored in more detail with the data of the four inverters, thus the generated power could be divided between the individual inverters and walls during a day. Solar power plant is explained further in Section 3.2.3 presenting the solar panels in Fig. 3.3. The inverters offered the values of voltages, currents and powers for DC and AC side, in addition to yield energy, frequency and condition of the inverter. The ICT system was able to receive new values from the inverters at 1 second interval. It is presumed that the values are time averages of 1 second.

Weather station enabled the monitoring of local weather conditions accurately and instantaneously. The weather station is located on the rooftop of laboratory of electrical energy engineering 100 meters away from Kampusareena. Measurements include temperature, air humidity, wind speed and direction and irrandiance of Sun with aspects of global, direct and diffuse radiation. The measurements are gathered at 1 second interval by the ICT system, although the weather station uses time resolution of 100 milliseconds. Instruments are manufactured by Vaisala and Kipp & Zonen. The data of the weather station will be utilized in the future studies, for instance, with the data of the electrical energy system and building automation.

Energy storage is a part of electric car charging demonstration in progress. The demonstration aims to economically charge the energy storage, the electric car, based on defined boundary conditions. Other planned use cases utilize V2G feature for peak power cutting and frequency reserve markets. The ICT system communicates with the energy storage by reading the state of the energy storage and by giving commands to charge and discharge according to optimization algorithm that receives input from the different data sources of the building, e.g., solar power plant. The demonstration is further discussed in the upcoming publications of TUT.

Weather forecast for the area of Kampusareena is downloaded from High Resolution Limited Area Model (HIRLAM) of Finnish Meteorological Institute (FMI). The forecast comprises, for example, temperature, air humidity, wind speed and direction, cloudiness and irradiance of Sun. The forecast is computed and downloaded at six hour intervals for the next 54 hours. Time resolution of the forecast is ten minutes at the databases of the ICT system.

The hourly electricity market spot price for Finland was collected from the website of Nord Pool. More specifically, the market is called Elspot Day-ahead, which determines the price of electricity individually for several countries including Finland. Additionally, electricity markets of different kinds are found in the website of Nord Pool. The prices are collected daily after the prices of the next day are published at 14:00 summer time latest.

The status of the national grid of Finland was gathered from the open database of Fingrid Oyj, Finland's transmission system operator. The database includes the real-time state of frequency, power production of various forms, e.g. nuclear and hydro, and the total production and consumption of Finland. Additionally, the hourly forecasts of total consumption and production of solar and wind power for the next 24 hours were downloaded. The real-time information is updated and downloaded every 3 minutes and the forecast once a hour.

The data sources of power quality, Laatuvahti 3, and power consumption, Schneider meters, are utilized in the analysis chapters 4 and 5 of the thesis. However, the other data sources were briefly introduced since the designing of the pilot environment and the ICT system were a part of the thesis work.

3.3.2 Data collection

The various sources of data required a component in the ICT system that particularly handles the data gathering. The data sources communicated with different protocols and the form of the data alternated. Also, the amount and confidentiality of the data needed management. These actions were performed by the Linux platform, in addition to storing the data in the local database and sending the data to the IoT platform. The number of different data variables per source, their update intervals at the data collection and the number of data points per day are listed in Table 3.2. The table exemplifies well the data flows in the pilot [25]. The external data sources are presented as one group in the table due to their minor numbers.

Table 3.2. *The number of variables, update interval, daily data values in Linux platform and daily data values in IoT platform for each data source on 14th of August 2018.*

Data source	Variables	Update interval	Daily values Linux platform	Daily values IoT platform
Building automation	2883	<1 s – 1 d	5 572 145	5 392 606
Power quality	1611	1 s	139 213 164	29 553 624
Power consumption	183	30 s	527 146	368 722
Solar power plant	149	1 s	12 183 637	8 986 430
Weather station	15	1 s	1 296 208	518 485
External data sources	37	3 min – 1 h	45 366	45 366
Overall	4878	<1 s – 1 d	158 837 666 (1 838 per second)	44 865 233 (519 per second)

Building automation contains the largest number of different variables but power quality measurements cause majority of the data flow in the ICT system. The values of building automation are updated when the values change in contrast to power quality measurements, which send the measurements every second. Also, the inverters of solar power plant are read at 1 second interval leading to the second highest amount of values for the day. It should be noted that the ICT system uses no time synchronization for the measurements, thus none of the measurements are measured exactly at the same time. This a noteworthy target for development in the future. The number of data points was reduced for the IoT platform because of the discarding the confidential information of tenants and variables irrelevant for applications and visualization. It was tested that the IoT platform would also suffer from severe delays, if all the data would be transferred there. Considering Table 3.2, the electrical energy system of the pilot building is monitored with a large amount of measurements.

3.3.3 Analysis, visualization and applications

The pilot and its ICT system enabled the analysis performed in this thesis and in several other applications and visualizations. The data analysis was mostly performed utilizing the data downloaded from the Linux platform because it stored every data variable. The

applications operating in real-time also extracted the data from the Linux platform. The IoT platform was mainly used for visualization of the data. MATLAB software of Mathworks was primarily used in the analyses and visualizations of this thesis.

Apart from the data analysis of the thesis, electrical energy accounting demonstration utilizing Ethereum blockchain technology was built to experiment the usefulness of blockchain in energy systems. In addition, an electric car charging demonstration is planned to study the optimization of charging and V2G feature. On the IoT platform, user-friendly dashboards were designed to deliver information of the refined data for the users of the building. Furthermore, the pilot of Kampusareena will be utilized in the next projects and collaborations. The public report of ProCem project ultimately describes the applications and analyses of the pilot [55].

The IoT platform, named IoT-Ticket, allowed a straightforward way to visualize the data of the pilot without further expertise on programming. As a branch of ProCem project, the author of this thesis constructed dashboards presented in Figures 3.6, 3.7 and 3.8 to visualize the data of the building in an intelligible manner. The dashboards depict the environmental impact, economic savings and indoor air quality of the pilot building and are updated as new data arrives from the data sources. The dashboards can be described as showcases of the data giving easily understandable information for the building users.

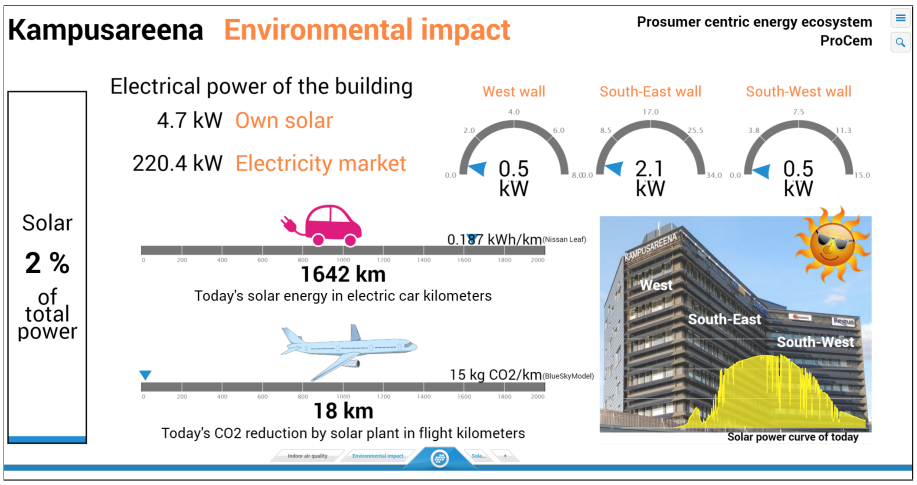

Figure 3.6. *IoT-Ticket dashboard of environmental impact of solar power plant in Kampusareena. Additionally, produced solar power is compared with power flowing from MV distribution network, and solar power produced by the panels on the three walls facing west, south-east and south-west is presented.*

The dashboard of Fig. 3.6 presents the kilometers that could be driven with an average energy consumption of Nissan Leaf electric car using the energy generated by solar power plant. Also the reduction in CO_2 emissions due to solar power plant is derived in terms of an average passenger plane kilometers. The dashboard shows the percentage of solar power of active power of the whole building. At the highest the percentage of solar power may rise to around 30 %. Lastly, the dashboard shows the solar power produced by the panels at each wall and what is the solar power curve of today.

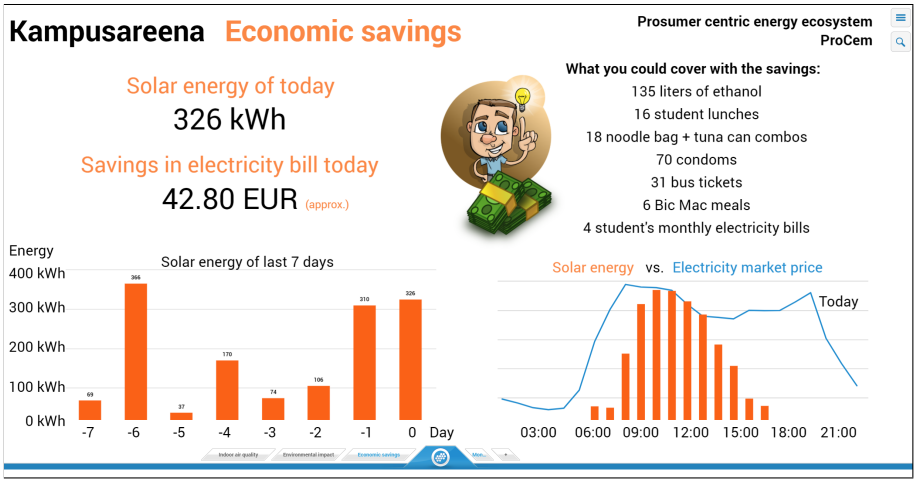

Figure 3.7. *IoT-Ticket dashboard of economic savings achieved with solar power plant at Kampusareena. A rough approximation of the savings is presented in euros and in goods one can buy. In addition, generated solar energy of the last seven days and the solar energy of the current day compared with the electricity market price is depicted.*

Economic aspects of solar power are speculated in Fig. 3.7. The dashboard shows today's solar energy and euros saved with the generated energy, in addition to various things you can buy with the savings. The value in euros is based on a rough approximation of the electricity price, electricity transfer price and taxes. Furthermore, the dashboard illustrates the solar energy of the last seven days and comparison between the solar energy of the current day and the hourly electricity market price. Evidently the highest solar power generation matches well with the fluctuation of the electricity price.

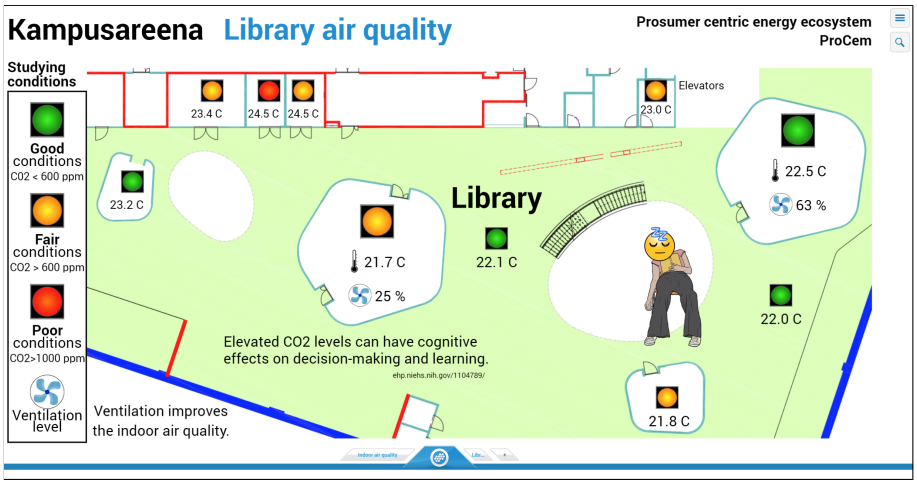

Figure 3.8. *IoT-Ticket dashboard of indoor air quality in the library of Kampusareena.*

The third dashboard, Fig. 3.8, utilizes the data of the building automation offering information about studying conditions in the library of Kampusareena. The different colors indicate CO_2 level in particles per million (ppm) for the premises. At certain concentration of CO_2 the effectiveness of studying may be affected. The dashboard also shows temperatures and the magnitude of the ventilation in some rooms.

Several other dashboards were also designed intended for general data browsing and monitoring of the building, however they are only mentioned here. One of the dashboards uses a version of Fig. 3.2 as the background while monitoring the electrical energy system of the building. The presented three dashboards will be displayed publicly as live versions in Kampusareena.

4. ELECTRICAL BEHAVIOUR OF BUILDING

Before further studies in the analysis chapter, a basic knowledge is provided considering the behaviour of the electrical energy system of the building. The behaviour of each measurement point of Fig. 3.2 is depicted in time-domain in terms of power, current and voltage for a day. The measurement points include the MV distribution network side of the transformer, the mains of service and tenants' electricity, ventilation, two cooling units, two elevators, EV charging station and solar power plant. The behaviour is illustrated in Figures 4.1– 4.17, in which the power and power quality quantities can be observed for the individual loads and their summation at the main distribution boards, and finally, for the aggregation of the whole building at the connection point to the 20 kV network. In case of certain measurements, a closer look of shorter time period is presented. The important findings from the measurements in general and from the figures are explained in each section and the results are summarized in the analyses of Chapter 5 in terms of powers and distortion.

The behaviour of the electrical energy system varies depending on the overall conditions of the building. External conditions have seasonal, daily and hourly variation. Internally, the building is populated differently during week days, weekends and holidays. Summer days are hotter but the building is less crowded due to the absence of the students. The university staff also has its holidays during the summer months. In winter, autumn and spring the outside temperature is lower but more people are using the building, and thereby warming and increasing the CO_2 content of the air inside. During weekdays people are at work but weekends are quiet. Ultimately, these conditions affect the electrical energy system of the building when people are connecting more appliances to the electrical network or more cooling and ventilation is required. Also, in Finland, Sun is significantly higher in summer than in winter, which has a remarkable effect on the power produced by a solar power plant.

In this behaviour study, the correlations between the prevailing outside and inside conditions and the electrical energy system of the building are neglected. However, the considerations include the impact of solar irradiance on solar power plant and the power flows affected by the power generation. In addition, the electrical behaviour of the building is defined by features of an office building, although the loads and solar power plant can be considered separately due to the positioning of the measurements. The ICT system of the pilot contains data of several months starting from 2017 but only three days are analyzed in this chapter because of presentation method of single days in time-domain. Besides, browsing of the data revealed that most of the loads behave in a very similar manner in terms of power during weekdays in the summer. Long-term data would require more sophisticated data analysis, as studied in Chapter 5, where correlations and machine learning methods are utilized with the data of three weeks.

The three days used in the behaviour figures were chosen as follows: Generally, Tuesday 3rd of July 2018 represents a reference for cloudy summer day when the influence of solar power plant on the electrical energy system is reduced. The summer day also requires cooling contrary to winter. The second day, Wednesday 25th of July 2018, was a mostly sunny summer day, and therefore solar power plant was operating at high power. The behaviour of this sunny day is presented for the measurements that were affected by solar power plant, e.g. ventilation. Finally, a third day, Tuesday 4th of July 2018, is presented for EV charging station since the day involved a few interesting occasions of electric car charging that were absent from the other studied days.

The behaviour figures consist of four parts: Powers, power factors, distortion current and voltage distortion and magnitude. The powers include full measurement bandwidth active power (P), fundamental frequency reactive power (Q_1), Fryze's full measurement bandwidth reactive power (Q_f) and full measurement bandwidth apparent power (S) for phase L1. Power factors (PF) are presented for all three phases. Distortion current is depicted comparing fundamental frequency related (TD_I) and absolute rms (I_{TD}) value of total distortion of current at L1. Voltage measurements involve full measurement bandwidth rms phase voltage of L1 (U) and fundamental frequency related total distortion of voltage (TD_U). The figure of point of connection to 20 kV network omits fundamental frequency reactive power and depicts total harmonic distortion of current (THD_I) and voltage (THD_U) instead of total distortion due to the features of different meter compared to other measurements. The fundamentals of the presented quantities in the behaviour figures are described in Chapter 2.

The measurements are presented utilizing the original data of 1 second rms from Laatuvahti 3 -meters, except for the point of connection to the 20 kV network, for which 1 second rms is collected once a minute from PM3255. The time resolution of 1 second rms introduces noise in the plotted curves but also depicts the behaviour in more detail. The effect of time averaging on powers is studied in Chapter 5. The bandwidth of the measurements is 2 kHz for Laatuvahti 3 and the manual of PM3255 only defines that 32 samples are taken per network cycle, which converts to the sampling frequency of 1600 Hz. Because of the extremely high short-circuit currents measured at the main distribution boards and solar power plant the voltage and total distortion of voltage remain fairly equal for the measurement points. In addition, fluctuations of powers and distortion current are hardly reflected to the voltage magnitude. Nevertheless, voltage distortion is the highest during working hours approximately between 6 and 18 o'clock when the load of the electrical energy system of the building is the highest.

The measurements shown in this thesis are limited to the quantities of single phase. This is due to LV network power quality standards usually giving recommendations for phase-to-neutral voltages and the consumer devices commonly being coupled between phase and neutral conductor [14, 60]. Additionally, the studying of power of one phase explicitly reveals the power flows of the phase, while a study of three-phase total power may conceal behaviour relating to an individual phase. On the other hand, three-phase appliances may

use no neutral conductor and the three-phase totals are normally used in power and energy measurements of the distribution networks. Thus, studies of line-to-line voltage distortion and calculation methods of three-phase total powers could be interesting subjects as well but for an another thesis.

4.1 Point of connection to 20 kV network

The measurement of point of connection to 20 kV network monitors the behaviour of the building from the MV side of the transformer at the access point to the MV distribution network, as is also shown in Fig. 3.2, thus the aggregation of the whole building is measured. The maximum three-phase active power of the building varies between 350 and 450 kW. The illustrated day in Fig. 4.1 is a cloudy Tuesday 3rd of July in 2018.

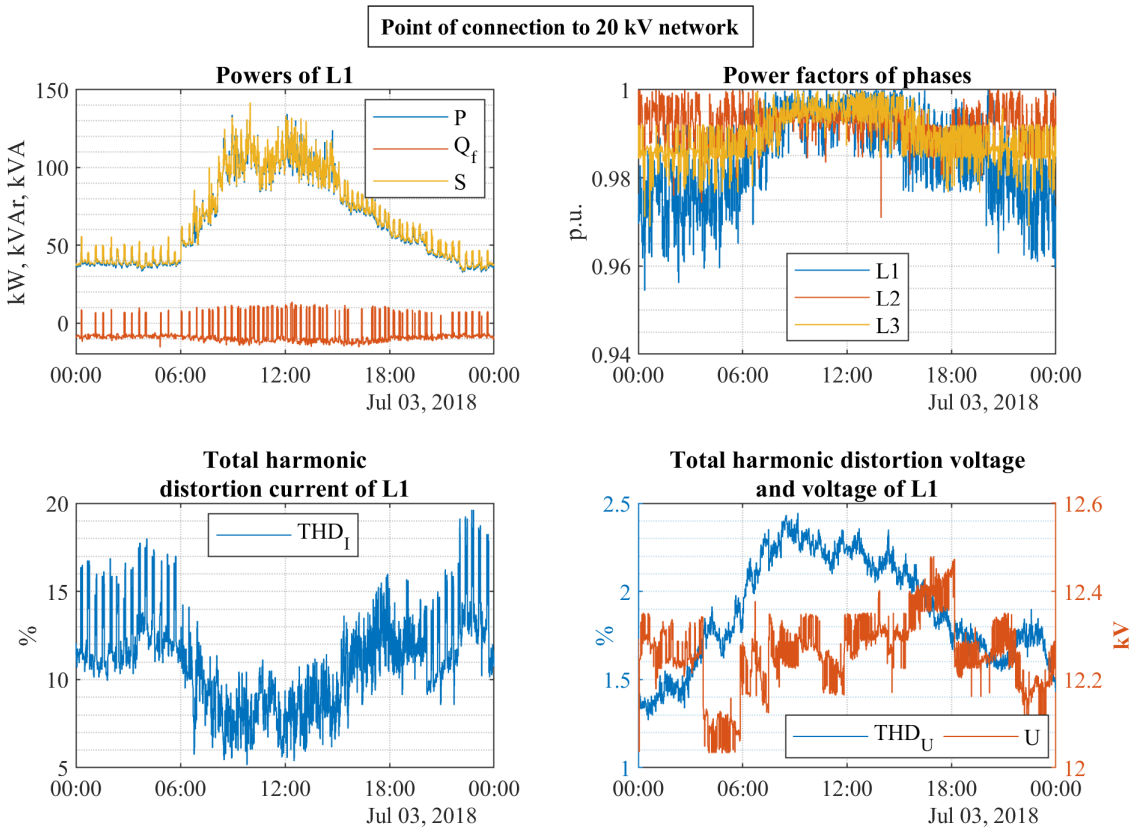

***Figure 4.1**. Overview of electrical quantities of point of connection to 20 kV network on 3rd of July 2018. Top-left: active (P), Fryze's reactive (Q_f) and apparent power (S) of L1. Top-right: Power factors (PF) of L1, L2 and L3. Bottom-left: Total harmonic distortion of current (THD_I) of L1. Bottom-right: Total harmonic distortion of voltage (THD_U) and voltage (U) of L1.*

Powers in Fig. 4.1 are visibly congruent with the measurements of the two main distribution boards, tenants' and service electricity, of Figs. 4.2 and 4.3 from the same day. The recurrent rapid changes of Q_f in Figs. 4.7 and 4.9 are caused by the cooling units because of their continuous starting and stopping. Q_f is mainly capacitive but continuously stepping to the inductive side. This is possibly due to the fact that the meter PM3255 is following

standard IEC 62053-23 that defines the sign of Q_f based on the reactivity of the fundamental frequency reactive power [11]. The maximum reactive power is slightly above 10 kVAr for inductive and capacitive reactive power.

Power factors of the phases are at the lowest in the morning and evening, when active power is the smallest but reactive power remains roughly the same. Tampereen Sähköverkko Oy, which owns the MV distribution network around the building, defines the pricing of fundamental frequency reactive power in their document [57]. According to the document, from 1st of January 2019, if Q_1 remains within -20–5 % of the reference active power used in billing, no additional cost is charged. This equals to DPF from 0.98 inductive to 0.999 capacitive. The billed reactive power is based on the two highest months of active power billing during sliding 12 months. The measurement of Fig. 4.1 indicates costs from capacitive reactive power, however the amount of distortion power in Q_f is unknown. It is strange that the MV network side measurement of the building provides only measurement of Q_f when the billing of the local DSO is utilizing Q_1, however most probably the DSO has its own electricity meter at the connection point to the MV network.

For L1 current, THD_I decreases for the working hours to around 8 % but is increased outside the working hours supposedly due to lower fundamental frequency current conditions. The operation of the cooling units also causes almost 10 % increase in THD_I at the low load conditions. For voltage, THD_U reached nearly 2.5 % during the day, however neither the voltage distortion nor the voltage magnitude correlate visibly with the powers or THD_I, and the voltage distortion is well below the limit of 8 % mentioned in SFS-EN 50160 [60]. Nevertheless, the voltage distortion rises from 1.5 % in the night to 2.5 % during the day.

4.2 Tenants' electricity

Tenants' electricity represents one of the two main distribution boards, which is mostly supplying the appliances and lighting of the tenants in the building. The tenants include, for example, the offices of companies, restaurants and library. The measurements of Fig. 4.2 depict a cloudy summer Tuesday of tenants' electricity on 3rd of July in 2018. Tenants' electricity is measured from the mains of the main distribution board as shown in Fig. 3.2. The electricity of the tenants usually constitutes majority of active power of the building as the maximum three-phase active power of tenants' electricity varies between 250 and 350 kW. The power can frequently be double or more, depending on the irradiance of Sun, to service electricity in Figs. 4.3 and 4.4.

Values of P and S overlap in Fig. 4.2 illustrating the fact that the reactive terms Q_1 and Q_f are relatively small compared to active power. The reactive powers are measured quite constant throughout the day, although some rapid variations are found around noon. The variations are presumably created by the operations of the larger appliances of the tenants, and higher activity of the building users in general disturbs the electrical energy system during the daytime. The values of reactive powers Q_1 and Q_f differ approximately 5 kVAr

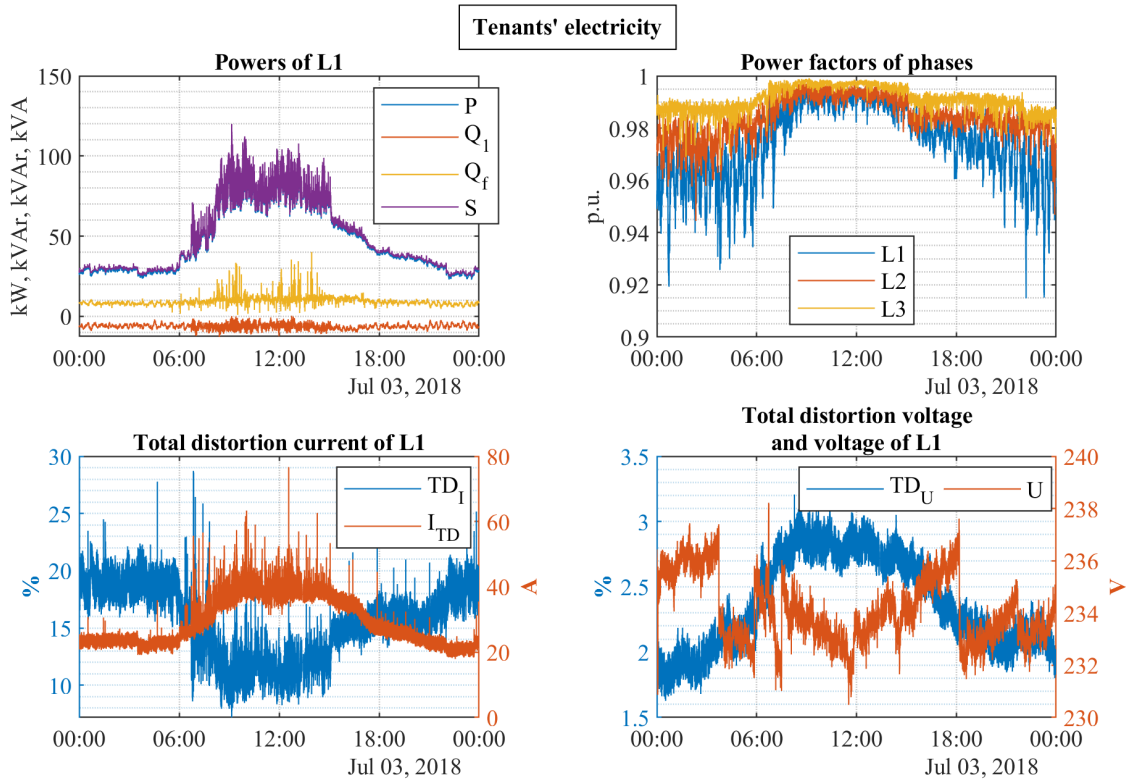

Figure 4.2. *Overview of electrical quantities of tenants' electricity on 3rd of July 2018. Top-left: active (P), fundamental frequency reactive (Q_1), Fryze's reactive (Q_f) and apparent power (S) of L1. Top-right: Power factors (PF) of L1, L2 and L3. Bottom-left: Total distortion of current (TD_I) and absolute value of distortion current (I_{TD}) of L1. Bottom-right: Total distortion of voltage (TD_U) and voltage (U) of L1.*

in average. The value of Q_1 remains capacitive the whole day. Power factors of the phases are measured to fluctuate around 0.99 p.u. during the working hours and decrease even to 0.92 p.u. outside the working hours.

Distortion current of tenants' electricity is observed using fundamental frequency related and absolute values of TD_I and I_{TD}. It is obvious that the absolute value in amperes and the value related to fundamental frequency component in percentages present inverse results: Absolute distortion current rises during the day, as can also be observed for Q_f, contrary to TD_I suggesting that the power quality conditions improve as the loading increases. Visual inspection of the distortion voltage measurement shows that the curves of current and voltage distortion are shaped similarly. Furthermore, the values of TD_U remain below the limit of 8 % in SFS-EN 50160 [60]. The magnitude of voltage supposedly has no relation to the electrical behaviour of the building due to the strength of the LV network. The stepwise variations in the voltage magnitude are likely to be caused by changes in the feeding network, e.g. tap changer operation.

The effect of various loads on the electrical quantities of tenants' electricity is left unclear because of only one measurement point and the aggregation of different types of loads. Assumptions were made that loads of the same type, e.g. lighting, and significant individual

loads, for instance, dish washing machines, ovens and cool rooms, may affect largely the electrical behaviour of the main distribution board of tenants' electricity. It is also possible that majority of the small tenants' appliances, e.g. laptops and lighting, are implemented with power factor correction (PFC), and thus the reactive power is only slightly capacitive. No capacitor banks or other compensation circuits are installed at the main distribution boards of the building.

4.3 Service electricity

The measurement point of the mains of the other main distribution board is called service electricity, which also shown in Fig. 3.2. This main distribution board supplies the rest of the loads examined in this chapter and is also interconnected to solar power plant through the ventilation feeder. Service electricity represents the main subject of this thesis as the individually measured loads are aggregated at this measurement point. The maximum three-phase active power of service electricity was usually around 150 kW during summer. Active power consumption of service electricity can be greatly affected by solar power plant in sunny days. In rare occasions during weekends, when solar power plant is operating near the nominal power of 57 kW, the active power flow of service electricity changes direction towards the transformer. In such a case service electricity is delivering energy for the tenants.

Here, two days, Tuesday 3rd of July 2018 and Wednesday 25th of July 2018, of Figs. 4.3 and 4.4 are used to illustrate the behaviour of service electricity. On 3rd of July minor effect of solar power plant, Fig. 4.16, is noticed because of cloudy weather contrary to sunny 25th of July, Fig. 4.17, when solar power plant is producing a higher power. The operation of solar power plant is especially observed in the behaviour of P and PF during midday in Fig. 4.4.

The cloudy day of Fig. 4.3 involves repetitive peaks in powers, power factors and distortion current. This a consequence of the cooling units restarting continuously over the day, which is also found later in Figs. 4.7 and 4.9 of the cooling units. In practice one of the compressors of the cooling units starts for a certain time and then stops repeatedly. The overall increase of powers and absolute distortion current during the day represents an another daily pattern of service electricity and is caused by ventilation, whose behaviour is depicted later in Fig. 4.5. Ventilation represents one of the largest loads of service electricity in addition to the cooling units. It can be noted, that besides active power, inductive Q_1 and relatively high amount of Q_f is measured, which indicates existence of distortion power at the main distribution board.

Power factors of the phases in Fig. 4.3 are observed to remain considerably low at 0.9 p.u. during the high loading, and power factors of L2 and L3 decrease near 0.8 p.u. outside the working hours. Heavier loading of L1 may hold its PF at higher values. The curve of I_{TD} seems to be directly proportional to the measurements of powers and distortion current

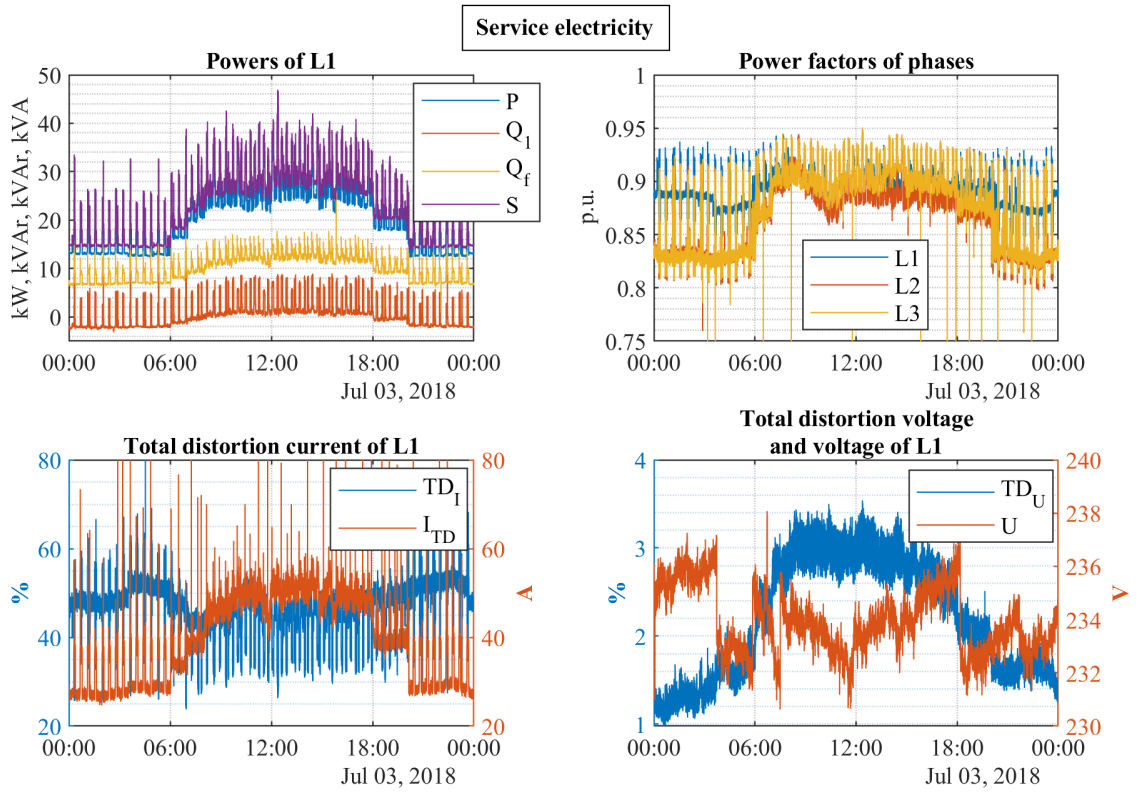

Figure 4.3. *Overview of electrical quantities of service electricity on 3rd of July 2018. Top-left: active (P), fundamental frequency reactive (Q_1), Fryze's reactive (Q_f) and apparent power (S) of L1. Top-right: Power factors (PF) of L1, L2 and L3. Bottom-left: Total distortion of current (TD_I) and absolute value of distortion current (I_{TD}) of L1. Bottom-right: Total distortion of voltage (TD_U) and voltage (U) of L1.*

can be estimated to present a large portion of the total rms current during the day. The percentage of TD_I in average varies around 50 % even at the high load conditions. Visual inspection of Fig. 4.3 also reveals a possible correlation between TD_U and I_{TD} for service electricity, which is studied further in the data analysis section 5.2.2. The level of TD_U remains well below the limit of 8 % of the standard SFS-EN 50160 [60].

Since the 25th of July embraced higher irradiance of Sun, the operation of solar power plant is observed in decrease of active power and power factors during the working hours in Fig. 4.4 of service electricity. The sunny day also requires more cooling, thus the power curves differ considerably from the cloudy of Fig. 4.3. More compressors are running simultaneously without interruption, which reduces the amount of the power peaks and elevates Q_1. The measurements of cooling unit 1 in the sunny day are presented later in Fig. 4.11.

4.4 Ventilation

Ventilation unit rooms, ventilation for brevity, is fed by the main distribution board called service electricity as shown in Fig. 3.2, which considers the main electricity distribution

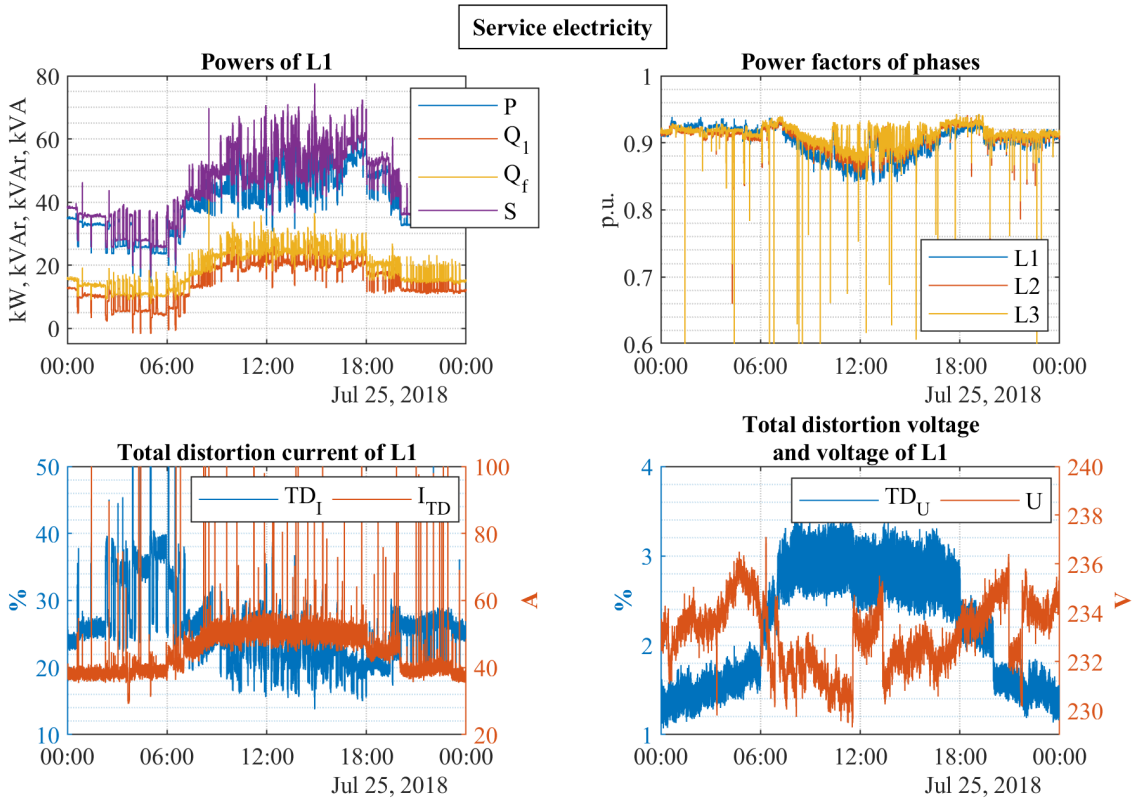

Figure 4.4. *Overview of electrical quantities of service electricity on 25th of July 2018. Top-left: active (P), fundamental frequency reactive (Q_1), Fryze's reactive (Q_f) and apparent power (S) of L1. Top-right: Power factors (PF) of L1, L2 and L3. Bottom-left: Total distortion of current (TD_I) and absolute value of distortion current (I_{TD}) of L1. Bottom-right: Total distortion of voltage (TD_U) and voltage (U) of L1.*

of the building. Ventilation maintains the air quality in appropriate condition inside the building representing one of the largest loads in service electricity and in Kampusareena. The gathered information during the pilot suggests that ventilation is mainly driven by frequency converters and other power electronics rotating the fans and other appliances of ventilation. The maximum three-phase active power of ventilation can be 100 kW or more. One of the ventilation unit rooms at the top of the building is also supplied by solar power plant.

The electrical behaviour of ventilation is presented for cloudy Tuesday 3rd of July and sunny Wednesday 25th of July in 2018 in Figs 4.5 and 4.6, respectively. If these figures are observed with Figs. 4.16 and 4.17 of solar power plant, the behaviour of ventilation can be compared with the operation of solar power plant during the corresponding days.

The operation of solar power plant is visibly observed around 12 o'clock when powers, power factors and distortion current are reduced momentarily in Fig. 4.5. Otherwise, the power consumption of ventilation is altered more or less stepwise especially in the morning and in the evening. Significant difference is measured between active and apparent power of ventilation, which is assumed to result from distortion power included in Q_f. If no reactive

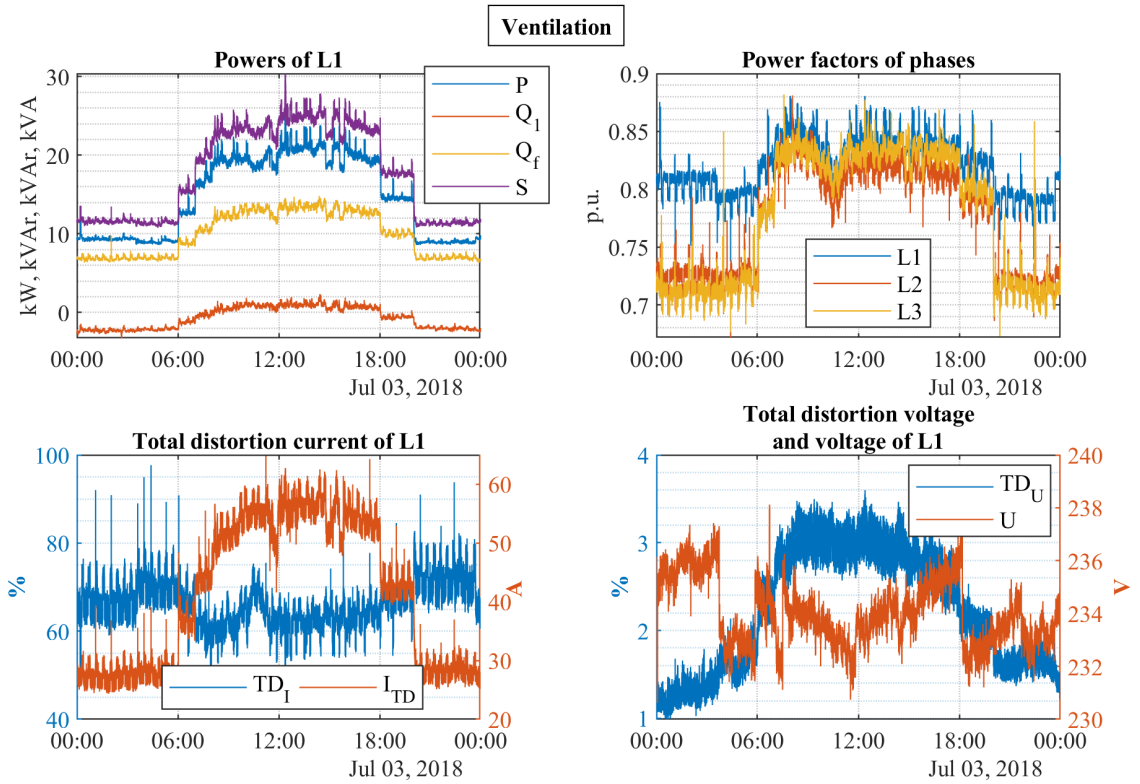

Figure 4.5. *Overview of electrical quantities of ventilation on 3rd of July 2018. Top-left: active (P), fundamental frequency reactive (Q_1), Fryze's reactive (Q_f) and apparent power (S) of L1. Top-right: Power factors (PF) of L1, L2 and L3. Bottom-left: Total distortion of current (TD_I) and absolute value of distortion current (I_{TD}) of L1. Bottom-right: Total distortion of voltage (TD_U) and voltage (U) of L1.*

distortion power would be present, the values of Q_1 and Q_f were equal, however in this case the maximum of Q_f reaches 15 kVAr while Q_1 is measured as 2 kVAr. In addition, the largest value of Q_1 is recorded outside the working hours being capacitive and nearly -3 kVAr when Q_f equals to 7 kVAr. These observations indicate a significant amount of distortion power in the system compared to the magnitude of active power.

As in the measurements of service electricity, power factor for L2 and L3 behave differently to L1 possibly due to unequal loads. The measurement of distortion current I_{TD} conforms with Q_f as it illustrates similar curve, and thus large part of distortion current is reactive as it is included in Q_f. The factor of TD_I also suggests a high concentration of distortion in current between 50 % and 80 %. Voltage distortion, TD_U, visibly resembles the magnitude changes in distortion current, however this studied more profoundly in Chapter 5.

During the data browsing of the thesis, the behaviour of ventilation in terms of power has been concluded to follow similar pattern from day to day, if no solar power is generated. Fig. 4.6 exemplifies the power variations caused by solar power plant detected by the measurement of ventilation at the main distribution board output. It is noteworthy that contrary to active power, the measurements of Q_f and Q_1 present minor correlation to the production of solar power plant. Reactive power is still delivered from the main distribution

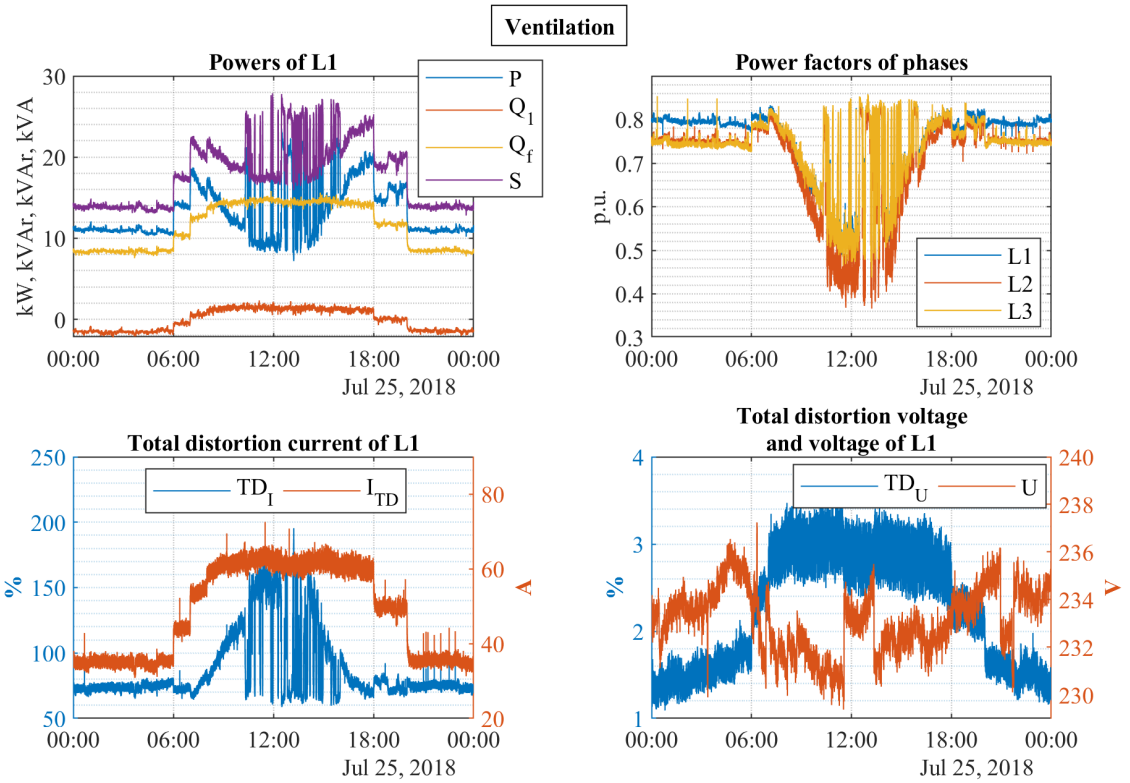

Figure 4.6. *Overview of electrical quantities of ventilation on 25th of July 2018. Top-left: active (P), fundamental frequency reactive (Q_1), Fryze's reactive (Q_f) and apparent power (S) of L1. Top-right: Power factors (PF) of L1, L2 and L3. Bottom-left: Total distortion of current (TD_I) and absolute value of distortion current (I_{TD}) of L1. Bottom-right: Total distortion of voltage (TD_U) and voltage (U) of L1.*

board in case of fundamental frequency and distortion power. Solar power plant provides no suitable reactive power for ventilation, which explains this kind of behaviour, and hence Q_1 and Q_f are still drawn from the main distribution board. Solar power plant is regulated to maintain DPF of 1 due to the parameters set in the inverters, thus no considerable Q_1 can be delivered, even though it would be possible by the inverters. The ability to compensate distortion current is seldom implemented in the solar inverters, however modern control designs allow generation of the desired distortion in current. Perhaps Q_f of ventilation even increases due to the operation of solar power plant as could be deduced from I_{TD} in Fig. 4.17. Furthermore, due to the fluctuation of active power of ventilation PF drops even below 0.4 p.u. and TD_I rises over 150 % occasionally.

4.5 Cooling units

The two cooling units of the building are supplied separately from the main distribution board of service electricity as depicted in Fig. 3.2. The cooling units maintain the temperature of coolant near set point, hence the indoor air temperature of the building can be regulated, if cooling is needed. The cooling units are called as cooling unit 1 and 2 in this thesis and are examined individually. Several parallel compressors are utilized in the

process of cooling. The highest observed three-phase active powers of the cooling units are 70 kW for unit 1 and 80 kW for unit 2.

Both of the cooling units are depicted on the cloudy Tuesday of 3rd of July 2018 and the operation of cooling unit 1 is also shown during the hot Wednesday of 25th of July 2018. In addition to Figs. 4.7, 4.9 and 4.11 illustrating the whole day, the behaviour of shorter time periods is presented in Figs. 4.8 and 4.10. The differences between the operation of the cooling units are due to technical specifications and cooling areas in the building.

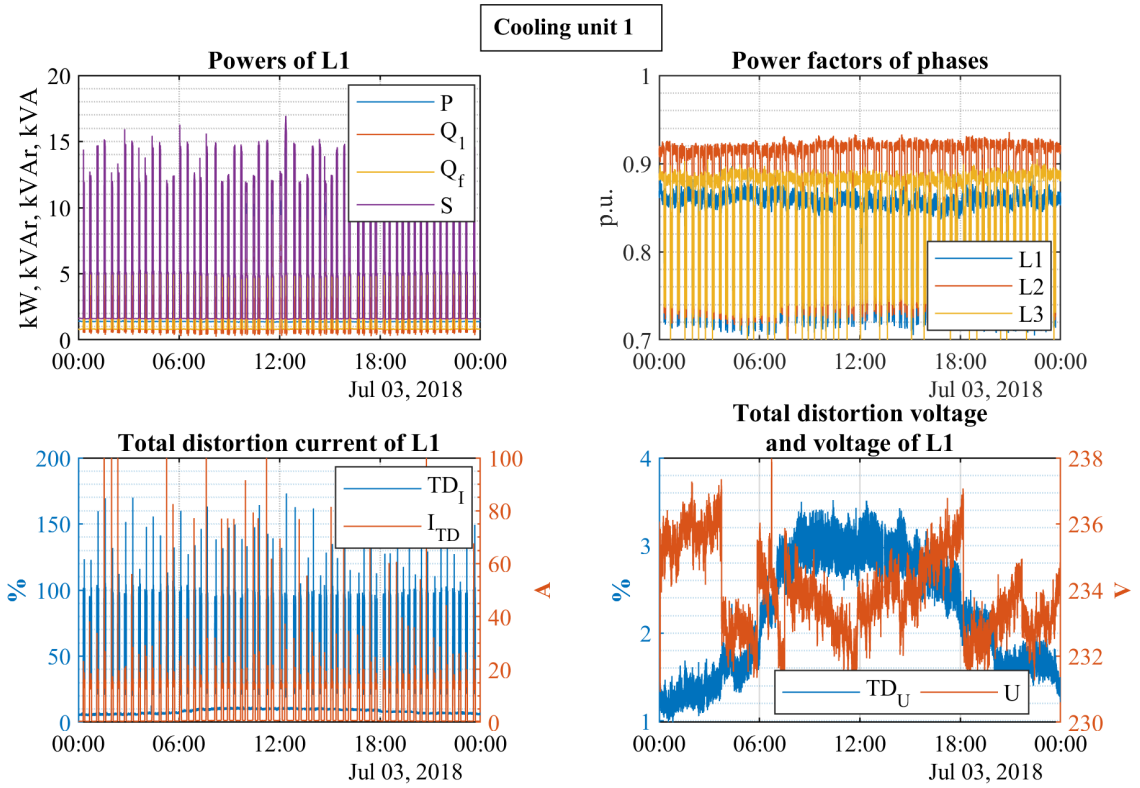

Figure 4.7. *Overview of electrical quantities of cooling unit 1 on 3rd of July 2018. Top-left: active (P), fundamental frequency reactive (Q_1), Fryze's reactive (Q_f) and apparent power (S) of L1. Top-right: Power factors (PF) of L1, L2 and L3. Bottom-left: Total distortion of current (TD_I) and absolute value of distortion current (I_{TD}) of L1. Bottom-right: Total distortion of voltage (TD_U) and voltage (U) of L1.*

The behaviour of cooling unit 1 in Fig. 4.7 is hardly observed apart from the recurrent peaks in powers and distortion current. Active power follows apparent power, thus the curve of P is under S. The peaks are caused by the compressors turning on and off and the occurrence of the peaks is greatly dependent on the outside temperature heating the indoor air. The operation of cooling unit 1 has no visible effect on voltage or its distortion. However, the base value of distortion current is increased during the day for TD_I and I_{TD}. A closer look on cooling unit 1 in time domain is provided in Fig. 4.8.

Two operating sequences of starting and stopping of cooling unit 1 are shown over 30 minutes in Fig. 4.8. The figure indicates that the cooling unit mainly consumes fundamental frequency reactive power because Q_1 and Q_f are nearly equal when the load is running.

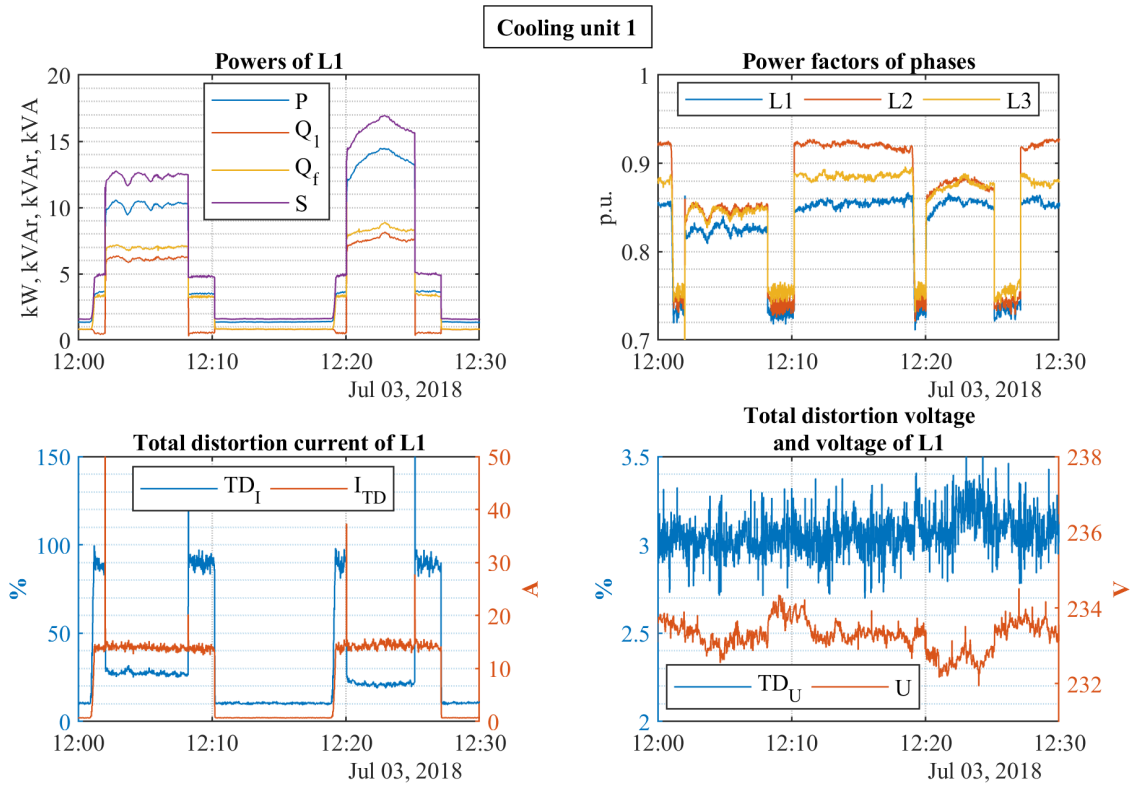

Figure 4.8. *Overview of short time period of electrical quantities of cooling unit 1 on 3rd of July 2018. Top-left: active (P), fundamental frequency reactive (Q_1), Fryze's reactive (Q_f) and apparent power (S) of L1. Top-right: Power factors (PF) of L1, L2 and L3. Bottom-left: Total distortion of current (TD_I) and absolute value of distortion current (I_{TD}) of L1. Bottom-right: Total distortion of voltage (TD_U) and voltage (U) of L1.*

This is a feature of directly coupled electric machine being a compressor in this case. A closer inspection also reveals start-up and turn-off periods of lower power, in which only reactive power of Q_f is measured. The measurements of power factors show that the system is electrically the most effective when the cooling unit is either completely turned on or off. The transition state of lower power results in the lowest value of PF since then the amount of Q_f and P are nearly equal in magnitudes. The absolute distortion current is found to be constant over the whole operating sequence excluding transients that occur at the start and end of the high power period. Perhaps a fan or other appliance of the cooling unit is operating during the whole operating sequence resulting in constant distortion current. The cooling seems to have no influence on voltage.

The behaviour of the second cooling unit, cooling unit 2, is depicted for one day and 1 hour in Figs. 4.9 and 4.10, respectively. The day is 3rd of July 2018 as for cooling unit 1 in the previous figures. The notable differences to cooling unit 1 are seen as less frequent appearance of power peaks and base active power of 2 kW and base Q_f of 3 kVAr. Obviously some appliance is consuming power continuously and power of the compressor is summed to that power. The closer look of cooling unit 2 in time domain is presented in Fig. 4.10.

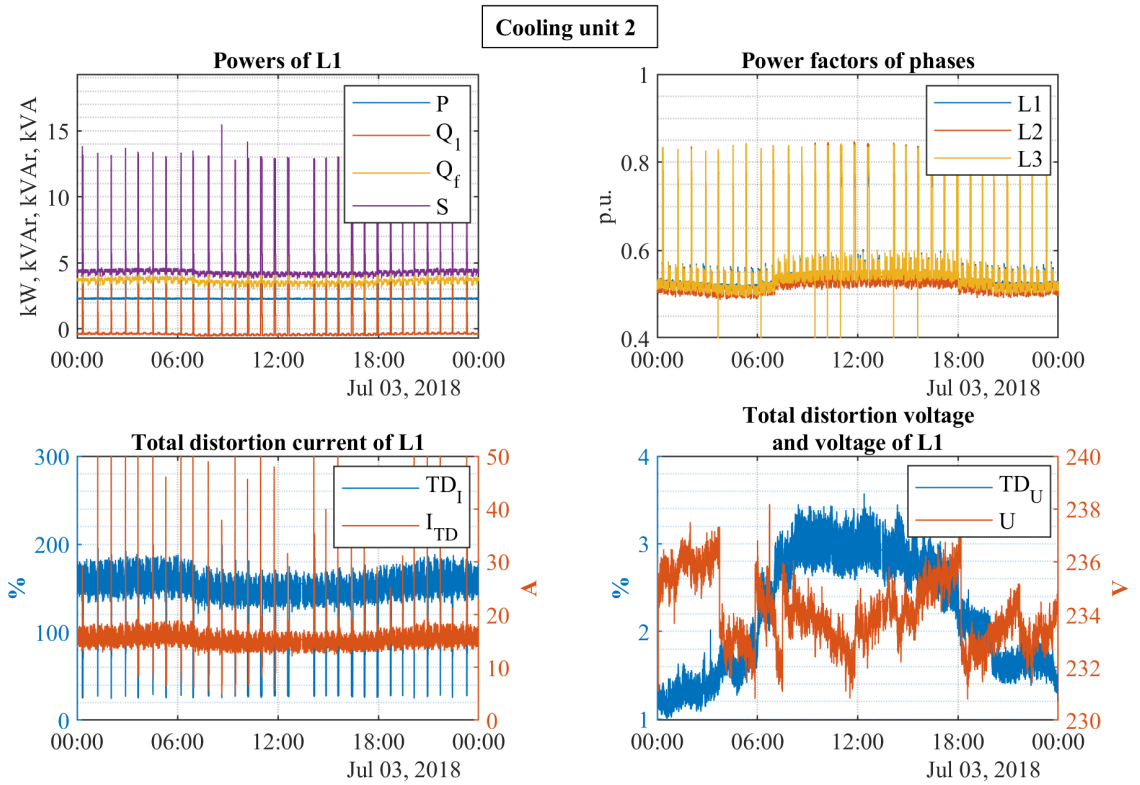

Figure 4.9. *Overview of electrical quantities of cooling unit 2 on 3rd of July 2018. Top-left: active (P), fundamental frequency reactive (Q_1), Fryze's reactive (Q_f) and apparent power (S) of L1. Top-right: Power factors (PF) of L1, L2 and L3. Bottom-left: Total distortion of current (TD_I) and absolute value of distortion current (I_{TD}) of L1. Bottom-right: Total distortion of voltage (TD_U) and voltage (U) of L1.*

Power factor of cooling unit 2 is measured at 0.55 p.u. outside of the higher power periods. The higher power events are again assumed to be caused by a compressor, furthermore the operation of the compressor has little effect on absolute distortion current, I_{TD}, in contrast to TD_I that is related to active power. Finally, the behaviour of cooling unit 1 is inspected in Fig. 4.11 on the sunny day of 25th of July 2018.

The clear summer day heats the building, which increases the demand of cooling as seen in Fig. 4.11 compared with Fig. 4.7 of the cloudy day. The higher demand of cooling starts more compressors and keeps them running for longer time periods, which is measured as the increments of powers. According to the measurements, the transitions of starting and stopping the compressors produce distortion current peaks of more than 100 A in 1 second averages of the meter. Thus also during the sunny summer days, when more cooling is required, large distortion currents are repeatedly induced to the electrical energy system due to the cooling units. However, the peaks of TD_I and I_{TD} can also result from the effect of the stepwise current change on the measurement method of distortion current.

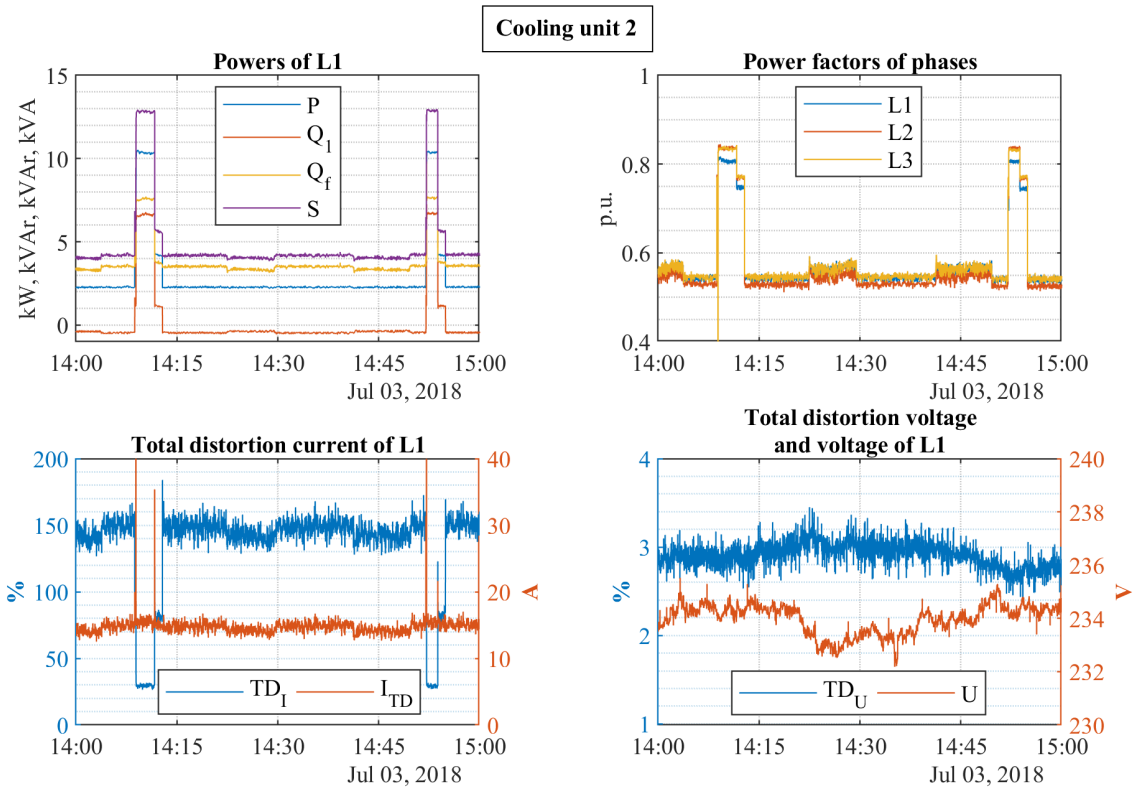

Figure 4.10. *Overview of short time period of electrical quantities of cooling unit 2 on 3rd of July 2018. Top-left: active (P), fundamental frequency reactive (Q_1), Fryze's reactive (Q_f) and apparent power (S) of L1. Top-right: Power factors (PF) of L1, L2 and L3. Bottom-left: Total distortion of current (TD_I) and absolute value of distortion current (I_{TD}) of L1. Bottom-right: Total distortion of voltage (TD_U) and voltage (U) of L1.*

4.6 Elevators

The passenger elevators of the building, elevator 1 and 2, are supplied from the main distribution board of service electricity as Fig. 3.2 illustrates. These two elevators are located physically next to each other and transfer people across eight floors in cooperation. Naturally, the elevators are used the most in daytime, and are lifting people numerous times during a day. The elevators are assumed to be driven by three-phase frequency converters regarding the measurements. Maximum three-phase peak active power was metered at approximately 7 kW for one elevator.

The behaviour of the elevators is presented over a day for elevator 1 and 2, and additionally the behaviour of shorter time period is depicted for elevator 1. The measurements proved that the elevators are electrically identical, hence only elevator 1 is studied in more detail. The daily behaviours of the elevators are found in Figs. 4.12 and 4.14 during Tuesday 3rd of July 2018, and Fig. 4.13 gives a closer look in time domain in case of elevator 1.

The operation of elevator 1 in Fig. 4.12 is difficult to observe because of the frequent lifts, which yield rapid power variations. Nevertheless, it can be concluded that the powers of the elevators are small regarding the other loads of service electricity, e.g. ventilation, and

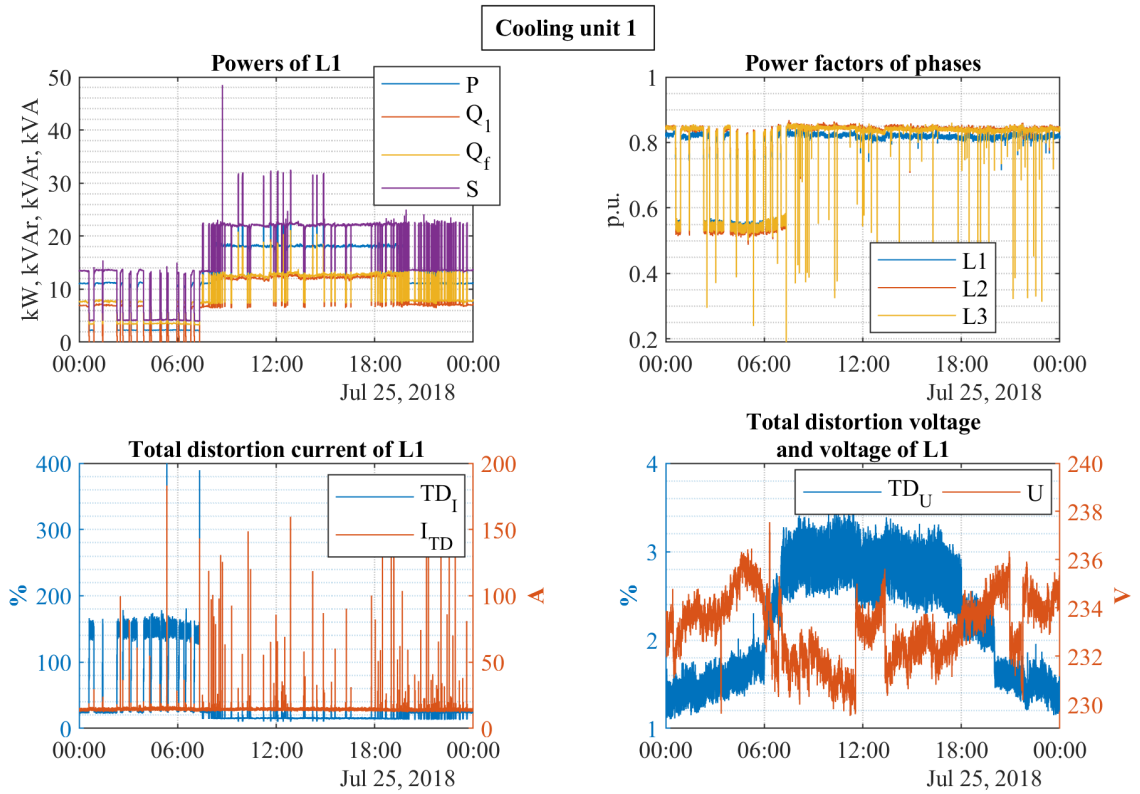

Figure 4.11. *Overview of electrical quantities of cooling unit 1 on 25th of July 2018. Top-left: active (P), fundamental frequency reactive (Q_1), Fryze's reactive (Q_f) and apparent power (S) of L1. Top-right: Power factors (PF) of L1, L2 and L3. Bottom-left: Total distortion of current (TD_I) and absolute value of distortion current (I_{TD}) of L1. Bottom-right: Total distortion of voltage (TD_U) and voltage (U) of L1.*

therefore the influence of the elevators to the total power of service electricity is low, even though the fast variations are measured. An elevator of higher power could represent a considerable peak in the power of the electrical energy system of a building. Power factors of the phases rise to 0.95 p.u. when the elevator is working at high power, and furthermore, L2 possibly contains an additional load deduced from the higher minimum power factor. The behaviour of elevator 1 is discussed further based on Fig. 4.13 showing 5 minutes time period from the same day.

The detailed consideration of Fig. 4.13 of elevator 1 illustrates how the up and down movement of the elevator differs, if measured electrically. When elevator 1 is rising up, the demand of power is minimal due to utilization of counterweight in the elevator, thus the downward movement requires the highest active power. The amount of distortion power in Q_f indicates that the elevators are controlled with power electronics and the measurement of I_{TD} verifies the presence of distortion current during the operation. Additionally, the elevator seems to draw small peaks of powers before settling during the accelerations. The time resolution of 1 second enables to identify the exact behaviour of the elevators and the studies in Chapter 5 propose that time domain information is remarkably lost even if time average of 1 minute is calculated.

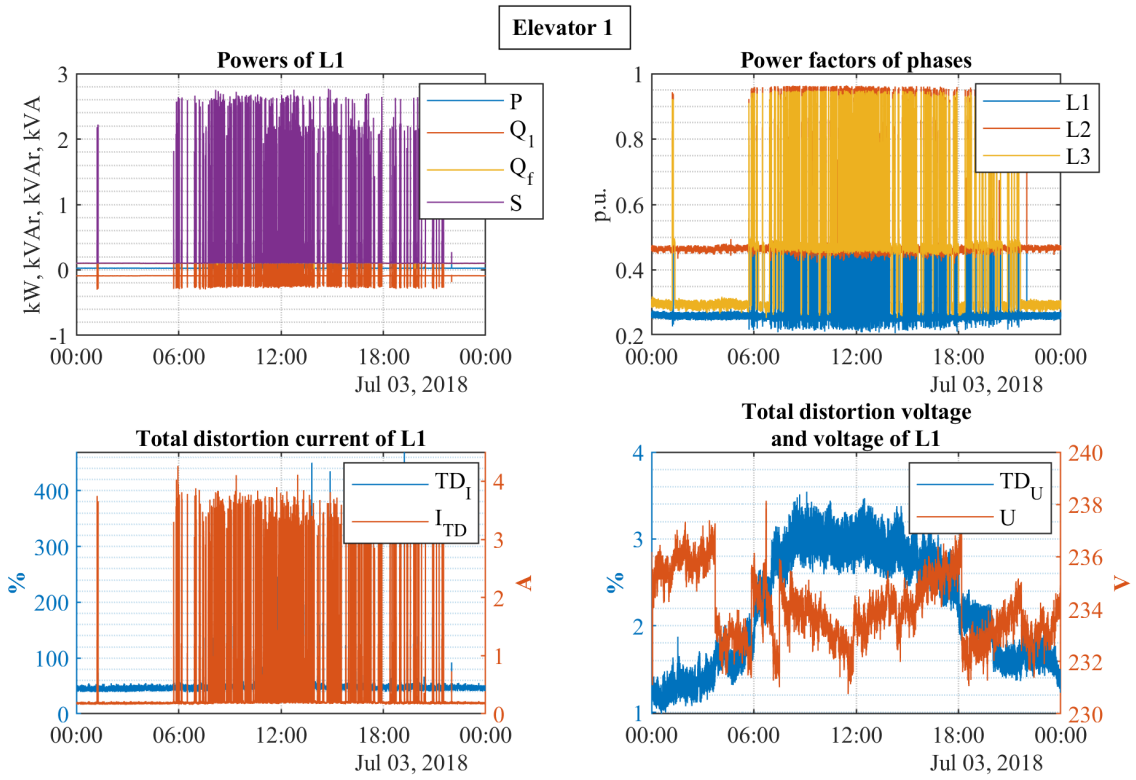

Figure 4.12. *Overview of electrical quantities of elevator 1 on 3rd of July 2018. Top-left: active (P), fundamental frequency reactive (Q_1), Fryze's reactive (Q_f) and apparent power (S) of L1. Top-right: Power factors (PF) of L1, L2 and L3. Bottom-left: Total distortion of current (TD_I) and absolute value of distortion current (I_{TD}) of L1. Bottom-right: Total distortion of voltage (TD_U) and voltage (U) of L1.*

As stated, the passenger elevators represent similar electrical behaviour, which is yet visualized with Fig. 4.14 of elevator 2. No other variations was discovered between the elevators than lesser usage of elevator 2 on 3rd of July 2018. The reason for the fewer lifts may result from the coordinated operation of the elevators with each other, in which elevator 1 is preferred to elevator 2 in lifting, if possible. A brief study of the elevators also demonstrated that the elevators seldom operate simultaneously or are lifting to the same direction. This reduces the power peaks due to the summation of the elevators at the main distribution board, yet it remains unconfirmed, if this behaviour is intended.

4.7 Electric vehicle charging station

Kampusareena offers five parking spots at the front of the building equipped with readiness to charge EVs. Each of the parking spots includes a pole with two Schuko sockets fused at 32 A. One of the poles additionally has a socket for three-phase charger. These parking spots are supplied from the main distribution board of service electricity as sketched in Fig. 3.2. Mostly electric cars have been recognized to use EV charging station, and the number of charged electric cars varies greatly in daily and yearly basis. Altogether, EV charging station represents perhaps the smallest load of service electricity in average due

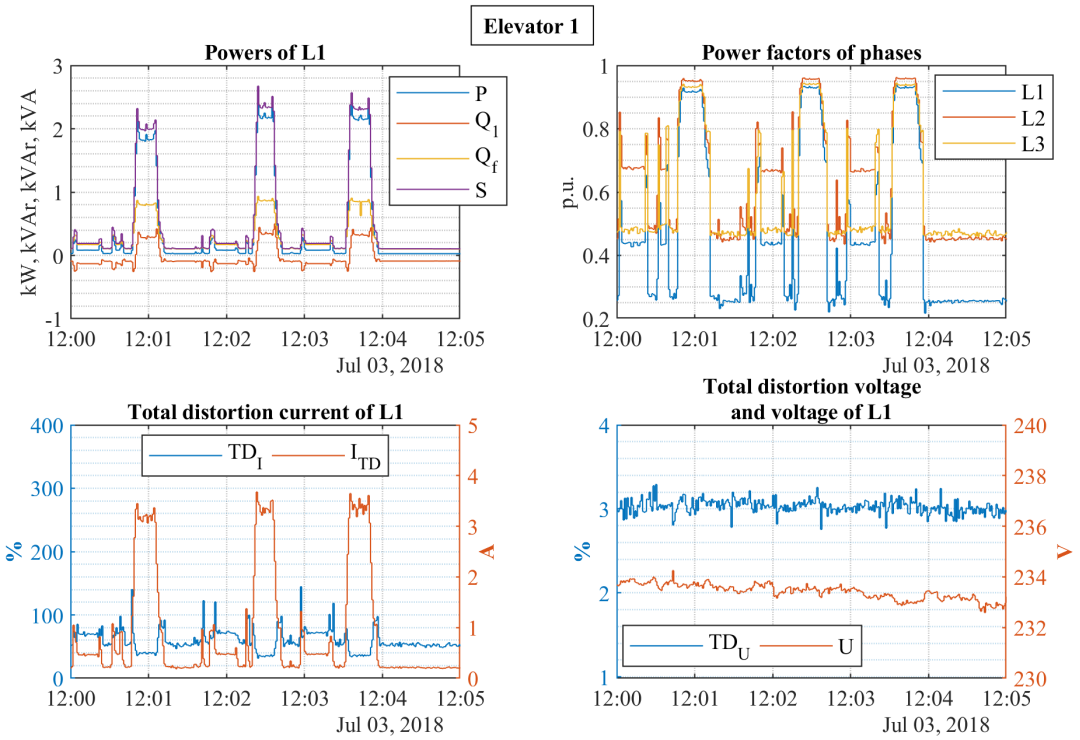

Figure 4.13. *Overview of short time period of electrical quantities of elevator 1 on 3rd of July 2018. Top-left: active (P), fundamental frequency reactive (Q_1), Fryze's reactive (Q_f) and apparent power (S) of L1. Top-right: Power factors (PF) of L1, L2 and L3. Bottom-left: Total distortion of current (TD_I) and absolute value of distortion current (I_{TD}) of L1. Bottom-right: Total distortion of voltage (TD_U) and voltage (U) of L1.*

to low usage but as the electric cars become more general the situation may change. The largest momentarily three-phase loading condition was measured at 22 kW.

The days studied in this chapter unfortunately involved no electric car charging, thus Wednesday 4th of July 2018 was selected for the examination of EV charging station behaviour. The day included two different occasions of electric car charging as shown in Fig. 4.15. If the magnitudes of the powers are neglected, the charging sequences of the two cars are rather similar.

The behaviour of EV charging station varies significantly due to alternating charging solutions of the electric and hybrid cars. The cars utilize either three-phase or one-phase charging, and the magnitude and pattern of the charging power differs from car to car. Power factors of the phases in Fig. 4.15 illustrate that the first event of charging has involved only L1 and the latter has used three-phases. In consequence, the second charged car has been a remarkably larger load in total than the first one. Both of the chargers represent a capacitive load according to Q_1 and draw a low amount of distortion current as Q_1 and Q_f are measured nearly equal and TD_I is observe as 5 %. However, the larger load generates double absolute distortion current, I_{TD}, at one phase to the smaller load. Power factors of the phases settle at approximately 0.993 p.u. during the maximum demand and drop only temporarily when the charging is close to completion.

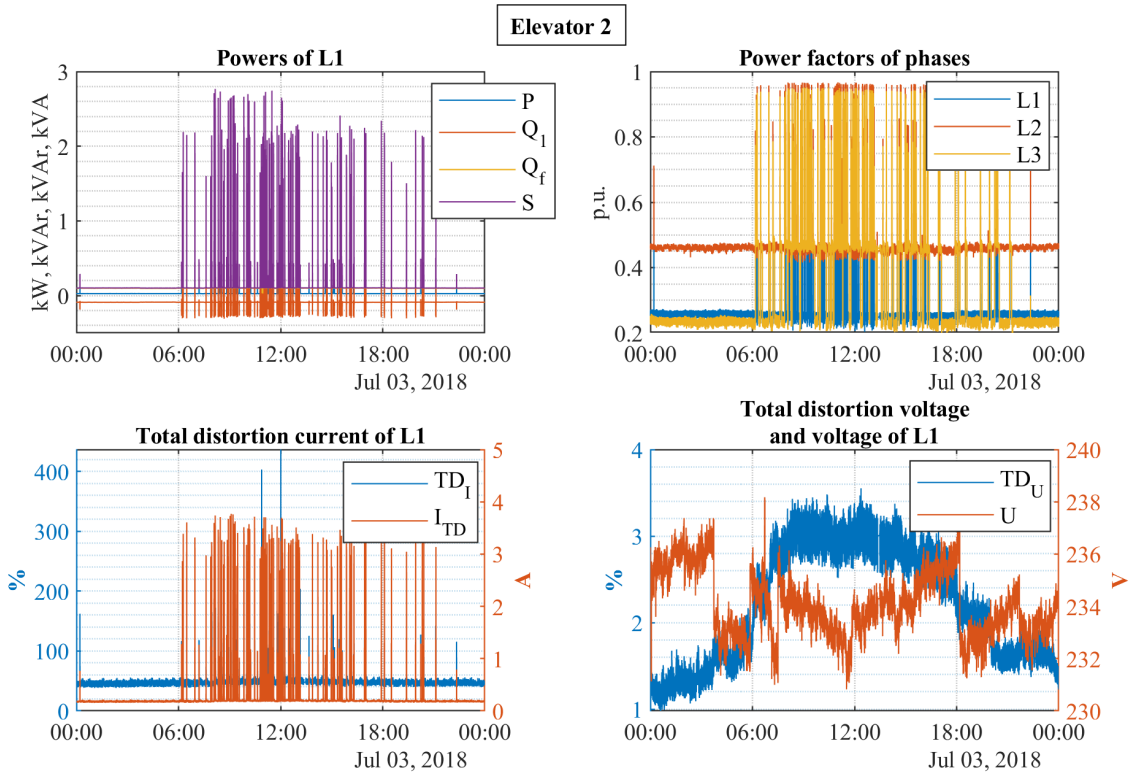

Figure 4.14. *Overview of electrical quantities of elevator 2 on 3rd of July 2018. Top-left: active (P), fundamental frequency reactive (Q_1), Fryze's reactive (Q_f) and apparent power (S) of L1. Top-right: Power factors (PF) of L1, L2 and L3. Bottom-left: Total distortion of current (TD_I) and absolute value of distortion current (I_{TD}) of L1. Bottom-right: Total distortion of voltage (TD_U) and voltage (U) of L1.*

4.8 Solar photovoltaic power plant

Solar power plant is generating power for the building, primarily for ventilation, as is illustrated in Fig. 3.2 of the main electricity distribution of Kampusareena. The three-phase inverters of solar power plant operate in parallel at the same point of common coupling (PCC) located at the top floor of the building contrary to the main distribution room at the bottom floor. In principle, the inverters are set to produce power at displacement power factor of 1 p.u. and the power is fed directly to the electrical energy system of the building because there is no battery storage. The measured maximum three-phase active power of solar power plant was 52 kW being close to the nominal of 57 kW. The nominal power of solar power plant is difficult to reach since the solar panels have been directed to different points of compass. However, solar power plant occasionally supplies the electricity of all the ventilation unit rooms and even the whole power of service electricity.

The operation of solar power plant is depicted in Figs. 4.16 and 4.17 for cloudy Tuesday of 3rd of July and sunny Wednesday of 25th of July 2018 respectively. The operation of solar power plant can also be observed at the measurement points of ventilation and service electricity in Figs. 4.6 and 4.4 on 25th of July. When inspecting the figures of solar power plant one should notice that active power, P, is positive, hence the measurement setup

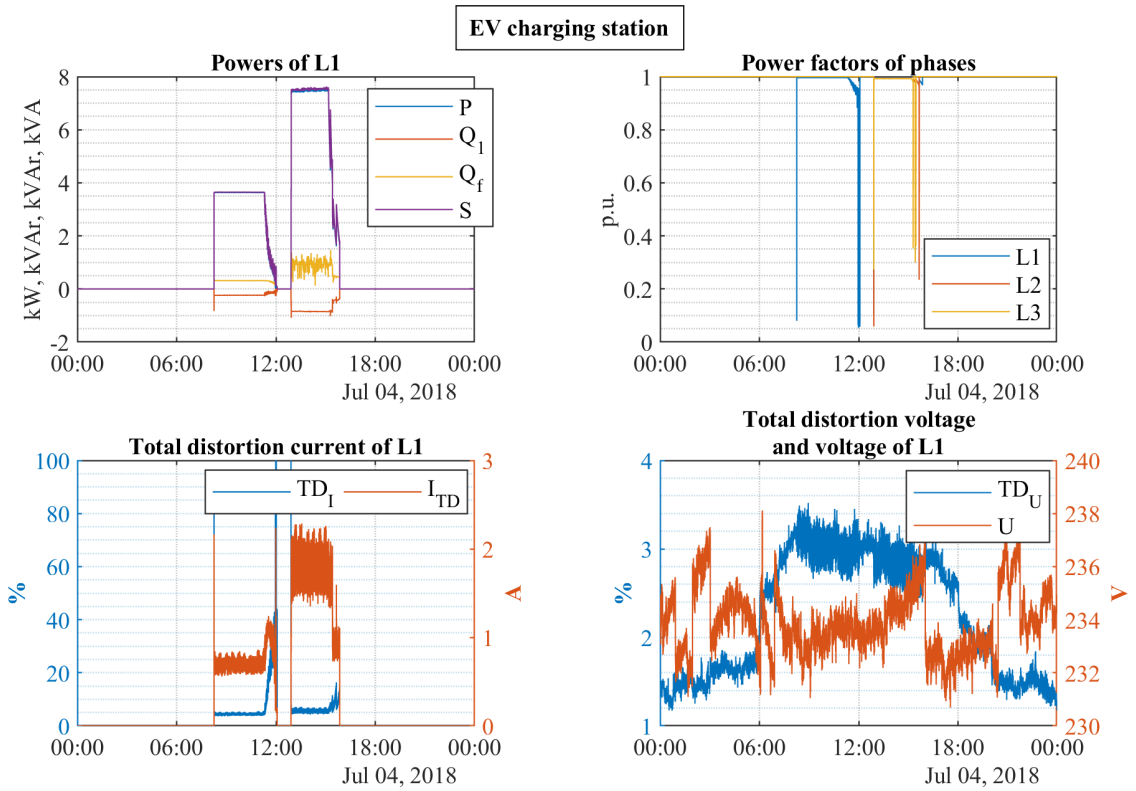

Figure 4.15. *Overview of electrical quantities of EV charging station on 4th of July 2018. Top-left: active (P), fundamental frequency reactive (Q_1), Fryze's reactive (Q_f) and apparent power (S) of L1. Top-right: Power factors (PF) of L1, L2 and L3. Bottom-left: Total distortion of current (TD_I) and absolute value of distortion current (I_{TD}) of L1. Bottom-right: Total distortion of voltage (TD_U) and voltage (U) of L1.*

considers the generated current positive in contrast to a conventional measurement that assumes the flow of current towards the load, i.e. the end of the feeder. On the other hand, active power is in principle flowing from solar power plant towards the loads of ventilation. Nevertheless, the used measurement configuration inverts the sign of Q_1 in comparison to the other measurements of the building, thus positive value of Q_1 represents capacitive reactive power.

The cloudy day of Fig. 4.16 involves low solar power production with a little peak around 11:00. The figure demonstrates the behaviour of solar power plant when its operating but only small power is generated. The plant starts operating before 6:00 and shuts down after 21:00, which is affect by the available irradiance. Because solar power plant aims to *DPF* of 1 p.u. the value of Q_1 is kept close to zero being slightly inductive during the bright hours and capacitive outside of the operating hours. Fryze's reactive power indicates that distortion power is present, and furthermore, Q_f is affected by the changes in active power: As the power production increases, also the amount of distortion power rises. This is supported by the measurement of I_{TD}, on the contrary to the value of TD_I that decreases towards the midday.

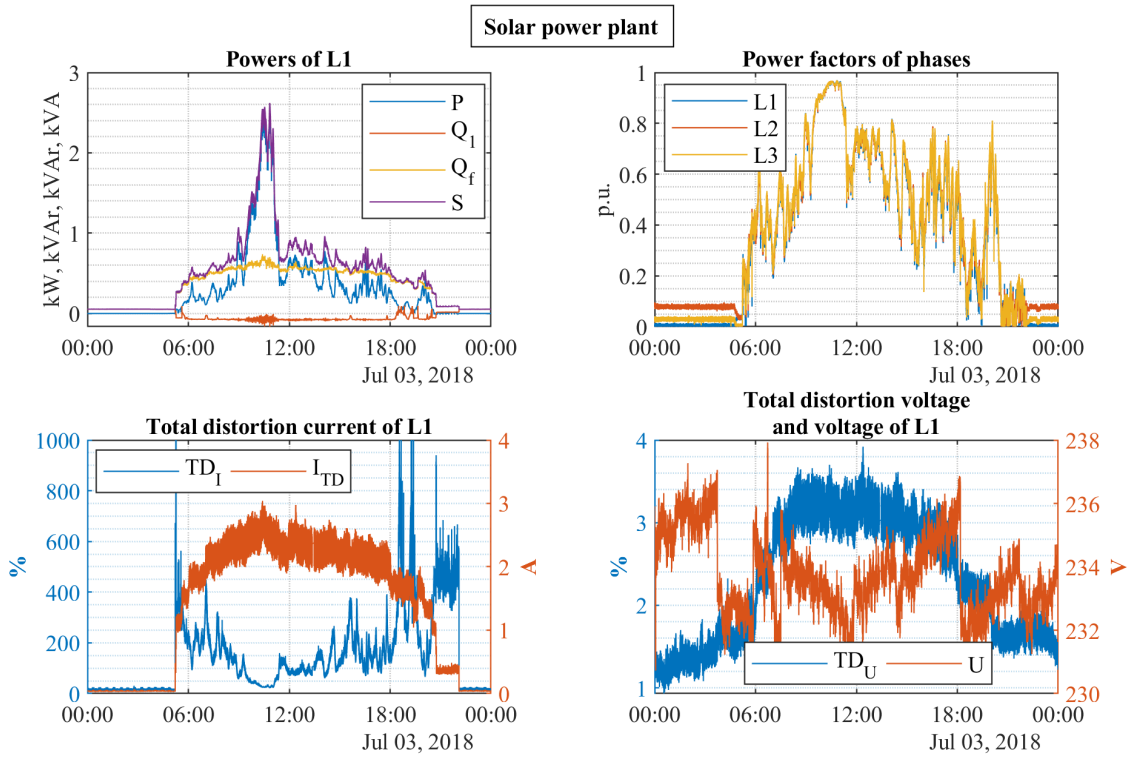

Figure 4.16. *Overview of electrical quantities of solar power plant on 3rd of July 2018. Top-left: active (P), fundamental frequency reactive (Q_1), Fryze's reactive (Q_f) and apparent power (S) of L1. Top-right: Power factors (PF) of L1, L2 and L3. Bottom-left: Total distortion of current (TD_I) and absolute value of distortion current (I_{TD}) of L1. Bottom-right: Total distortion of voltage (TD_U) and voltage (U) of L1.*

Power factors of solar power plant are measured remarkably below 1 p.u. in Fig. 4.16 due to low power generation when distortion power constitutes a significant portion of S. Total distortion of voltage at solar power plant is visibly higher than, for example, in Fig. 4.3 of service electricity, which depicts during the same day the main distribution board that connects also to solar power plant. Voltage distortion of solar power plant exceeds 3.5 %, while at the main distribution board voltage distortion is measured to remain below 3.5 %. The higher voltage distortion of solar power plant presumably results from the same feeder of solar power plant and ventilation and the impedance of 100 meter long cable between the bottom and top floor of the building, at which the main distribution board and solar power plant are located respectively. As shown in Fig. 4.5, ventilation is drawing a high amount of distortion current, which due to voltage drop distorts the voltage at PCC of solar power plant and the ventilation unit room at the top of the building.

The fluctuating nature of solar power plant is illustrated in Fig. 4.17 for the sunny day with a few clouds covering Sun. As the figure demonstrates, active power can drop to one-fifth within minutes and rise in similar manner, and this kind of fluctuations may occur continuously during a day. Moreover, the behaviour of the figure is frequently measured in Finland because few completely clear days occur annually.

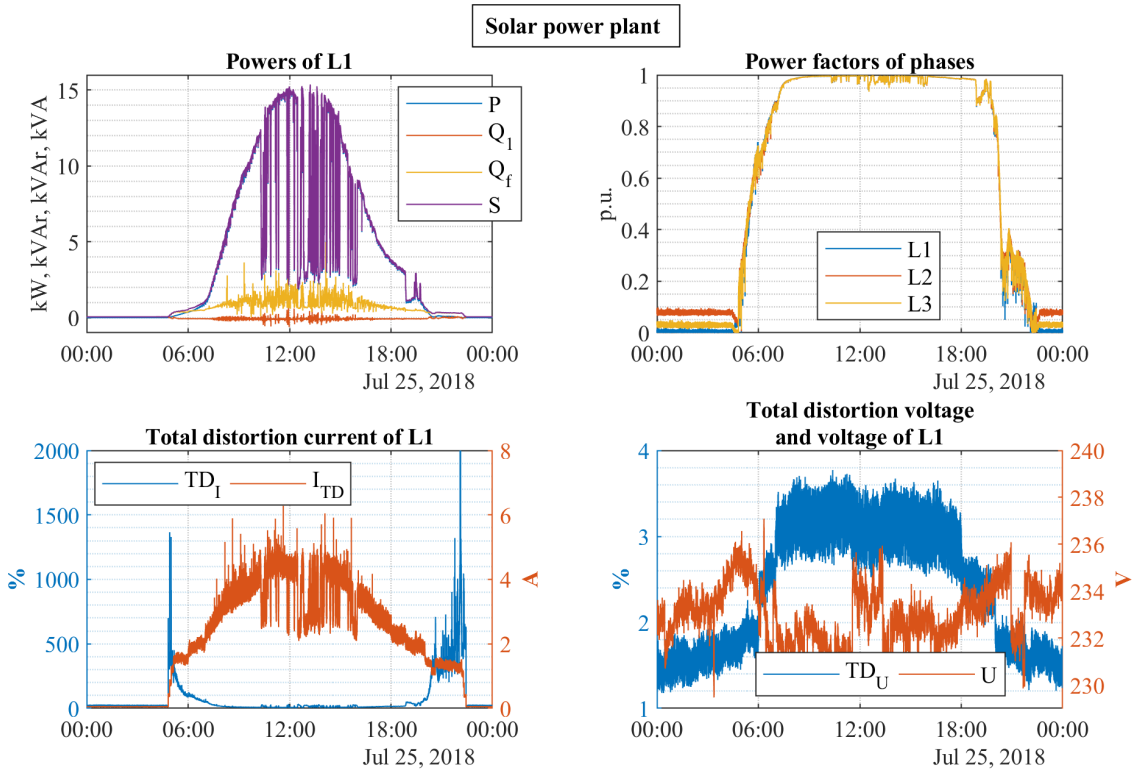

Figure 4.17. *Overview of electrical quantities of solar power plant on 3rd of July 2018. Top-left: active (P), fundamental frequency reactive (Q_1), Fryze's reactive (Q_f) and apparent power (S) of L1. Top-right: Power factors (PF) of L1, L2 and L3. Bottom-left: Total distortion of current (TD_I) and absolute value of distortion current (I_{TD}) of L1. Bottom-right: Total distortion of voltage (TD_U) and voltage (U) of L1.*

The fluctuation of power generation also affects the values of Q_1 and Q_f causing them to seem noisy in the measurements. This is a consequence of solar power plant attempting to maintain *DPF* near 1 p.u., and how distortion power relates to the magnitude of active power. The effect of power fluctuation on distortion current is perhaps the most obviously observed in the absolute value of I_{TD}, from which it is evident that increase in P leads to an increment in distortion current. In addition, the higher power production of July 25th in Fig. 4.17 results in higher distortion current than during the cloudy day of Fig. 4.16. The measurements of power factors prove that the plant achieves a proper value of *PF*, if the active power production is close enough to the nominal power. In this case, active power of L1 can decrease to around 3 kW before *PF* is reduced visibly, which means that three-phase active power is lowered to 9 kW being 16 % of the nominal power of 57 kW.

5. DATA ANALYSIS

The various time periods, and their shortening, in the price setting of electricity markets with the emerging power tariffs for distribution network motivated the studies in this chapter. In addition, the inevitably increasing amount of power electronics, and growing concern on power quality and its costs, led for a deeper look in measuring of power. These issues are covered in the analyses by emphasizing the significant features of the piloted building: short time interval of measurements, simultaneous measurements across the electrical system, wide range of measured power and power quality quantities and large amount of data acquired during a long period of time. Overall, the pilot of Kampusareena laid the foundation for the studies in this chapter.

Eventually, the analyses present the effect of time averaging on power measurements for different load types and solar power plant, and consider the quantification of power. Especially reactive power is considered from the aspects of voltage and current distortion and power quality. More generally, the analyses promote the capabilities of available data in the pilot building and summarize the findings in the behaviour of the electrical energy system considered in Chapter 4.

The analyses are presented under three sections. Firstly, with the aid of 1 second resolution multiple time averages for active and reactive power of the loads and solar power plant were calculated to examine how the perception of power changes over various time periods. Based on results a viable time averaging interval was selected to be used in the following analyses. Secondly, the sources of distortion current and voltage are studied with the simultaneous measurements around the electrical energy system. The distortion current is straightforwardly observed from the measurements but the source of distortion voltage is traced with machine learning (ML) methods and correlations. Also, the summation of distortion current is briefly stated inspired by the diverse measurements. Thirdly, comparison is presented between the conventional fundamental frequency powers and full measurement bandwidth powers, including Fryze's reactive power measurements. Fryze's power theory involves the distortion of voltage and current into measurements of power in an electrical network, and thus addresses power quality by quantifying disturbances in the network.

The qualities of the pilot environment and the selected scope of the thesis limit the analyses of the thesis, as more profoundly explained in the beginning of Chapter 4. Examinations are mainly performed for L1 meaning three-phase values are excluded and the comparisons of phases are in a minor role. The loads, power generation and their coupling as a whole practically represent electrical energy system of an office building. Still, device specific information is provided in the individual studies of various load types and solar power.

5.1 Time averaging

Currently DSOs are starting to place active power tariffs even for smaller private customers in Finland. In Europe, the hourly day-ahead electricity market of Nord Pool is shifting its imbalance settlement period (ISP) from 1 hour to 15 minutes at latest by 1st of January 2025 [56]. These changes and the introduction of numerous solar PV power plants in the distribution networks presumably have a remarkable effect on the electricity markets and the available business cases, and furthermore, encourage the studies of time averaging in this thesis. Solar power plants generate continuously and rather rapidly fluctuating power flows, hence their time domain behaviour deviates from the conventional power production [23,49]. In addition, EV charging may significantly affect the electricity distribution of the future. The time averaging study of this thesis utilizes the combination of the high time resolution measurements and the various types of the loads and solar power plant found in the pilot building. The pilot also demonstrated that the data should be gathered only in a time resolution necessary for the practical application. Otherwise, problems may occur in the data transfer and storing resulting in delays and interruptions in the data collection.

Majority of the electrical system data in the pilot building is measured in time resolution of 1 second average allowing to compute time averages of several different intervals for power quantities. Time averages are calculated for active, fundamental frequency reactive and Fryze's reactive power at L1 using time periods of 1 hour, 15 minutes, 5 minutes and 1 minute. The average of 1 hour represents the current ISP in the day-ahead market, in addition to the averaging time of power tariffs commonly [57], and the time period of 1 minute is calculated to speculate the future of power measurements and to utilize the full potential of the measured 1 second averages. This study used the measurements of various days to illustrate the active time domain behaviour of the each measurement point, and furthermore only one of the cooling units and elevators was included in the study because of their similar behaviour. The time averages of point of connection to 20 kV network, tenants' electricity, service electricity, ventilation and elevator 1 are based on the measurements of 3rd of July 2018. Solar power plant and cooling unit 1 are calculated for the day of 25th of July 2018 and EV charging station averages contain the measurements of 4th of July 2018. The time domain behaviours of these days are found in Chapter 4 with further descriptions.

Comparison of the time averages expresses how, for instance, elevator is perceived over different time periods, and in what extent time domain information is lost in averaging. The study especially concerns solar power plant in contrast to the various load types of the building. The time averages of power can be converted to energy by integrating the averages over a time period. The overall amount of energy is independent on the time averaging of power, however the increase in time resolution of energy still reveals the peaks of consumption as with power. On the contrary, the time averaging can conclusively hide the behaviour of power due to the instantaneous nature of power. The time averaged power can also be called as demand, and frequently maximum, minimum and average demand are recorded by power meters. The maximum and minimum demands express the

extreme values of power during a time period and the average demand equals to the time averaging in this thesis. It should also be mentioned that voltage and current distortion are recommended to be quantified with time averages of 3 seconds and 10 minutes in standard IEC 61000-4-30, and the standard defines time averaging as time aggregation [13].

According to standard IEEE Std 1459 [30], the time averages of powers are calculated arithmetically instead of root mean square (rms) as suggested in power quality standard [13]. Empirical cumulative distribution function (ecdf) of MATLAB software was chosen to depict the results of the time averaging. The cumulative probability computed by ecdf-function shows how the magnitudes of power are distributed in the various time average calculations of the different devices and time periods. The calculations of the longer time period averages filter the power measurements by reducing the magnitude of maximums and increasing the minimums. This is demonstrated in Figure 5.1 with active power of solar power plant and ventilation.

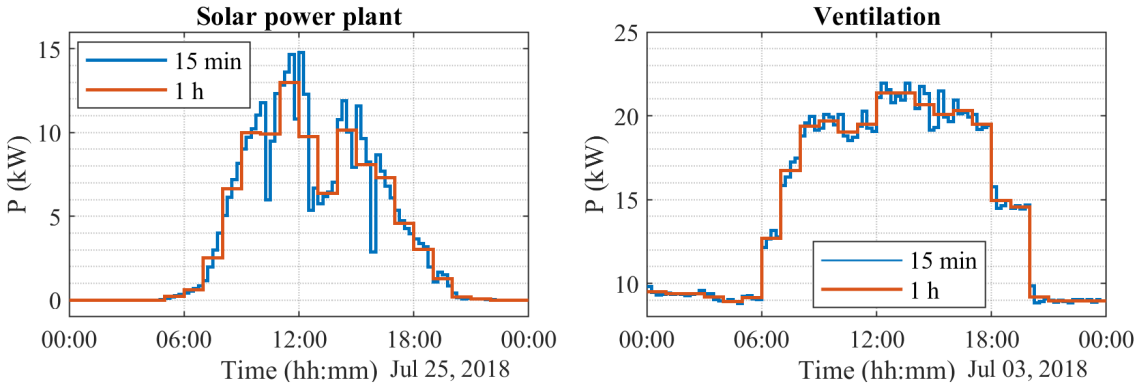

Figure 5.1. *Time averaging example of active power for solar power plant and ventilation at L1 using 1 hour and 15 minutes averages.*

In case of solar power plant, the average of 1 hour diminishes the maximums and minimums of active power compared with 15 minutes average. Whereas the power curve of ventilation, in Fig. 5.1, is only slightly affected by the change in the time averaging period. This demonstrates the differences between the time domain behaviours of the measurements in the pilot building.

5.1.1 Active power

For private customers and smaller connections in the LV distribution networks, active power solely contributes to electrical energy the customer is paying for in Finland. Also the developed power tariffs for the smaller customers only consider active power at the moment. Altogether, in Finland the price of electricity comprises the cost of energy and its transfer, energy tax and possibly the payment of power tariff. More specifically, the quantity of active power is considered, e.g. in the standard IEEE Std 1459, as active power of the fundamental and harmonic frequencies [30]. Also standard IEC 62052-11 defines

power quantities for power metering [9]. However, the energy of harmonic active power can be negligible and is discussed in section 5.3.

Since the electricity bill of the private and smaller customers in the LV distribution networks fully depends on active power the shorter ISP and power tariffs can considerably elevate the electricity costs, if no actions are taken by the customers. As a counteract, the controllability of the modern loads could be utilized in demand response (DR), or e.g. in aggregated power reserves of the future, and thereby the changes in electricity markets could be turned into profit. If implemented well, the control of the loads also benefits DSOs by making the capacity of the distribution network utilized more effectively, and therefore investments in the networks can be delayed. In addition, distributed generation, for instance solar power, will decrease the amount of energy needed from the distribution network for a customer. Conversely, solar power plant may cause unpredictable active power variation due to its intermittent nature but this can be resolved with an energy storage. Decrease in energy consumption is also achieved with more energy efficient devices in general.

The time averaging comparison of active power (P) is shown in Figure 5.2 for each load type, solar power plant and their aggregation at the main distribution boards of service and tenants' electricity, and at the access point to the distribution network. The effect of time averaging on the magnitude of P is illustrated using cumulative distributions and the averages include original data of 1 second and the calculated averages of 1 hour, 15 minutes, 5 minutes and 1 minute. In case of point of connection to 20 kV network, no 1 second measurement was available. Active power is measured with the full bandwidth of 2 kHz of Laatuvahti 3 meter at L1. Perhaps the most obvious differences between the time averages are found at the lowest and highest values of power. The origin of x-axis varies in Fig. 5.2 depending on the measurement point, which should be noted in the observations.

In Fig. 5.2, the time averages of 1 second depict the power curve of the measurement at the highest accuracy, and 1 hour averages deviate the most from the real behaviour of the power in time-domain. In addition to the maximum and minimum values of power, the figure demonstrates the effects of time averaging for a particular measurement and between different loads and solar power plant. The results indicate that 1 minute average describes every measurement point, except elevator 1, in a reasonable precision, and thus the average of 1 second provides little additional information. Newborough has expressed a similar view and also Richardson utilizes 1 minute resolution in his study [48, 50]. In case of point of connection to 20 kV network, tenants' electricity and ventilation even 1 hour average follows the curve of 1 minute accurately until the highest magnitudes of power. For these measurement points 1 hour and 1 minute average maximums differ each other from 4 kW to 20 kW and the power values of 1 minute average above the maximum of 1 hour average comprise around 10 % of the measurements. Also Widen has reported the smoothing impact of load aggregation to active power in time domain considering measurements of domestic loads and solar power plant [61].

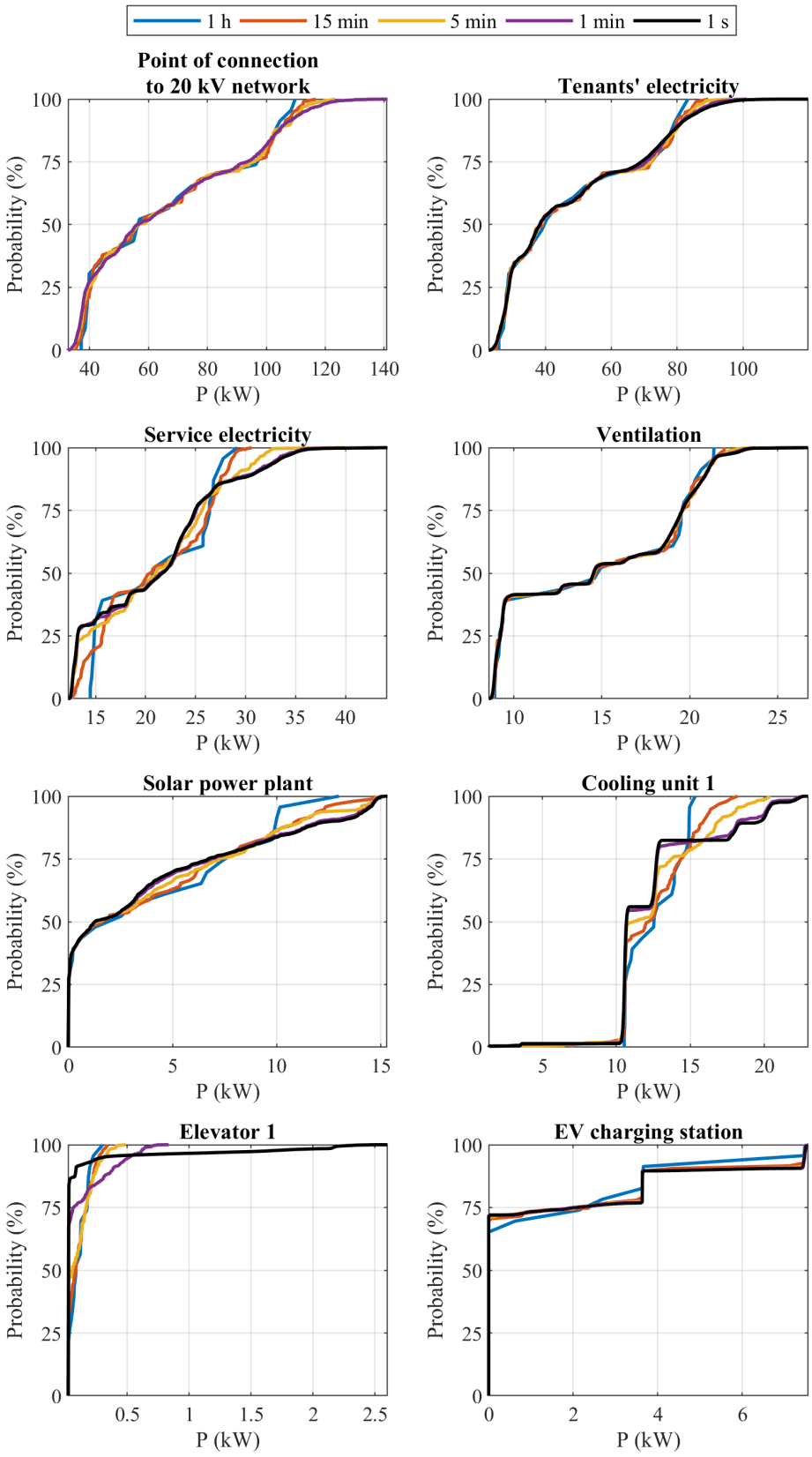

Figure 5.2. *Time averaging of active power (P) at L1 for the measurement points of the building in various days. Averaging intervals include 1 h, 15 min, 5 min and 1 min, with original data of 1 s, except for point of connection to 20 kV network, depicted with cumulative distribution functions.*

Active power of service electricity is affected by solar power plant, the cooling units, the elevators and EV charging station that generally induce considerable variations in P, and this is also proven by the cumulative distributions of Fig. 5.2. For elevator 1, even the alternation between 1 second and 1 minute average is still remarkable making the elevators the most rapidly fluctuating in terms of active power in time-domain. When EV charging station is considered, the upcoming ISP of 15 minutes seems to depict accurately the behaviour. In the cumulative distributions of cooling unit 1 the steps of power are illustrated evidently, and they nearly conform in the averages of 1 minute and 1 second. It can be concluded that active power fluctuation is found especially at solar power plant, the cooling units and the elevators in this study. In addition, the fluctuation of P is reduced when the powers are aggregated at the point of connection to 20 kV network measurement.

5.1.2 Fundamental frequency reactive power

Nowadays only larger customers of the distribution networks are billed for fundamental frequency reactive power (Q_1) in Finland. For example, in the tariff document of Tampereen Sähköverkko Oy, the DSO of TUT, the tariffs are presented for fundamental frequency reactive power, and especially capacitive Q_1 yields a high cost compared with inductive fundamental frequency reactive power [57]. Increase in capacitive Q_1 has been reported in Finland, which is assumed to result from the underground cabling of the distribution networks and from the development of the customer appliances towards electronic coupling [35]. This section highlights the time domain behaviour of Q_1 of the various types of the loads and solar power plant in the pilot building. Additionally, the reactivity of the measurements is discussed.

Similarly to the previous section considering active power, Figure 5.3 presents the cumulative distributions of Q_1 using the same measurement points and days. In case of point of connection to 20 kV network, the value of Q_1 is presumed to represent Q_f according to the examination of the summation of the two Laatuvahti 3 measurements from the main distribution boards. Moreover, the value of Q_f is assumed to change sign according to the reactivity of Q_1. No other value of reactive power was available in the meter at the access point to the 20 kV network, thus the measurement is utilized in the studies of Q_1 and Q_f later on. The original measurement is shown to avoid misleading results because the exact definitions of the power quantities in the 20 kV network meter are unknown. Overall, the reader should be cautious when comparing point of connection to 20 kV network to the other measurements in Fig. 5.3.

An overview of Fig. 5.3 reveals the maximum and minimum magnitudes Q_1 and reactivity of the each measurement point. During the whole observation day the building appears capacitive from the viewpoint of the 20 kV network, if time averages of 1 hour or 15 minutes are used. The averages of 1 minute and 5 minutes of the 20 kV network contain approximately 15 % inductive values. Reactive power of the 20 kV network is fluctuating rapidly due to the measurement principles of the meter, which results in large differences in

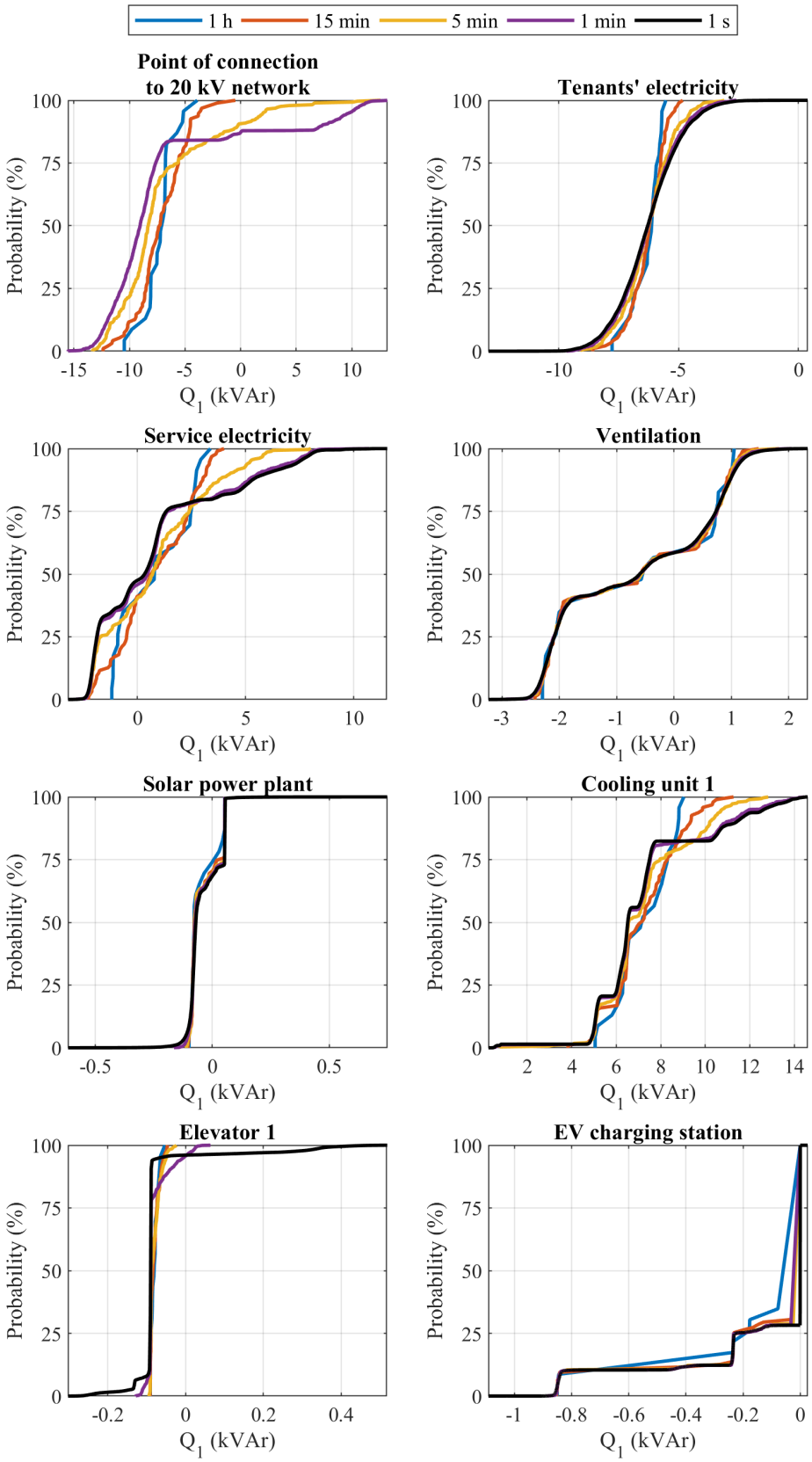

Figure 5.3. *Time averaging of fundamental frequency reactive power (Q_1) at L1 for the measurement points of the building in various days. Averaging intervals include 1 h, 15 min, 5 min and 1 min, with original data of 1 s, except for point of connection to 20 kV network, depicted with cumulative distribution functions.*

the cumulative distributions. In addition to point of connection to 20 kV network, tenants' electricity, ventilation and EV charging station are depicted as mostly capacitive loads. The highest magnitudes of Q_1 are found at the cumulative distributions of cooling unit 1, service electricity and tenants' electricity. Solar power plant, the elevators and EV charging station are measured as minor contributors to Q_1. In time domain, 1 minute average seems to follow the curve of 1 second for the all measurement points except in case of elevator 1, as was stated for P previously. However, the powers of elevator 1 are small in the pilot building. For service electricity, the computed difference of 8 kVAr between the maximums of 1 hour and 1 minute values origins from the time variation of the cooling units. In general, the only considerable contributors to the magnitude of Q_1 regarding the whole building are tenants' electricity, the cooling units and ventilation.

As also discussed in Chapter 4, the compressors of the cooling units consume Q_1 and ventilation and tenants' electricity produce Q_1 in significant manner. The operation of the cooling units turns service electricity on the inductive side. If the tariffs of Q_1 are introduced also for the smaller customers, the controlling of Q_1 may be more difficult to comprehend and implement in general than active power control. The regulating of Q_1 can be easily performed with power converter including active front-end. Otherwise, for example, a compensation reactor is needed. The active front-end power electronics allow also the selling of Q_1, if a business case appears. In the case of the pilot building solar power plant regulates its Q_1 to nearly zero but Q_1 of the cooling units has to be compensated with capacitors.

5.1.3 Fryze's reactive power

Distortion of voltage and current constitute important part of the thesis, thus also Fryze's reactive power (Q_f) is studied by means of time averaging congruently to active (P) and fundamental frequency reactive power (Q_1). The thesis examines Fryze's reactive power as an option to quantify disturbances of distortion in LV distribution networks, and furthermore speculates the usage of Q_f, if the costs of the disturbances are shared between DSO and customers. This section studies the time domain features of Q_f, and hence discovers the influence of distortion regarding time variation in power measurements and how the fundamental frequency dependent P and Q_1 differ in behaviour.

The time averaging results of Q_f are presented in Figure 5.4 identically to active power in Fig. 5.2 and fundamental frequency reactive power in Fig. 5.3, in which the same points and days of the measurements are utilized. Reactive power of point of connection to 20 kV network equals the measurements of Fig. 5.3 due to limited availability of power quantities and uncertainty in the exact measured values of the meter. The other results are computed as explained in the theory section of 2.4 of power theories.

Generally, the time variation of Q_1 presented in Fig. 5.3 seems to be dampened by the distortion in the Q_f measurements of Fig. 5.4. However, cooling unit 1 clearly represents an

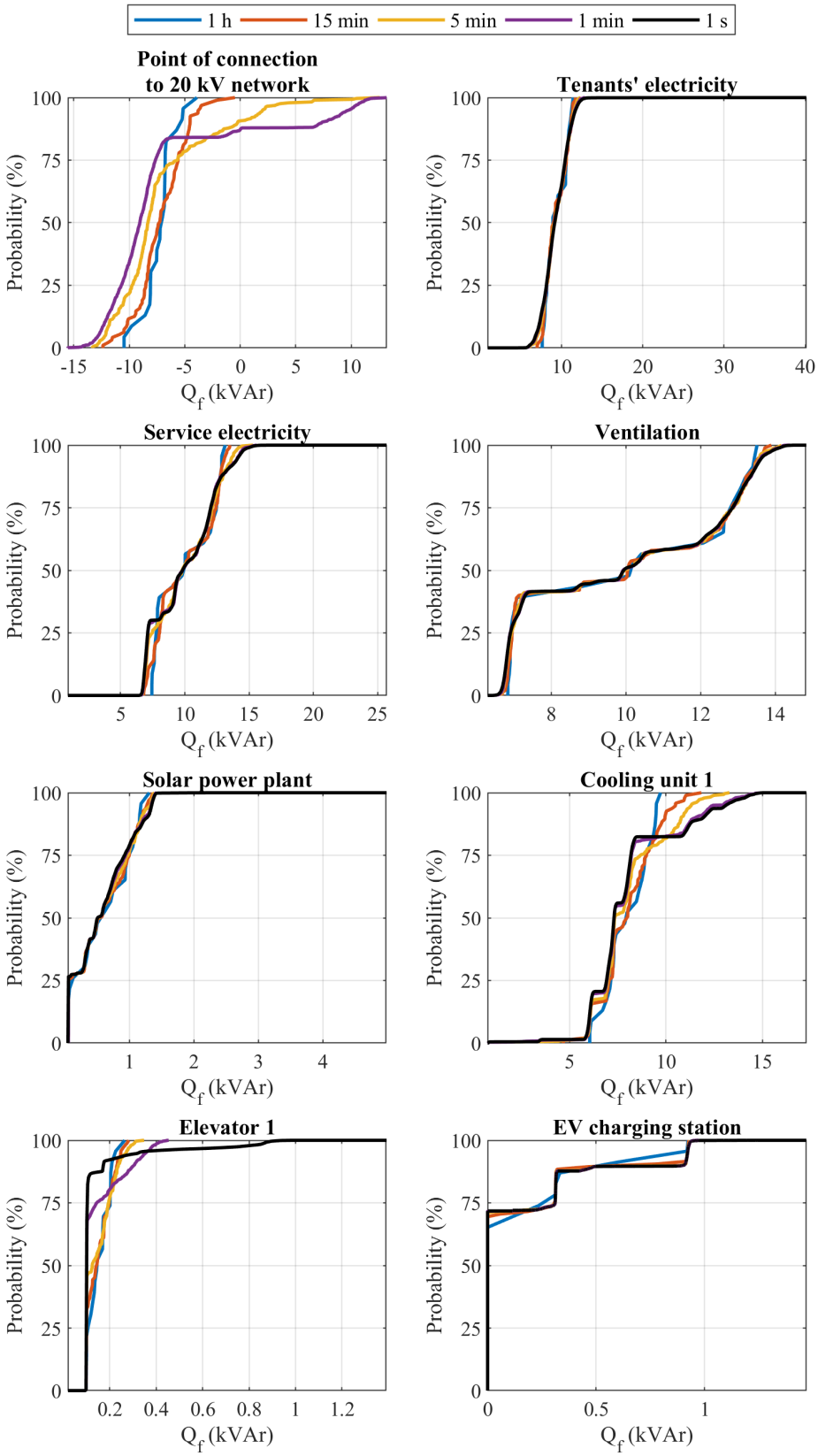

Figure 5.4. *Time averaging of Fryze's reactive power (Q_f) at L1 for the measurement points of the building in various days. Averaging intervals include 1 h, 15 min, 5 min and 1 min, with original data of 1 s, except for point of connection to 20 kV network, depicted with cumulative distribution functions.*

exception. Also the maximum values of the cumulative distributions in Fig. 5.4 comprise higher magnitudes than in case of Q_1 because of the added distortion. The different time averages especially resemble each other in the figures of tenant's electricity, ventilation, solar power plant and consequently service electricity. Cooling unit 1 again shows the steps of the compressors that are due to the component of Q_1, and therefore only 1 minute average follows the average of 1 second. The behaviour of elevator 1 still remains measured the most accurately with the averages of 1 second. For EV charging station, the time averages apart from 1 hour depict the power similarly. The access point to the 20 kV network illustrates the largest variation between the cumulative distributions as well as in Fig. 5.3 of Q_1.

Distortion elevates the maximum magnitudes of the time averages remarkably in the measurements points of tenants' electricity, ventilation and solar power plant, as also stated in sections 5.3 and 5.2.1, where distortion is considered specifically. Overall, distortion changes the time domain behaviour of reactive power towards active power by lessening fluctuation. Yet, it can be concluded that 1 second average is rarely required to model the time domain behaviour of a device in the electrical energy system of the pilot building, and 1 minute average in several occasions provides sufficient time resolution.

5.2 Total distortion current and voltage

The overviews in Chapter 4 considered, among others, the behaviour of current and voltage distortion at the measurement points of the electrical energy system of the building. This section focuses on the distortion measurements by summarizing the overviews and finding the sources of distortion. More specifically, the distortion current measurements are contrasted with each other to discover the main sources of distortion current and the relationships between the magnitudes of distortion and fundamental frequency currents. Summation of distortion currents is also briefly examined inspired by the simultaneous measurements around the electrical energy system. The actual source of voltage distortion is searched by means of correlations and machine learning (ML) methods.

The study of distortion currents supports the assessment of voltage distortion source with the summary of the largest sources of distortion current, and thus aids to evaluate the validity of trained ML models. Eventually, the results guide section 5.3, which considers power measurements from the viewpoints of different types of loads, solar power generation and power theories.

5.2.1 Sources of distortion current

The amount electronically coupled nonlinear devices in the distribution networks rises continuously the latest additions being EV chargers and solar power plants. Consequently, the research considering current distortion remains essential, and especially practical measurements are still valuated. The source of distortion current is easily measured in contrast to determining the source of voltage distortion. Distortion current can be explicitly

measured from the conductor of an appliance but distorted voltage may either result from the background distortion of the distribution network or be caused by the distorted current at the measurement point. On the other hand, distortion current can increase because of the interaction between the background voltage distortion and the dynamics of the appliance [19]. The thesis illustrates total distortion currents of the loads and solar power plant and compares them with each other. In addition, the summation of the total distortion currents at the main distribution board of service electricity is briefly discussed.

The measurements are presented as 1 minute averages inherited from the time averaging analysis in 5.1, in which 1 minute average was concluded to sufficiently depict 1 second average. The averages are calculated according to standard IEC 61000-4-30 that defines the time aggregation of the measurements as the square root of the arithmetic mean of the squared measurements [13]. Distortion current is expressed using the absolute value of total distortion current (I_{TD}), which is further explained in the theory chapter part 2.3.3. The absolute values make the measurements of the building comparable on the contrary to the fundamental frequency related value of TD_I. The difference between I_{TD} and TD_I can be observed, for instance, from the behaviour of solar power plant in Fig. 4.17 in Chapter 4, where the misleading nature of TD_I is noted during low load conditions.

In order to compare and understand the proportions of distortion and fundamental frequency (I_1) currents in the building Figure 5.5 is presented. The figure depicts distortion current of the loads and solar power plant of service electricity and tenants' electricity. The main electricity distribution of the building was presented in Fig. 3.2 including the measurement points concerned here. The measurements in Fig. 5.5 are stacked on top of each other using a method of area plotting. In practice, the values of each measurement point are on the top of the underlying values of the other measurement, and thus only tenants' electricity has base value of zero. The addition of the measurements in the figure requires the calculation of the square root of the squared currents (rms). The stacked presentation was utilized to visualize the magnitudes of the distortion currents more intelligibly.

The measurement data in this study represents the various days of Chapter 4: Tuesday 3rd of July for tenants' electricity, cooling units, elevators and ventilation, Wednesday 4th of July for EV charging and Wednesday 25th of July for solar power plant in 2018. The approach to utilize various measurement days was chosen to illustrate the behaviour of each measurement point when the loads and solar power plant are operating at higher active power. Especially solar power plant and EV charging station have variation in the operation in daily basis. Additionally, the aim of Fig. 5.5 is to show distortion current of ventilation when solar power plant minimally influences active power of ventilation. Because the measurement points are depicted for separate days one should avoid making further conclusions of distortion current summation or interactions between the measurement points based on Fig. 5.5. The summation of distortion current at the main distribution board of service electricity is studied for 3rd of July later in Fig. 5.6. In the measurements of Fig. 5.5, defect is noticeable around 13:00 due to an interruption in the data collection on 3rd of July 2018.

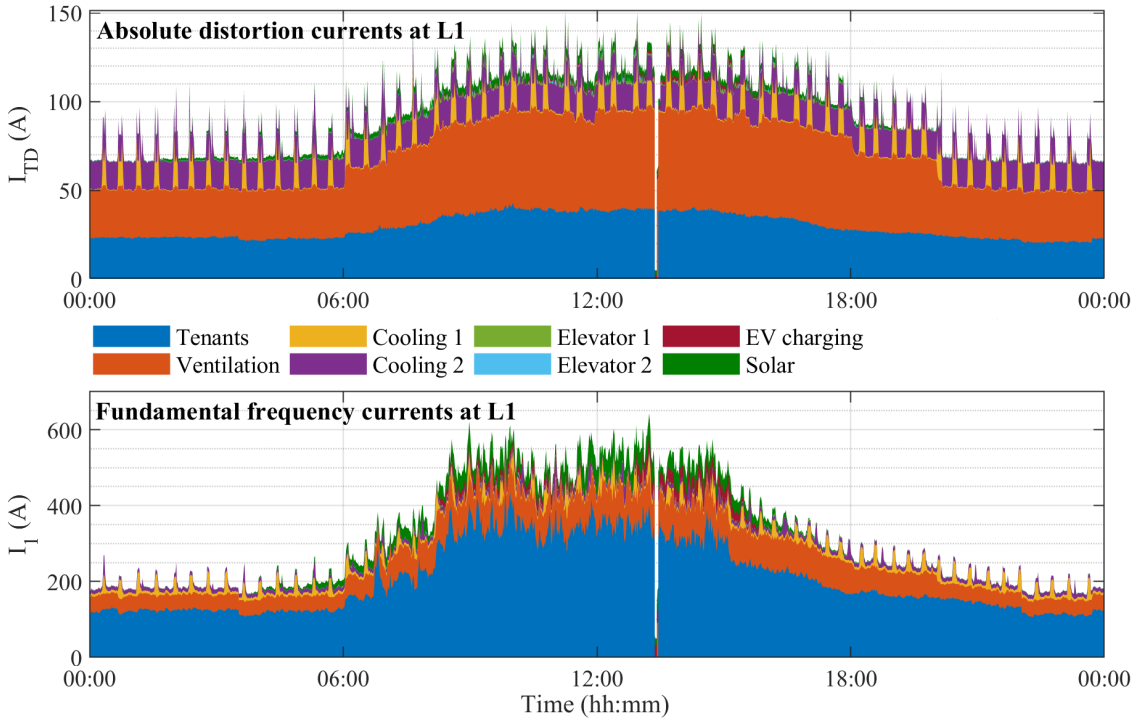

Figure 5.5. *Distortion and fundamental frequency currents of loads and solar power plant at L1 stacked on each other in area plot of 1 min averages of various days. Top: Absolute distortion current (I_{TD}). Bottom: Fundamental frequency current (I_1).*

Apart from tenants' electricity, the distortion currents in Fig. 5.5 are aggregated at the main distribution board called service electricity, that is further studied in Figure 5.6 considering the measured and calculated summation of distortion current. The main causes for distortion current are observed from Fig. 5.5 pointing at tenants' electricity and ventilation. The reason for the distortion of ventilation may result from numerous power electronics converters designed with similar principles including, for example, diode rectification. Tenants' electricity however constitutes of larger blend of aggregated loads. Additionally, the cooling units are showing considerable amounts of distortion current. Solar power plant represents the last recognizable measurement of distortion current indicating that the elevators and EV charging are comparably low sources of distortion in this case.

The bottom part of Fig. 5.5 relates the magnitudes of distortion currents to fundamental frequency currents that transfer the actual net energy and illustrate the connection to active power behaviour. Tenants' electricity draws the majority of I_1, yet ventilation dominates the amount of I_{TD} especially during the working hours, when the demand of change of air is the highest. For the cooling units the flow of I_1 is roughly equal, even though cooling unit 2 is drawing remarkably more distortion current. Furthermore, EV charging and solar power plant are more apparent when I_1 is considered. Overall, the amount of distortion currents seems to comprise less rapid fluctuations during a day than fundamental frequency currents. Furthermore, it can be concluded that increase in the magnitude of I_1 generally results in higher distortion current.

Another area plot in Fig. 5.6 presents a closer examination of distortion currents of the measured loads fed by the main distribution board of service electricity during the day of 3rd of July 2018. The figure uses time period of 1.5 hours for low and high load conditions. Additionally, the distortion current measurement at the mains of service electricity is plotted with the calculated maximum summation of distortion currents of the loads. The calculated summation depicts distortion current that would be measured in case of maximum superposition of distortion currents of the loads. This means that the individual frequency components of the load currents would have equal phase shift when currents are summed at the main distribution board of service electricity. A book of McGranaghan [54] provides further guidance in this matter, in addition to section 2.3.1 in the theory chapter of this thesis.

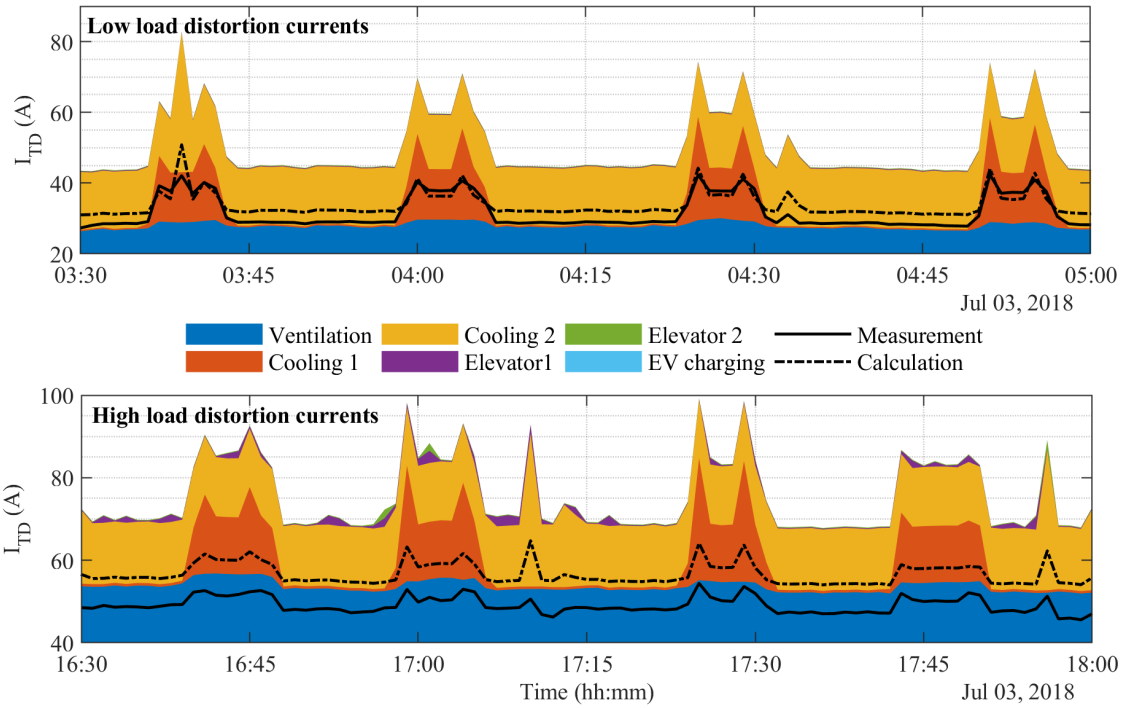

Figure 5.6. *Distortion currents of loads with measured and calculated summation of distortion current of service electricity main distribution board. Measurements are stacked on each other with area plot, excluding the lines of summations, and 1 minute averages of L1 are used from the day of 3rd of July 2018. Top: Distortion currents of low load condition in the morning during 1.5 h. Bottom: Distortion currents of high load condition in the afternoon during 1.5 h.*

According to Fig. 5.6, an evident difference is found between the summation of distortion currents in low and high load conditions. Although the current curves of the cooling units, if magnitude is neglected, remain similar, the measured sum of distortion differs more from the calculated maximum distortion in the high load condition. In low load condition, the calculation and measurement of distortion current match, when the compressor of cooling unit 1 operates. It is notable that I_{TD} of ventilation and the cooling units rise simultaneously in both conditions. These four events of distortion increase in Fig. 5.6 were timed in data browsing to the operation of cooling unit 1, thus ventilation and cooling unit 2 are

somehow excited by cooling unit 1 to produce more distortion current. However, ventilation is only slightly affected. The operation of cooling unit 2 is unnoticeable because it draws no additional distortion current when a compressor starts. During the inspected day no EV charging was measured and the elevators represent merely a ripple on top of the other distortion currents.

Generally, the measured and calculated summations prove that distortion current at the aggregation point of service electricity considerably depends on the load conditions and concurrently operating appliances. Also, the maximal addition of distortion components is rarely achieved and usually cancelling of a some degree occurs for the distortion currents as stated also, for example, by Meyer studying lighting devices [45]. A day with heavier EV charging load should be studied as well as individual harmonics, which are available in the measurements of the building. Eventually, this thesis presents an introduction to the available measurement data and a more profound study considering distortion currents and their summation is possible in the future.

5.2.2 Importance of loads and solar power plant in voltage distortion

In addition to total distortion current, the reasoning for the rather elevated voltage distortion level in the building was studied by means of machine learning (ML) and correlations utilizing data of three weeks. The causes for voltage distortion are generally complex, and thus the source of voltage distortion is often difficult to determine as explained in section 2.3.2 [54]. Therefore, studies have proposed multiple methods to identify the sources of voltage distortion [33]. No similar studies was found in the literature regarding the examinations of this section, however a few other studies were noted using neural networks to detect and classify power quality disturbances [59] and ML to predict energy consumption of a building [47]. Currently ML represents a universally trending topic among researchers and the definitions of ML and other sophisticated data analysis methods remain wide. The studies of this thesis utilizing ML and correlations were made possible by Nyyti Kinnunen from laboratory of pervasive computing at TUT. Kinnunen gives a deeper insight of the used ML methods in her thesis [37]. Without the large amount of data gathered in the pilot the information of this study would have been unfeasible to create.

At first, the idea of ML and correlation studies was to receive another aspect to the previously performed distortion current analysis and study, if the results have common indications. It was also possible that these analyses might reveal new considerable research questions. The voltage distortion analysis began with calculations of correlation coefficients between total voltage distortion (TD_U) of service electricity and powers and currents of the loads and solar power plant within the same main distribution board. Pearson's, Spearman's and Kendall's coefficients were computed to determine the correlation between the studied quantities. The data set of each correlation study was also scatter plotted on a figure for visual inspection. The correlation coefficients of Pearson, Spearman and Kendall differ in

the manner they assess linear relationship and the order of the values. Pearson's coefficient represents the basic understanding of linear correlation and considers the correlation of the quantities in the time domain order of the measurements. Spearman and Kendall utilize ordinal association described further in the book [26]. In brief, the methods of Spearman and Kendall rank the input values during the correlation calculation. The values of the used correlation coefficients vary between -1 and 1, and 0 represent the situation of no correlation.

After the correlation calculations, the importance of features for TD_U of service electricity was examined with ML methods using the measured electrical quantities of the loads and solar power plant as the features. The ML methods involved decision tree and random forest techniques. In more detail, scikit-learn Python library was utilized due to the ease of the feature importance extraction. The model of the ML method was required to include human understandable features, thus black box methods including neural networks were excluded from the studies. The used methods assume the model is sufficiently well trained and has evidently learnt from the data, and therefore the important features can be extracted with confidence from the trained model. In other words, the trained model should adequately predict the studied quantity, TD_U in this case, to have reliable results for the important features.

Decision tree constitutes a structure of if-clauses, questions expressed by the model, that classify the input data. Data elements are directed by the if-clauses until the last level of the decision tree, which is the final classification for the data elements. The decisions at each level of the decision tree present mean squared error (mse), the number of classified samples and the value of the prediction accuracy as the qualities of the model at that level. An example decision tree in Figure 5.7 also demonstrates how the value of the prediction accuracy increases at each level and mse is lowered as the classification improves. Decision tree is generated automatically based on the input data that only consists of the studied quantity and the features of it. Classical examples of test data sets used for ML methods include measures of flowers, e.g. Iris flower data set introduced by Fisher [26]. The ML method called random forest was mainly utilized in this thesis. The method generates a set number of decision trees and derives the model and its quality based on, for example, the average of the individual decision tree classifications. And finally, the model provides the importance of the features. The benefits of random forest, and ML in general, appeared as a great way to develop interdisciplinary research with little expertise requirements on each other's field, in addition to being a straightforward technique to utilize a larger amount of data.

The quantities of the electrical energy system of the building that were involved in the correlation calculations and as the features of service electricity total distortion of voltage (TD_U) are listed as follows: current (I), fundamental frequency active power (P_1), active power (P), fundamental frequency reactive power (Q_1), Fryze's reactive power $\left(Q_f\right)$, fundamental frequency apparent power (S_1), apparent power (S), total distortion of current (TD_I) and

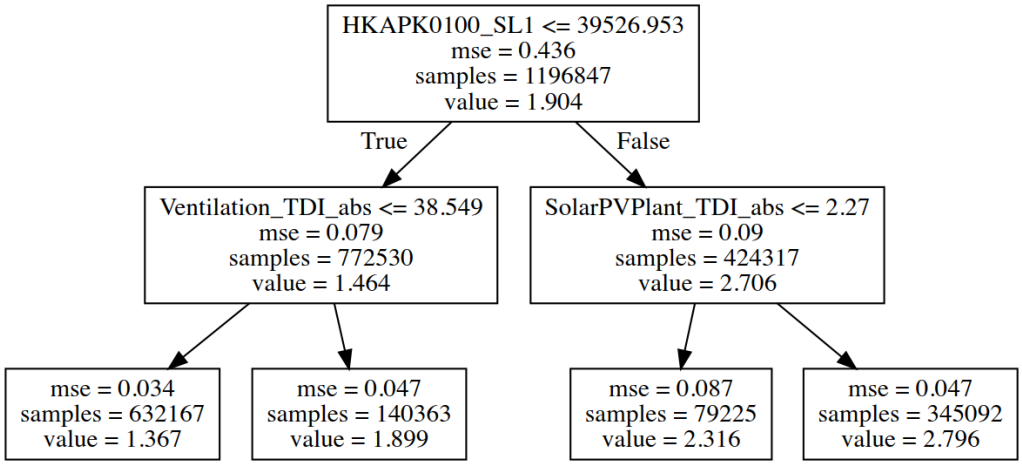

Figure 5.7. *Example of two-level decision tree presenting the questions, if-clauses, created for features of studied total distortion of voltage (TD_U) of service electricity. Each decision lists its mean squared error (mse), number of classified samples and prediction quality.*

absolute total distortion current (I_{TD}). The correlations and random forest model later on utilize three weeks data of 1 second averages between 23.7. and 12.8.2018.

The strongest correlations were found with Pearson's and Spearman's coefficients Kendall generally presenting distinctly the weakest correlation. The most significant correlations were surprisingly computed between service electricity (TD_U) and tenant's electricity. As expected considering distortion current study in section 5.2.1, ventilation and service electricity itself also correlated considerably with distortion voltage, especially in case of I_{TD}, I, Q_f, Q_1 and S. In addition, I_{TD} and negative correlation of Q_f of solar power plant distinguished from the others. Elevator 1 and 2 represent the weakest correlation in Table 5.1, in which the quantities having at least one correlation coefficient > 0.5 are listed. Thus, unexpectedly the cooling units were left outside of the table. The significance of correlation coefficients is difficult to determine, hence the limit of 0.5 for the table was chosen more or less arbitrarily. However, Cohen provides guidance regarding the interpretation of the coefficients in his book [32].

A great portion of the coefficients in Table 5.1 remain below 0.5 and even weaker correlation was calculated for the cooling units and EV charging station that were completely excluded from the table. The highest correlations were found with the linear correlation coefficient of Pearson and the results also indicated that active power relates to the amount of distortion as was observed in the distortion current study of section 5.2.1. The active harmonic distortion has evidently no effect on voltage distortion deduced from the equal numbers of P and P_1 in the correlation table. During the correlation calculations the data was also visualized with scatter plots as shown in Figure 5.8 as an example. The figure presents correlations between TD_U of service electricity and I_{TD} of service and tenants' electricity, which are also found in Table 5.1. The correlation could be demonstrated by fitting a straight line on the scattered data.

Table 5.1. *Pearson's, Spearman's and Kendall's correlation coefficients for total distortion of voltage (TD_U) of service electricity and quantities with at least one coefficient > 0.5 at three phases.*

Quantity		TD_U								
		Pearson			**Spearman**			**Kendall**		
		L1	**L2**	**L3**	**L1**	**L2**	**L3**	**L1**	**L2**	**L3**
Service	I_1	0.58	0.56	0.57	0.53	0.52	0.52	0.37	0.37	0.36
	I	0.6	0.58	0.59	0.56	0.55	0.54	0.39	0.38	0.37
	I_{TD}	0.83	0.76	0.76	0.79	0.77	0.75	0.58	0.54	0.53
	P_1	0.57	0.55	0.56	0.53	0.52	0.52	0.36	0.36	0.36
	P	0.57	0.55	0.56	0.52	0.52	0.52	0.36	0.36	0.36
	Q_1	0.56	0.52	0.5	0.54	0.52	0.5	0.38	0.37	0.35
	Q_f	0.58	0.42	0.39	0.63	0.53	0.5	0.43	0.38	0.36
	S_1	0.58	0.56	0.56	0.53	0.52	0.52	0.37	0.37	0.36
	S	0.6	0.58	0.58	0.55	0.55	0.54	0.38	0.38	0.37
Tenants	I_1	0.85	0.84	0.83	0.78	0.8	0.79	0.57	0.6	0.58
	I	0.85	0.84	0.83	0.78	0.8	0.79	0.57	0.6	0.58
	I_{TD}	0.82	0.83	0.8	0.74	0.76	0.74	0.52	0.55	0.52
	P_1	0.85	0.84	0.83	0.78	0.8	0.79	0.57	0.59	0.58
	P	0.85	0.84	0.83	0.78	0.8	0.79	0.57	0.59	0.58
	S_1	0.85	0.84	0.83	0.78	0.8	0.79	0.57	0.59	0.58
	S	0.85	0.84	0.83	0.78	0.8	0.79	0.56	0.59	0.58
Solar	I_1	0.65	0.64	0.64	0.7	0.66	0.68	0.48	0.45	0.47
	I	0.65	0.64	0.64	0.72	0.67	0.7	0.51	0.47	0.49
	I_{TD}	0.87	0.85	0.86	0.85	0.82	0.83	0.65	0.61	0.63
	P_1	0.65	0.64	0.64	0.71	0.67	0.7	0.5	0.47	0.5
	P	0.65	0.64	0.64	0.71	0.67	0.7	0.5	0.47	0.5
	Q_1	-0.56	-0.5	-0.54	-0.64	-0.47	-0.6	-0.45	-0.32	-0.42
	Q_f	-0.79	-0.76	-0.77	-0.8	-0.76	-0.78	-0.6	-0.56	-0.58
	S_1	0.65	0.64	0.64	0.7	0.66	0.68	0.48	0.45	0.47
	S	0.65	0.64	0.64	0.71	0.67	0.69	0.5	0.47	0.48
Elevator 1	I	0.25	0.24	0.25	0.7	0.64	0.74	0.48	0.43	0.53
	I_{TD}	0.29	0.3	0.29	0.67	0.51	0.73	0.47	0.35	0.52
	S	0.25	0.24	0.25	0.56	0.55	0.71	0.37	0.36	0.5
Elevator 2	I	0.16	0.16	0.18	0.7	0.59	0.76	0.49	0.39	0.55
Ventilation	I_1	0.54	0.52	0.59	0.53	0.52	0.58	0.36	0.37	0.39
	I	0.8	0.79	0.79	0.74	0.78	0.75	0.51	0.54	0.52
	I_{TD}	0.92	0.91	0.91	0.84	0.83	0.81	0.62	0.62	0.6
	P_1	0.53	0.51	0.58	0.53	0.53	0.59	0.36	0.37	0.4
	P	0.52	0.5	0.57	0.52	0.52	0.59	0.35	0.37	0.4
	Q_1	0.94	0.89	0.88	0.85	0.84	0.83	0.65	0.63	0.62
	Q_f	0.87	0.51	0.25	0.53	0.01	-0.29	0.31	-0.05	-0.24
	S_1	0.54	0.52	0.59	0.52	0.51	0.58	0.35	0.36	0.39
	S	0.79	0.79	0.79	0.74	0.77	0.75	0.5	0.54	0.51

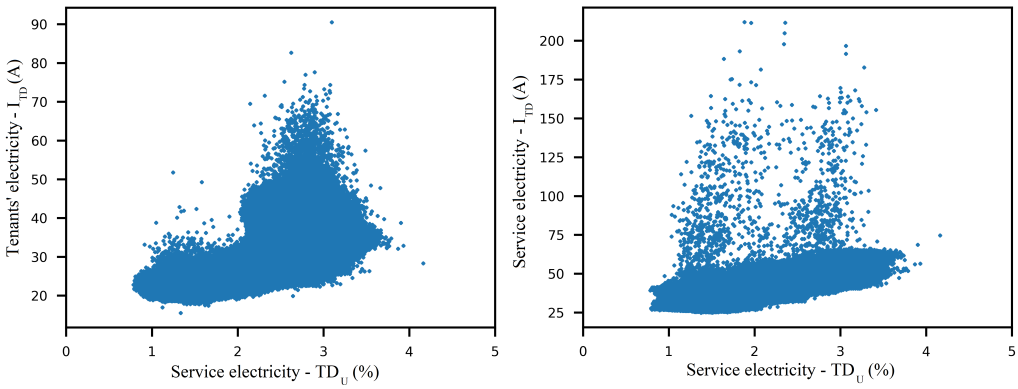

Figure 5.8. *Correlation demonstrated with scattered plot between TD_U of service electricity and I_{TD} of service and tenants' electricity at L1.*

The model of random forest method was trained with a promising prediction accuracy, when the data of 1 second averages from the time period of 23.7.-12.8.2018 was utilized. These summer weeks included a high usage of the cooling units and production of solar power plant. Timestamps of the measurements were deleted denying the time to be overly dominant feature since the electrical quantities were the main focus. The model was set to use 20 decision trees and three phases were considered separately. The measurement data was fed to the random forest model in chronological order as the data sets of each 1 second average. The quality of the trained random forest model can be inspected with R^2 and *mse* values in Table 5.2. The value of R^2 evaluates the correlation between the prediction and the original data of the studied quantity during the studied time period. *mse* is the square of the average of the error between the prediction and the actual value of the quantity. Table 5.2 also compares the prediction to the average and median of the studied quantity to illustrate the feasibility of the trained model. The average represents a constant prediction computed as the arithmetical average of the values of the studied quantity TD_U. Similarly the median predicts TD_U as the middlemost value of TD_U when the values are sorted by the magnitude.

Table 5.2. *Quality of trained 20-tree random forest model compared with quality of average and median of studied quantity TD_U using R^2 and mse values.*

	TD_U								
	Average			**Median**			**Trained model**		
	L1	**L2**	**L3**	**L1**	**L2**	**L3**	**L1**	**L2**	**L3**
R^2	0.000	0.000	0.000	-0.168	-0.146	-0.140	0.979	0.976	0.977
mse	0.436	0.410	0.354	0.510	0.470	0.404	0.008	0.009	0.007

When inspecting Table 5.2, it is concluded that the quality of the prediction, R^2, equals zero for the average and a negative value for median. This means that the average of the studied value is a more successful estimate than the median of the studied quantity data set. However, R^2 of the average is still zero giving no proper prediction of TD_U. The prediction

of the trained model represents a fair correlation with the actual measurement of TD_U because R^2 nearly equals to 1, which is the maximum correlation. Thus, if the original data of the feature quantities of TD_U is fed to the trained model in chronological order, the model can predict the value of TD_U accurately throughout the studied time period. The error, *mse*, is evaluated below 0.01 for the trained model, however no explanation of respectable value of *mse* or R^2 was found, thus they are concerned as ambiguous as the correlation coefficients. Nevertheless, the quality of the trained model is considered acceptable and potential for future studies, and overall the study proposes that the data of the electrical energy system is capable to create a model that predicts the behaviour of the system.

The importance of each feature of the trained model was extracted and inspected for three phases. In practice, the model yielded a sorted feature importance list that consisted of the electrical quantities of the measurement points. The sum of the importance equals to 1, which is divided between the features. Figure 5.9 shows ten most important features for three phases based on the trained random forest model. Importance is further described by Breiman [5] and here importance represents a factor derived by the model. The trained model claims that tenants' electricity represents the most meaningful factor for TD_U of service electricity in all three phases. In addition, ventilation and solar power plant and cooling unit 1 are considered important. The importance of these measurements is in line with the study of distortion current in section 5.2.1, although the great importance of tenant's electricity was unforeseen. Quantity wise the most frequently are listed I_{TD}, TD_I, Q_f and I_1, of which TD_I raised interest because the rest were expected after the study of distortion currents in section 5.2.1.

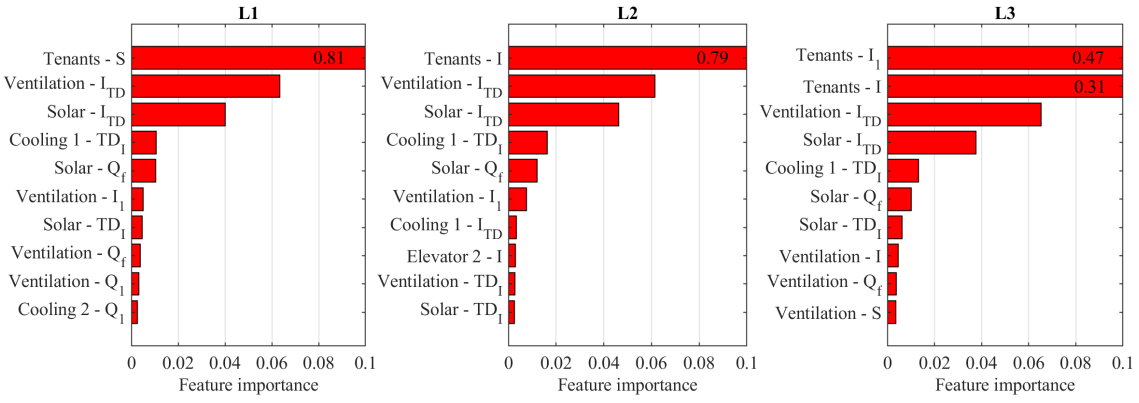

Figure 5.9. *Top ten of feature importance for total distortion of voltage (TD_U) of service electricity at three phases.*

Tenants' electricity represents occasionally three times larger load than service electricity, which could provide a reasoning for the importance of it in Fig. 5.9. The importance of tenants' electricity relates to the magnitudes of S, I and I_1 that closely correlate with active power demand. In contrast, the importance of solar power plant and ventilation relies on I_{TD} and Q_f, which are still connected, but more loosely, to active power. The analysis of distortion current in section 5.2.1 revealed that active power and distortion current are

related, however ventilation was concluded as the main source of distortion current instead of tenants' electricity. Eventually, voltage distortion is caused by distortion current, which should be acknowledged when considering the results of the trained model. Additionally, it remains unclear is the reason of elevated service electricity TD_U the result of distortion current of tenants' electricity, or is voltage distortion affecting the distortion current of tenants' electricity. This study also promotes the absolute value of distortion, I_{TD}, over the fundamental frequency related TD_I as an indicator of the source of voltage distortion.

Overall, the correlation coefficient calculations, the trained random forest model and the study of total distortion currents conform with their outcomes. Tenants' electricity and ventilation are deduced as the main sources of distortion and the quantities including I_{TD} and Q_f are emphasized. Ultimately, the studies are raising more questions than answers, and therefore the upcoming studying possibilities are diverse. For instance, more profound familiarization with ML methods and addition of the data of building automation and weather would utilize more widely the capabilities of the pilot.

5.3 Differences in power quantities

Since the installed meters in the pilot provide a wide variety of electrical quantities the measuring of power can be analyzed diversely and especially reactive and distortion power are considered in this section. The concern on power quality has increased as numerous new solar power plants and power electronics devices, e.g. EV chargers, are connected to LV distribution networks every year. This study is motivated by an idea to quantify disturbances possibly induced by the new devices by means of voltage and current distortion using a power measurement. One day the disturbances may yield a cost for distribution network customers, and that requires a proper practice to quantify the caused disturbances. Here, the measurements of Fryze's reactive power (Q_f) are compared with distortion of current and voltage and also with active (P) and fundamental frequency reactive power (Q_1). The measurements include the loads and solar power plant of service electricity and tenants' electricity.

The analysis uses time averages of 1 minute as the result of the time averaging study in section 5.1. The presented power quantities are based on the explanations in the theory part of the thesis in section 2.4. The theory and the measurements of the section emphasize the difference between Q_1 and Q_f due to alternative frequency components they contain. The value of Q_1 solely consists of the magnitude of the fundamental frequency reactive power resulting from phase shift between fundamental frequency voltage and current. On the contrary to Q_1, the reactive quantity of Q_f involves reactive power of the whole measurement bandwidth, until 2 kHz in these measurements. More specifically, also non-harmonic distortion power, interharmonics below and above fundamental frequency, is concerned in Q_f in this case. Furthermore, Fryze's power theory divides apparent power to active and reactive power, and moreover active power can be split to distortion and fundamental frequency components. In Figure 5.10 Fryze's reactive power (Q_f) is compared with the

absolute values of current (I_{TD}) and voltage distortion (U_{TD}) and fundamental frequency reactive power (Q_f), in addition to active power (P) and active distortion power (P_{TD}).

Fig. 5.10 mainly utilizes the measurements of 3rd of July 2018. However, solar power plant and EV charging are presented on 25th and 4th of July 2018, respectively, to illustrate their behaviour due to low active powers on 3rd of July. The reasoning for the using of various days within the same figure is discussed in the beginning of section 5.2.1, in which it is emphasized that one should make no conclusions about the summation of the quantities or the interaction between the measurement points based on the figure, which is Fig. 5.10 in this case. Defect is found in the measurements of 3rd of July due to short interruption in the data collection, anyhow the day represents a good example case, and thus the data is utilized in this study. From Fig. 5.10 one can observe the effect of I_{TD}, U_{TD} and Q_1 on Q_f and how P relates to their magnitudes. Additionally, the amount of P_{TD} in contrast to reactive powers can be observed. Except for Q_1, the measurements are stacked on each other with area plot method similarly to currents in Fig. 5.5. This practice of presentation is used to demonstrate the relation between the measurement points more visibly.

The behaviour of Q_f and I_{TD} in Fig. 5.10 suggest that distortion current induces a large portion of Q_f. This is understandable when the magnitudes of I_{TD} and U_{TD} are compared the value of I_{TD} generally being ten times higher. The magnitude of Q_f also contains Q_1 in absolute manner, although especially for ventilation Q_1 represents a minor magnitude to distortion power according to Fig. 5.10. These observations indicate that the source of distortion current can be traced with the value of Q_f in this electrical energy system. Yet, the cause of voltage distortion still remains complex. Additionally, the curves of Q_f seem to include noise-like behaviour regarding I_{TD}, which can result from the varying voltage in general and the component of Q_1. To support the visual inspections from Fig. 5.10, the correlations between Q_f and the other studied measurements are listed in Table 5.3. The correlation coefficients of the table utilize Pearson's method, which was also studied, and indicated the highest correlations, in voltage distortion section 5.2.2. The table indicates that other quantities than U_{TD} embrace notable correlation with Q_f for all of the loads excluding cooling unit 2. The studied measurements of cooling unit 2 in this case included a constant magnitude of I_{TD} that may result in low correlation.

Conventionally, the electrical engineers consider the value of Q_1 in reactive power tariffs and, for example, in the evaluation of the distribution network performance [57]. The measurements of Fig. 5.10 prove that the other frequency components than fundamental frequency have a remarkable impact on the reactive power measurement. The values of Q_f depict a completely different feature of the system than Q_1, thus the engineer responsible of the measurements must be aware of the definition of the used power quantity. This is emphasized in the increasingly distorted conditions of the distribution networks and also concerned in Emanuel's paper [18], in which the separation of fundamental frequency and distortion component of reactive power is argued for. The usage of Q_f may find its place in the LV distribution network measurements because it quantifies distortion and fundamental frequency reactive power of the measurement point both of them representing

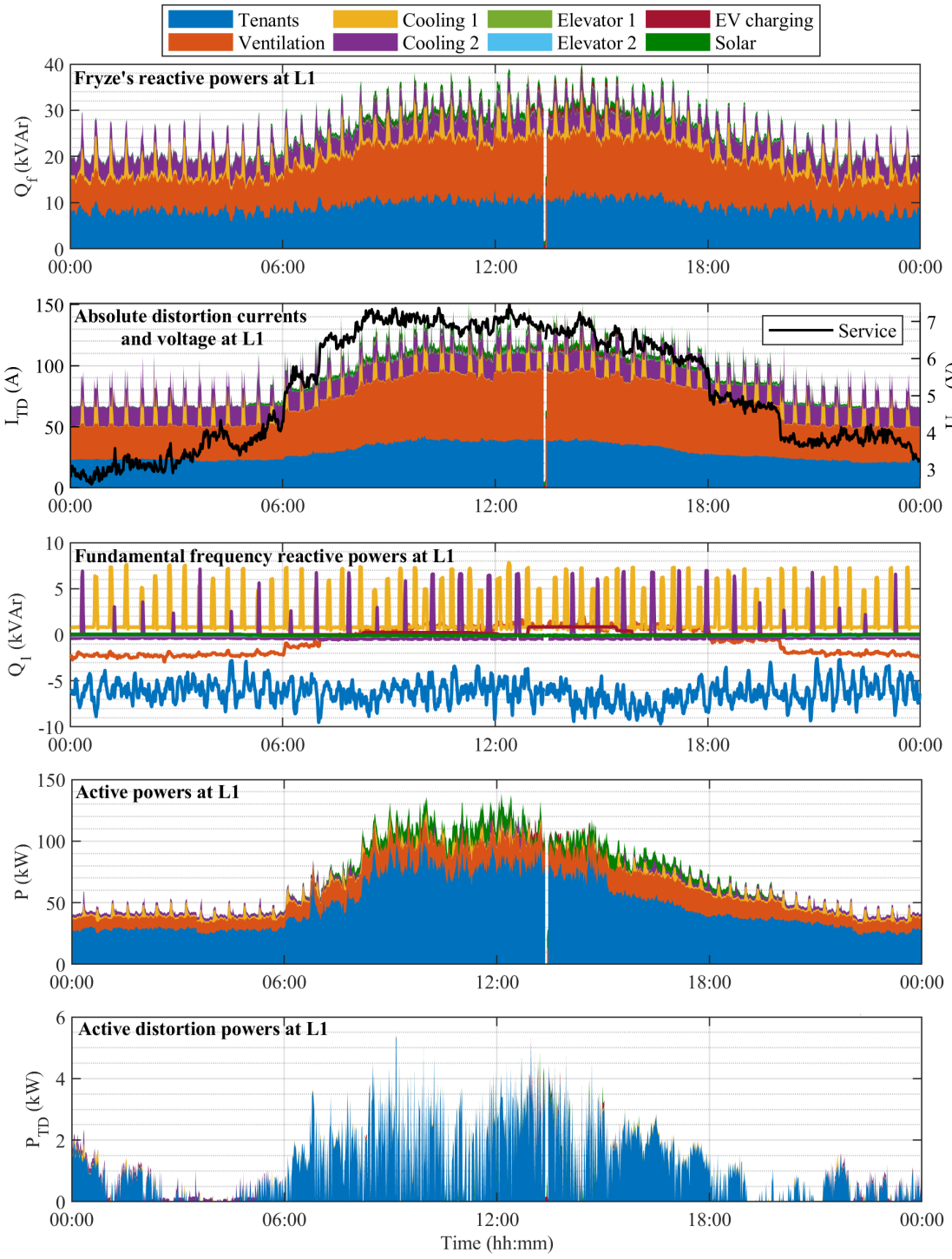

Figure 5.10. *Fryze's reactive power (Q_f) compared to distortion current (I_{TD}) and voltage U_{TD} and fundamental frequency reactive power (Q_1). In addition, active power (P) and active distortion power (P_{TD}) are presented for a day. The measurements are shown for the loads and solar power plant of service electricity and tenants' electricity at L1 as 1 minute averages.*

uncontrollable and undesired quantity at the customer's access point. The conventional LV distribution networks are considered usually majorly resistive in nature, thus reactive power cannot be well utilized, e.g. in voltage control. However, currently Finland is investing in underground cabling of MV and LV distribution networks, which shifts the reactivity of the networks. Discussion is also going on considering the responsibilities of the customers and DSOs on disturbances in the distribution networks. For example, Marnay speculates two visions of power quality in the future considering super grid and dispersed grid that either provide homogeneous or heterogeneous quality of electricity [42]. The billing of disturbances will probably require simple and practical measures that reveal the disturbances, such as the distortion studied in this thesis, and reliably allocate the disturbances to the correct source.

Active power is also shown in Fig. 5.10 to relate the amount of reactive powers to the power actually transferring energy. Similar comparison was made in Fig. 2.7, and active power was concluded to correlate strongly with distortion as also can be read from Table 5.3. To demonstrate the significance of active distortion power P_{TD} was added to Fig. 5.10. The figure indicates that active distortion power is hardly present except for tenants' electricity, although the origin of P_{TD} remains unclear. Either an error is found in the measurements or calculations, or the numerous electrically coupled devices of tenants generate also active distortion power. Nevertheless, the values of P_{TD} confirm that most of the distortion can be quantified with Q_f.

Table 5.3. *Pearson's correlation coefficients for Fryze's reactive power (Q_f) and the compared quantities in cases of different loads.*

		I_{TD}	U_{TD}	Q_1	P
Q_f	Tenants	0.82	0.73	-0.68	0.73
	Ventilation	0.99	0.94	0.99	0.98
	Cooling 1	0.84	0.06	0.94	0.98
	Cooling 2	0.41	-0.05	0.97	0.97
	Elevator 1	0.99	0.44	0.87	0.99
	Elevator 2	0.99	0.28	0.84	0.98
	EV charging	0.98	0.52	0.99	-0.9760
	Solar	0.97	0.92	-0.84	0.94

The development of the power and power quality measurement practices in the future depends on standardization, legislation and the financial motives of DSOs. The power meter manufacturers follow certain standards, e.g. IEC 62053-22 and -23 for the quantification of active and reactive power and energy. Still during the thesis it was noted that the manuals of power meters may inaccurately describe the actual measurement techniques and quantities of the meters, which was also demonstrated by comparing two meters at the same measurement point. For example, it should be verified is the measurement of reactive

power representing Q_1, Q_f or something else. In critical cases the billing of electricity can be affected by false measurements [6, 18]. In addition to utilized power theory and implementation of it in the meter, inaccuracies in distortion power measurements may result from inappropriate current transformers or other instruments used in the measurements.

This study encourages into a deeper survey of power theories and their application in the modern distribution networks. The capabilities of the unutilized measurements of the pilot building include the data of over an year from three-phases of the electrical energy system. Additionally, the diverse measurement quantities enable calculations of various other electrical quantities that could be utilized, e.g. in finding the origins of voltage distortion and in other studies considering the quantification of disturbances of distortion in distribution networks.

6. CONCLUSION

The thesis is based on a research project relating to the pilot building of Kampusareena and the implementation of the ICT system, which collected the utilized measurements. The measurements enabled the electrical behaviour study of the building and the more sophisticated analyses of time averaging of power and the sources of voltage and current distortion and their impact on distortion power. The chapters of the thesis examine the theory and practices of measuring voltage and current distortion and power, describe the designed pilot environment and lastly illustrate and analyze the measurement data.

The topical power quality and power concerns about voltage and current distortion and fluctuation of power originate from the development of technologies, which promote the utilization of distributed power generation and modern power electronics loads. Moreover, the intermittent features of distributed generation, e.g. solar power, with the generalizing load control and the evolving electricity markets introduce changes in the power flows of the conventional distribution networks. The nonlinear loads of power electronics cause distortion in current that can be measured with the quantity of total distortion, which is expressed either in relation to the fundamental frequency component or in an absolute manner. Even if easily measured, the source of voltage distortion remains as a complex research question due to the background voltage distortion and its interaction with the devices. Currently power quality monitoring relies on customer complaints voltage distortion being one of the causes of poor power quality.

Several power theories are available to quantify power in addition to the conventionally used practices. Apparent power can be divided into parts containing various frequency components and physical meanings. However, complicated power theories are found impractical by a regular electrical engineer. Thus, the simpler theory of Fryze is studied further in the analyses. The literature demonstrated that the measuring of power requires revising due to the increasingly distorted conditions of distribution networks. The distorted conditions result in varying readings of power meters, and therefore inaccurate power measurements and false electrical energy billing may occur. In general, the advanced technology enables the design of any desired electricity meter, however, the measuring in distorted conditions should be handled.

The pilot taught lessons regarding the management and unification of the collected data while the ICT system was implemented with the measurements of the electrical energy system. Choices had to be made considering the time resolution and measurement quantities because it was infeasible to gather the all available data of every data source. The issues in the data collection involved the transferring and storing of the data without large delays and filling of data storage. The measurements of the electrical energy system comprise different

types of appliances including elevators, cooling units, EV charging devices, ventilation units, solar photovoltaic power plant and their aggregation at the main distribution boards of service electricity and tenant's electricity. Ultimately, the measurements describe the conditions of the multi-user office building of Kampusareena, even though the thesis also generally discusses LV distribution networks. Overall, the pilot served as a diverse research platform during the ProCem project.

The electrical behaviour of the measurement points was inspected using the quantities of powers, power factors and distortion current and voltage during three individual days. The conditions of the days varied regarding solar irradiance and EV charging. The time resolution of 1 second depicted the behaviour of the electrical energy system in detail, and thereby also the behaviours of certain short time period operations during the day are illustrated for the elevators and cooling units. The study indicates that the impact of solar power plant on the electrical energy system relates mostly to active power. Additionally, the inverse difference was shown between the measurements of fundamental frequency related and absolute total distortion currents. Voltage distortion was stated similar across the measurement points due to the voltage stiffness of the electrical network, however the voltage distortion increased by approximately 2 percent during the working hours.

With the aid of cumulative distributions the study of the time averaging revealed the time domain characteristics of active, fundamental frequency reactive and Fryze's reactive power at the measurement points of the building. It was noted that 1 minute averaging mostly conforms with 1 second averages, thus the measurements of 1 second provide only little additional information in time domain. However, for the elevators 1 second represented distinctly the most accurate average. The time averaging study also summarized the maximum and minimum powers and concluded that tenants' electricity, ventilation and the cooling units consume the largest active power while the elevators and EV charging have in general a minor effect on the electrical energy system. Fundamental frequency reactive power contains the fastest fluctuations regarding the influence of the time averaging. The cooling units were found the most inductive loads because of the compressors, and tenants' electricity produces the highest capacitive reactive power. Fryze's reactive power involved significantly less time variation due to the addition of distortion power and the largest magnitudes were quantified in cases of ventilation, the cooling units and tenant's electricity.

The source of distortion current was traced by comparing the absolute values of total distortion. The results showed that tenants' electricity and ventilation draw the highest distortion current before the cooling units and solar power plant. The same comparison also indicated that distortion current increases with fundamental frequency current and the magnitude of distortion current contains less variation than fundamental frequency current. The current distortion of ventilation is assumed to origin from numerous frequency converters with diode rectification. The blend of tenants' devices includes the lighting equipment and the appliances of tenants. In addition, the brief study of the summation of

distortion current at the main distribution board demonstrated that more cancellation of harmonics occurs in the high load than low load conditions.

Considering the source of voltage distortion the machine learning method of random forest and correlation coefficients resulted in similar indications as the study of distortion currents. Tenants' electricity was highlighted as the main cause of voltage distortion for the main distribution board of service electricity, and ventilation and solar power plant were listed the next in significance. Generally, the quantities of I_{TD}, Q_f and I_1 had the strongest relation to voltage distortion. The model of random forest was trained promisingly well as it predicted the voltage distortion accurately, although the sources of voltage distortion were left undefined. The distortion was further analyzed using Fryze's reactive power and it was recognized that current represents the main contribution to distortion in Fryze's reactive power due to the low amount of absolute voltage distortion. Furthermore, the measurements of Fryze's and fundamental frequency reactive power differ remarkably because of the majorly reactive nature of distortion current, thus Fryze's theory seems to quantify well the disturbances of current distortion.

The thesis promotes several areas of further research as multiple aspects of the measurements were analyzed. The normal practice of total powers in distribution networks supports expanding the studies to three phases. On the other hand, the development of Fryze's power theory towards practical cases considering its limitations and weaknesses seems relevant. The summation study of distortion would yield more profound results, if the available magnitudes of individual harmonics were used. In addition, different machine learning methods could be investigated to fully utilize the data of the pilot by including the weather conditions and building automation variables in the studies.

REFERENCES

[1] J. Arrillaga, D.A. Bradley, P.S. Bodger, Power system harmonics, Wiley, Chichester, 1985.

[2] R. Arseneau, Y. Baghzouz, J. Belanger, K. Bowes, A. Braun, A. Chiaravallo, M. Cox, S. Crampton, A. Emanuel, P. Filipski, E. Gunther, A. Girgis, D. Hartmann, S.D. He, G. Hensley, D. Iwanusiw, W. Kortebein, T. McComb, A. McEachern, T. Nelson, N. Oldham, D. Piehl, K. Srinivasan, R. Stevens, T. Unruh, D. Williams, Practical definitions for powers in systems with nonsinusoidal waveforms and unbalanced loads: a discussion, IEEE Transactions on Power Delivery, Vol. 11, Iss. 1, 1996, pp. 79–101.

[3] M.H. Bollen, Understanding Power Quality Problems: Voltage Sags and Interruptions, Vol. 5, John Wiley & Sons, 1999.

[4] M.H. Bollen, R. Das, S. Djokic, P. Ciufo, J. Meyer, S.K. Rönnberg, F. Zavodam, Power quality concerns in implementing smart distribution-grid applications, IEEE Transactions on Smart Grid, Vol. 8, Iss. 1, 2017, pp. 391–399.

[5] L. Breiman, Random forests, Machine Learning, Vol. 45, Iss. 1, Oct, 2001, pp. 5–32.

[6] A. Cataliotti, V. Cosentino, S. Nuccio, The measurement of reactive energy in polluted distribution power systems: An analysis of the performance of commercial static meters, IEEE Transactions on Power Delivery, Vol. 23, Iss. 3, 2008, pp. 1296–1301.

[7] L.S. Czarnecki, What is wrong with the Budeanu concept of reactive and distortion power and why it should be abandoned, IEEE Transactions on Instrumentation and Measurement, Vol. 36, Iss. 3, 1987, pp. 834–837.

[8] F.C. De La Rosa, Harmonics and Power Systems, CRC Press, Baton Rouge, 2006.

[9] Electricity metering equipment (AC) – General requirements, tests and test conditions – Part 11: Metering equipment, IEC 62052-11:2003+AMD1:2016 CSV, 2016, p. 85.

[10] Electricity metering equipment (AC) – Particular requirements – Part 21: Static meters for active energy (classes 1 and 2), IEC 62053-21:2003+AMD1:2016 CSV, 2016, p. 45.

[11] Electricity metering equipment (AC) – Particular requirements – Part 23: Static meters for reactive energy (classes 2 and 3), IEC 62053-23:2003+AMD1:2016 CSV, 2016, p. 35.

[12] Electromagnetic compatibility (EMC) – Part 3-2: Limits – Limits for harmonic current emissions (equipment input current ≤ 16 A per phase), IEC 61000-3-2:2018, 2018, p. 73.

[13] Electromagnetic compatibility (EMC) – Part 4-30: Testing and measurement techniques – Power quality measurement methods, IEC 61000-4-30:2015, 2015, p. 150.

[14] Electromagnetic compatibility (EMC) – Part 4-7: Testing and measurement techniques – General guide on harmonics and interharmonics measurements and instrumentation, for power supply systems and equipment connected thereto, IEC 61000-4-7:2002+A1:2008, 2008, p. 86.

[15] A.I. Elombo, T. Morstyn, D. Apostolopoulou, M.D. McCulloch, Residential load variability and diversity at different sampling time and aggregation scales, in: 2017 IEEE AFRICON, 2017, pp. 1331–1336.

[16] A.E. Emanuel, Powers in nonsinusoidal situations – a review of definitions and physical meaning, IEEE Transactions on Power Delivery, Vol. 5, Iss. 3, 1990, pp. 1377–1389.

[17] A.E. Emanuel, Summary of IEEE standard 1459: definitions for the measurement of electric power quantities under sinusoidal, nonsinusoidal, balanced, or unbalanced conditions, IEEE Transactions on Industry Applications, Vol. 40, Iss. 3, 2004, pp. 869–876.

[18] A.E. Emanuel, Non-sinusoidal reactive power and its impact on smart meter infrastructure in the era of smart grid, in: 2012 IEEE Power and Energy Society General Meeting, 2012, p. 4.

[19] J.H.R. Enslin, P.J.M. Heskes, Harmonic interaction between a large number of distributed power inverters and the distribution network, IEEE Transactions on Power Electronics, Vol. 19, Iss. 6, 2004, pp. 1586–1593.

[20] P.S. Filipski, Y. Baghzouz, M.D. Cox, Discussion of power definitions contained in the IEEE Dictionary, IEEE Transactions on Power Delivery, Vol. 9, Iss. 3, 1994, pp. 1237–1244.

[21] P.S. Filipski, P.W. Labaj, Evaluation of reactive power meters in the presence of high harmonic distortion, IEEE Transactions on Power Delivery, Vol. 7, Iss. 4, 1992, pp. 1793–1799.

[22] S. Firth, K. Lomas, A. Wright, R. Wall, Identifying trends in the use of domestic appliances from household electricity consumption measurements, Energy and Buildings, Vol. 40, Iss. 5, 2008, pp. 926–936.

[23] J.M. Guerrero, F. Blaabjerg, T. Zhelev, K. Hemmes, E. Monmasson, S. Jemei, M.P. Comech, R. Granadino, J.I. Frau, Distributed generation: Toward a new energy paradigm, IEEE Industrial Electronics Magazine, Vol. 4, Iss. 1, 2010, pp. 52–64.

[24] Guidelines of good practice on the implementation and use of voltage quality monitoring systems for regulatory purposes, Council of European Energy Regulators (CEER), 2012, p. 56.

[25] V. Heikkilä, Data gathering from IoT devices, Master of Science Thesis, In progress.

[26] M. Hollander, D.A. Wolfe, E. Chicken, Nonparametric Statistical Methods, 3rd ed., John Wiley & Sons Ltd, USA, 2014.

[27] IEEE recommended practice and requirements for harmonic control in electric power systems, IEEE Std 519-2014, 2014, p. 29.

[28] IEEE Recommended Practice for Monitoring Electric Power Quality, IEEE Std 1159-2009, 2009, p. 81.

[29] IEEE Recommended Practice for the Instrumentation and Metering of Industrial and Commercial Power Systems, IEEE Std 3001.8-2013, 2013, p. 31.

[30] IEEE Standard definitions for the measurement of electric power quantities under sinusoidal, nonsinusoidal, balanced, or unbalanced conditions, IEEE Std 1459-2010, 2010, p. 50.

[31] A. Ipakchi, F. Albuyeh, Grid of the future, IEEE Power and Energy Magazine, Vol. 7, Iss. 2, 2009, pp. 52–62.

[32] C. Jacob, Statistical Power Analysis for the Behavioral Sciences, 2nd ed., Lawrence Erlbaum Associates, USA, 1988.

[33] A. Kalair, N. Abas, A. Kalair, Z. Saleem, N. Khan, Review of harmonic analysis, modeling and mitigation techniques, Renewable and Sustainable Energy Reviews, Vol. 78, 2017, pp. 1152–1187.

[34] Kampusareena: A new spark to campus life -web page, http://www.tut.fi/en/kampusareena/. Accessed: 31.10.2018.

[35] A.I. Kenttälä, Jakeluverkon loistehohallinnan suunnitelma, Diplomityö, 2016, p. 101.

[36] J. Kilter, J. Meyer, B. Howe, F. Zavoda, L. Tenti, J.V. Milanovic, M. Bollen, P.F. Ribeiro, P. Doyle, J.M.R. Gordon, Current practice and future challenges for power quality monitoring - CIGRE WG C4.112 perspective, in: 2012 IEEE 15th International Conference on Harmonics and Quality of Power, 2012, pp. 390–397.

[37] N. Kinnunen, Decision tree learning with hierarchical features, Master of Science Thesis, 2018, p. 67.

[38] P. Koponen, Sparse sampling methods for power quality monitoring, Dissertation, Vol. 379, 2002, p. 301.

[39] LEMENE project -web page, http://www.lempaalanenergia.fi/content/fi/1/20126/LEMENE.html. Accessed: 31.10.2018.

[40] Loistehon kompensointi ja yliaaltojen rajoittaminen, Sähköenergialiitto ry Sener, 1999, p. 75.

[41] J. Luoma, Liike- toimisto- ja koulurakennuksien sähkökuormat kysynnän jouston reserveinä, Diplomityö, 2015, p. 96.

[42] C. Marnay, Microgrids and heterogeneous security, quality, reliability, and availability, in: 2007 Power Conversion Conference - Nagoya, 2007, pp. 629–634.

[43] C. Marnay, S. Chatzivasileiadis, C. Abbey, R. Iravani, G. Joos, P. Lombardi, P. Mancarella, J. von Appen, Microgrid evolution roadmap, in: 2015 International Symposium on Smart Electric Distribution Systems and Technologies (EDST), 2015, pp. 139–144.

[44] J. Meyer, M. Bollen, H. Amaris, A.M. Blanco, A.G. de Castro, J. Desmet, M. Klatt, L. Kocewiak, S. Rönnberg, K. Yang, Future work on harmonics - some expert opinions: Part II – supraharmonics, standards and measurements, in: 16th International Conference on Harmonics and Quality of Power (ICHQP), 2014, pp. 909–913.

[45] J. Meyer, P. Schegner, K. Heidenreich, Harmonic summation effects of modern lamp technologies and small electronic household equipment, Conference on Electricity Distribution (CIRED), Jan. 2011, p. 4.

[46] J.V. Milanovic, J. Meyer, R.F. Ball, W. Howe, R. Preece, M.H.J. Bollen, S. Elphick, N. Cukalevski, International industry practice on power-quality monitoring, IEEE Transactions on Power Delivery, Vol. 29, Iss. 2, 2014, pp. 934–941.

[47] J. Moon, J. Park, E. Hwang, S. Jun, Forecasting power consumption for higher educational institutions based on machine learning, The Journal of Supercomputing, Vol. 74, Iss. 8, Aug, 2018, pp. 3778–3800.

[48] M. Newborough, P. Augood, Demand-side management opportunities for the UK domestic sector, IEE Proceedings - Generation, Transmission and Distribution, Vol. 146, Iss. 3, 1999, pp. 283–293.

[49] P. Pakonen, A. Hilden, T. Suntio, P. Verho, Grid-connected PV power plant induced power quality problems – Experimental evidence, in: 18th European Conference on Power Electronics and Applications (EPE'16 ECCE Europe), 2016, p. 10.

[50] I. Richardson, M. Thomson, D. Infield, A. Delahunty, A modelling framework for the study of highly distributed power systems and demand side management, in: 2009 International Conference on Sustainable Power Generation and Supply, 2009, pp. 1–6.

[51] S.K. Rönnberg, M.H. Bollen, H. Amaris, G.W. Chang, I.Y. Gu, L.H. Kocewiak, J. Meyer, M. Olofsson, P.F. Ribeiro, J. Desmet, On waveform distortion in the frequency range of 2 khz–150 khz – Review and research challenges, Electric Power Systems Research, Vol. 150, 2017, p. 10.

[52] H. Saari, P. Koponen, E. Tahvanainen, T. Lindholm, Remote reading and data management system for kWh-meters with power quality monitoring, in: Eighth International Conference on Metering and Tariffs for Energy Supply (Conf. Publ. No. 426), 1996, pp. 11–15.

[53] I.A. Sajjad, G. Chicco, R. Napoli, A statistical analysis of sampling time and load variations for residential load aggregations, in: 2014 IEEE 11th International Multi-Conference on Systems, Signals and Devices (SSD14), 2014, pp. 1–6.

[54] S. Santoso, M.F. McGranaghan, R.C. Dugan, H.W. Beaty, Electrical power systems quality, 3rd ed., McGraw-Hill, New York, 2012.

[55] Social Energy – Prosumer Centric Energy Ecosystem (ProCem) -web page, http://www.senecc.fi/projects/procem-2. Accessed: 31.10.2018.

[56] Sähkömarkkinalaki, 9.8.2013/588, 2013.

[57] Tampereen Sähköverkko Oy, Loistehon hinnoittelu ja kompensointi, 2018, p. 4.

[58] Tilastokeskus, Sähkön ja lämmön tuotanto 2016, 2017, p. 12.

[59] M. Valtierra-Rodriguez, R. de Jesus Romero-Troncoso, R.A. Osornio-Rios, A. Garcia-Perez, Detection and classification of single and combined power quality disturbances using neural networks, IEEE Transactions on Industrial Electronics, Vol. 61, Iss. 5, May, 2014, pp. 2473–2482.

[60] Voltage characteristics of electricity supplied by public electricity networks, SFS-EN 50160, 2010, p. 66.

[61] J. Widén, E. Wäckelgård, J. Paatero, P. Lund, Impacts of different data averaging times on statistical analysis of distributed domestic photovoltaic systems, Solar Energy, Vol. 84, Iss. 3, 2010, pp. 492–500.

[62] A. Wright, S. Firth, The nature of domestic electricity-loads and effects of time averaging on statistics and on-site generation calculations, Applied Energy, Vol. 84, Iss. 4, 2007, pp. 389–403.

[63] F. Zavoda, R. Langella, G.C. Lazaroiu, M. Bollen, S.K. Rönnberg, J. Meyer, P. Ciufo, Power quality in the future grid - Results from CIGRE/CIRED JWG C4.24, in: 17th International Conference on Harmonics and Quality of Power (ICHQP), 2016, pp. 931–936.